| Title | MOLECULAR MECHANISM OF MICROTUBULE-SEVERING BY KATANIN P60( Dissertation_    ) |
|---|---|
| Author(s) | Iwaya, Naoko |
| Citation | Kyoto University (        ) |
| Issue Date | 2012-01-23 |
| URL | http://dx.doi.org/10.14989/doctor.k16511 |
| Right | |
| Type | Thesis or Dissertation |
| Textversion | author |

# MOLECULAR MECHANISM OF MICROTUBULE-SEVERING BY KATANIN P60

**NAOKO IWAYA**

Department of Molecular Engineering

Graduate School of Engineering

Kyoto University

2011

# PREFACE

The projects in genome science try to understand the mechanism of the life phenomenon by analyzing genomes, which are often called the genetic blueprints for life. After the complete nucleotide sequence of the human genome was released in April 2003, research in life science has reached a new stage so called "Post-genome Era". Supporting by the enormous genome information including various organisms, analyses of gene functions and structures and functions of proteins have been extensively carrying out during this period. For example, although there are estimated about 25,000 human protein-coding genes, several tens of thousands of different proteins would be produced in human cells. There are two main mechanisms to a huge variety of protein: a single gene can generate different protein isoforms through the alternative splicing; most proteins after its synthesis undergo chemical modifications called post-translational modifications. Many scientists are very interested in the protein functions, because the life phenomenon has been controlled by the enormous network system among diverse proteins.

This thesis containing collected papers and discussion of my studies at Field of Supramolecular Biology, International Graduate School of Arts and Sciences, Yokohama City University during April 2003–March 2005 and at Department of Molecular Engineering, Graduate School of Engineering, Kyoto University and Yokohama City University during April 2005–March 2008 and at Kyoto University and Division of Structural Biology, Graduate School of Medicine, Kobe University during September 2008–September 2011. The aim of this thesis is to elucidate the molecular mechanism of microtubule-severing by katanin p60 in terms of structural biology. PART I provides introductions of above theme. PART II provides the studies about katanin p60 from the process of determining the novel structure to the novel hypothesis of microtubule-severing mechanism. Finally, the summaries and conclusions of this thesis are described in PART III.

# ACKNOWLADGEMENTS

December, 2011

Kyoto, Japan

Naoko Iwaya

# LIST OF PUBLICATIONS

**PART II**

**CHAPTER 1**

Fine-tuning of protein domain boundary by minimizing potential coiled coil regions

Naoko Iwaya, Natsuko Goda, Satoru Unzai, Kenichiro Fujiwara, Toshiki Tanaka, Kentaro Tomii, Hidehito Tochio, Masahiro Shirakawa and Hidekazu Hiroaki

*Journal of Biomolecular NMR*, **2007**, 37(1), 53-63

**CHAPTER 2**

A common substrate recognition mode conserved between katanin p60 and VPS4 governs microtubule severing and membrane skeleton reorganization

Naoko Iwaya, Yohta Kuwahara, Yoshie Fujiwara, Natsuko Goda, Takeshi Tenno, Kohei Akiyama, Shogo Mase, Hidehito Tochio, Takahisa Ikegami, Masahiro Shirakawa and Hidekazu Hiroaki

*The Journal of Biological Chemistry*, **2010**, 285(22), 16822-16829

**CHAPTER 3**

Effect of $Ca^{2+}$ on the microtubule-severing enzyme p60-katanin: insight into the substrate-dependent activation mechanism

Naoko Iwaya, Kohei Akiyama, Natsuko Goda, Takeshi Tenno, Yoshie Fijiwara, Daizo Hamada, Teikichi Ikura, Masahiro Shirakawa and Hidekazu Hiroaki

*The FEBS Journal*, revised

**OTHER PUBLICATIONS**

LBT/PTD dual tagged vector for purification, cellular protein delivery and visualization in living cells

Natsuko Goda, Takeshi Tenno, Kohsuke Inomata, Naoko Iwaya, Yoshiyuki Sasaki, Masahiro Shirakawa and Hidekazu Hiroaki

*Biochimica et Biophysica Acta,* **2007**, 1773(2), 141-146

Structure and function of the N-terminal nucleolin binding domain of nuclear valosin-containing protein-like 2 (NVL2) harboring a nucleolar localization signal

Yoshie Fujiwara, Kenichiro Fujiwara, Natsuko Goda, Naoko Iwaya, Takeshi Tenno, Masahiro Shirakawa, Hidekazu Hiroaki

*The Journal of Biological Chemistry*, **2011**, 286(24), 21732-21741

$^1$H, $^{13}$C, and $^{15}$N resonance assignment of the SPFH domain of human stomatin

Tomoyuki Tsuruta, Natsuko Goda, Yoshitaka Umetsu, Naoko Iwaya, Yohta Kuwahara, Hidekazu Hiroaki

*Biomolecular NMR Assignments*, in press

# CONTENTS

# PART I


# GENERAL INTRODUCTION

# Structural biology and the aim of this thesis

*The life is understood by the three-dimensional structure of protein*

The protein, which exists everywhere in the cell, is the most important material supporting the life activity. Although proteins are chemical synthetic polymer compounds that consist of 20 different amino acids, each protein has a unique structure and biological function due to the variety of amino acid sequences among proteins. The various proteins exhibit their functions by interacting with ions and electrons, as well as with molecules such as other proteins, nucleic acids, and sugars. In the cells, these interactions are organized into exquisite, highly complex networks, which are governed by the three-dimensional (3D) structures of proteins. Therefore, it is important that we clarify the 3D structure and function of each protein to understand the life phenomena in the cells. Research into the 3D structure and function of protein is called "Structural Biology".

*The methods of protein structure determination*

In structural biology, there are three major approaches, X-ray crystallography, nuclear magnetic resonance (NMR) spectroscopy, and cryo-electron microscopy to determine the 3D structures of proteins. Each method has advantages and disadvantages, and can be used according to sizes and characters of molecules. For X-ray crystallography, proteins are crystallized and analyzed their X-ray diffraction patterns to determine the distributions of electrons. While X-ray crystallography is an excellent method for determining the structures of rigid proteins that form ordered crystals, flexible proteins are difficult to observe in this method, because crystallography relies on having molecules aligned in the same orientation. For NMR spectroscopy, proteins are placed in a strong magnetic field and analyzed the resonance signals of their atomic nuclei such as $^1$H, $^{13}$C, and $^{15}$N to determine the distances between atoms. NMR samples are limited to small or medium proteins, because large proteins present problems with overlapping peaks in the NMR spectra. On the other hand, a major advantage of NMR spectroscopy is that provides information on

proteins in solution, as opposed to those locked in a crystal or bound to a microscopy grid. Thus, NMR spectroscopy is the premier method for studying the atomic structures of flexible proteins, the protein–protein interactions, and the protein dynamics. For cryo-electron microscopy, proteins are bound to a microscopy grid at liquid nitrogen temperatures and analyzed their electron microscopy images to determine the overall shapes of molecules. Although one of the disadvantages of cryo-electron microscopy is that the resolution obtained is low, this method can determine structures of large macromolecular complexes with no symmetry, as opposed to both X-ray crystallography and NMR spectroscopy.

The enormous data of protein structures has been accumulated now. According to the database such as Protein Data Bank (PDB) (http://www.pdb.org/pdb/home/home.do), one can compare and classify them. For example, it is possible to predict systematically the structure and function of unknown protein, by using the structural data and amino acid sequences.

### *Multidomain protein*

The protein domain is a unit of the structure. A majority of proteins in higher eukaryotes consist of multiple domains and are called multidomain proteins. Advanced research has been demonstrated that each domain exhibits a unique function and contributes to diverse biological processes in cooperation with each other. Although each domain has been determined the structure and correlated with the function in structural biology approaches, we would need to assemble interactive networks among multidomain proteins for our understanding of the various life phenomena.

### *The Protein is responsible for the diseases as well as the fundamental life phenomena*

The protein plays a key role in understanding and overcoming diseases, because diseases would result from aberrant networks among proteins in the cells. Many therapeutic drugs target

proteins (e.g. receptor and channel proteins). In recent years, structural biology has become indispensable not only in the understanding of fundamental life phenomena but also in the elucidation of disease mechanisms. Thus, the 3D structure-based investigations such as *in silico* screening and drug design are expected to develop drugs. For example, the structures of G protein coupled receptor (GPCR), one of the membrane proteins, are applied to the discovery and the development of drugs[1]. A cytoskeleton protein, microtubule related to the cell division is also paid attention as one of targets of the anticancer drug[2]. Additionally, since the proteins that interact with microtubule might cause critical diseases such as Alzheimer's disease, these proteins can be targeted for the drug development[3].

Interactions between microtubules and its associated proteins are organized into complex networks and involved in the various life phenomena including diseases. The mechanisms of how microtubule-associated proteins regulate microtubules remain poorly understood because of the lack of detailed 3D structural information. Therefore, in this thesis I performed analyses of the 3D structure and function of katanin, one of microtubule-associated proteins, in terms of structural biology to understand a part of the phenomena induced by the interactions between microtubules and microtubule-associated proteins.

## Microtubule, one of cytoskeleton

### *Cytoskeleton*

The cell is the basic structural and functional unit of life. The cytoskeleton is the most fundamental part of the cell. The cytoskeleton acts to organize and maintain the cell shape and is also responsible for strength and motility of the cell. The concept for cytoskeleton as an organized network of protein molecules extending throughout the cell was proposed by Peters in 1930. In 1931, the term "cytoskeleton" (cytosquelette, in French) was first introduced by Wintrebert[4]. Then,

electron microscopy has been instrumental in visualizing the cytoskeleton for the first time, and also in investigating its structural organization in different cells and conditions. The initial progress in the cytoskeletal studies closely paralleled the development of electron microscopy techniques.

The cytoskeleton is a 3D meshwork of crosslinked biopolymers that fills the cytoplasm in every cell. It was for a long time believed to be a characteristic feature of cells with a nucleus (eukaryotic cells) as both unicellular organisms such as yeast and amebas and multicellular organisms such as fungi, plants, and animals. Recently it became clear that even cells without a nucleus (prokaryotic cells) such as bacteria have homologous proteins that form a cytoskeleton[5]. Eukaryotic cells contain three major cytoskeletal filaments: actin filaments (also called microfilaments), microtubules, and intermediate filaments. On the other hand, prokaryotic cells contain MreB, FtsZ, and CreS, respectively, as homologues for major cytoskeletal filaments in eukaryotic cells. Each cytoskeleton exhibits diverse functions according to their species and cell types, because they drastically differ in their own stiffness and flexibility. One may think of a skeleton as a rigid framework. However, the structures of cytoskeletons act as muscle as well as skeleton, for movement and stability. In fact, they are very dynamic and involved in active cellular processes including cell movement, strength, adhesion, and polarity as well as intracellular transport. Therefore, structural information about cytoskeleton organization is critical for understanding its functions and mechanisms.

### *The structure of microtubule*

Microtubules (MTs) are major dynamic structural components in eukaryotic cells. They play important roles in a variety of cellular processes. During cell division, MTs form mitotic spindles and organize the spatial distribution of chromosomes[6]. They can serve as the principal structural element of cilia and flagella which are involved in swimming of cells[7]. They further serve as a rail on which motor proteins, such as kinesin and dynein proteins, convey their cargoes such as

organelles in intracellular transport[8]. In the same fashion, MTs within the axon in the neuron are used to transport substances to different parts of the cell[9]. MTs are also involved in granule transport in pigment cells[10].

MTs[11,12] are polymers of tubulin, which is a heterodimer composed of two different globular protein subunits, α- and β-tubulin. These heterodimers stack head to tail at 8 nm intervals to compose long liner chains so called protofilaments, where always a α-tubulin is followed by a β-tubulin. Within the most MT, thirteen protofilaments associate laterally to form a hollow cylindrical structure that measures 25 nm in diameter. (Fig. 1) This polymer structure of MT was first observed using electron microscopy in 1950s. The robust multifilament bundles are stabilized as compared to a single filament, while both termini of filaments are dynamic, in common with three cytoskeletons. Since all heterodimers are arranged in the same direction, MTs have a polar structure. The cellular functions of MTs critically depend on their polarity. For example, this polarity is central to the ability of motor proteins to move unidirectionally on the polymer lattice. MT polarity is also reflected in the distinct dynamic properties of the two polymer ends (see the following paragraph). On one end, the slower polymerizing end, in which α-tubulin is exposed, was termed the 'minus' end. On the opposite end, the faster polymerizing end, in which β-tubulin is exposed, was termed the 'plus' end.
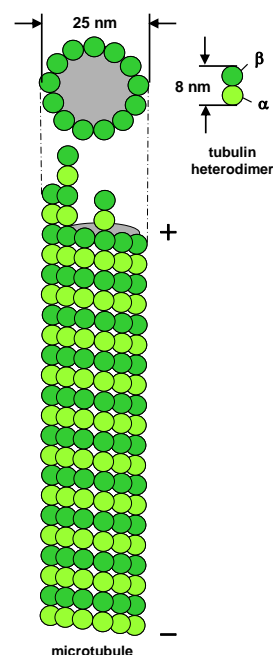
FIGURE 1. **MT structure.** Head-to-tail interactions of αβ dimers form liner protofilaments. 13 protofilaments associate laterally to form hollow cylindrical polymers.

In 1998, the 3D structure of tubulin heterodimer was determined by electoron crystallography to 3.7 Å resolutions (Fig. 2)[13]. The next year, a model of the MTs has been obtained by docking the 3D structure of tubulin into a 20 Å reconstruction of the MTs according to cryo-electron microscopy[14]. α- and β-tubulin are highly related proteins, ~50% identical at the amino acid sequence[15]. The structural analysis demonstrates that the 3D structure of α- and β-tubulin are basically identical as expected, while dimer is asymmetric because each monomer arrays in the same direction. This has been emphasized that the MTs have a polar structure and a particular dynamic property. The 3D structure information of tubulin was great success to provide impetus to the MT research afterwards.
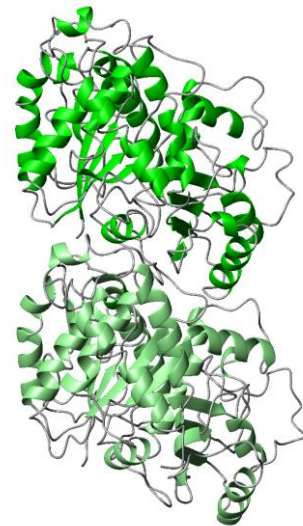


FIGURE 2. **Ribbon diagram of the tubulin dimmer showing α-tubulin (bottom), and β-tubulin (top).** (PDB code: 1tub).

*Dynamic instability of microtubule*

MTs are highly dynamic because of the constant transition between polymerizing (growing) and depolymerizing (shrinking) phases. This dynamics is described in terms of "dynamic instability"[16]. When first discovered, this unique behavior of MT dynamic instability was surprising to many researchers. The energy to drive the dynamic instability comes from guanosine triphosphate (GTP) hydrolysis. Tubulin is a GTPase whose activity is stimulated by polymerization.

When a new tubulin heterodimer is incorporated into the MT, the GTP bound to β-tubulin is hydrolyzed, and the resulting guanosine diphosphate (GDP) does not exchange in the polymer lattice. In contrast, the GTP bound to α-tubulin faces β-tubulin of heterodimer and is not hydrolyzed. The kinetics of GDP-tubulin is different from those of GTP-tubulin. GDP-tubulin is prone to depolymerization. Since tubulin adds onto both ends of the MT only in the GTP-bound state, there is generally a cap of GTP-tubulin at the tip of the plus end (β-tubulin). The GTP-cap protects the MT from disassembly. If hydrolysis catches up to the tip of the MT, growing MT suddenly begins a rapid depolymerization so called a 'catastrophe'. On the other hand, shrinking MT can often begin a slow polymerization again so called a 'rescue', by adding GTP-tubulin enough to the tip of the MT. Both catastrophe and rescue are also included in dynamic instability (Fig. 3)[17]. At the plus ends, the polymerizations of MTs are faster as compared with the minus ends. Additionally, the frequency of the catastrophe is higher at the plus ends, while the frequency of the rescue is higher at the minus ends. Therefore, MT plus ends show dynamic instability at a higher rate than the minus ends. In both test-tube studies (*in vitro*) and the cell (*in vivo*), such dynamics of MTs can occur spontaneously, while it is tightly regulated by the balance of MT stabilizing and destabilizing factors.
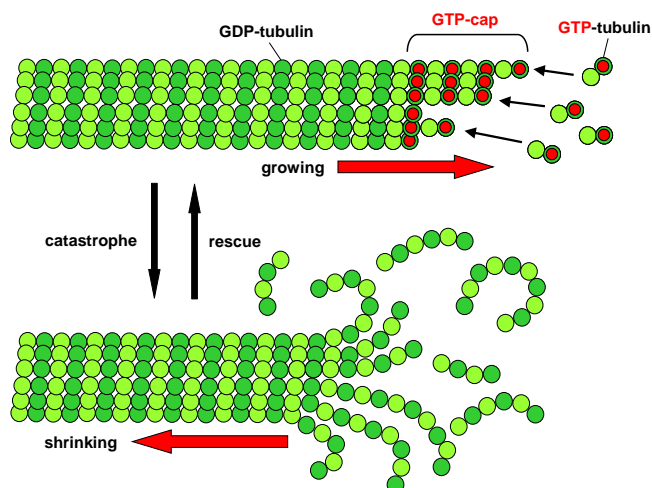


FIGURE 3. **MT dynamic instability.** Dynamic instability is characterized by the coexistence of polymerizing and depolymerizing MTs (see the text). At polymerizing MT end, the bound GTP is hydrolyzed during or soon after polymerization. The MT lattice is predominantly composed of GDP-tubulin. Polymerizing MTs suddenly transit to the depolymerization phase (catastrophe). Depolymerizing MTs can transit back to the polymerization phase (rescue).

## *Regulators for dynamic instability of microtubule*

MT dynamic instability is regulated by microtubule-associated proteins (MAPs) that interact with MT/tubulin (Fig. 4). There are two main types of MAPs which stabilize and destabilize MTs. MT stabilizing proteins include MAP1, MAP2, MAP4, and tau termed classical MAPs[18,19]. XMAP215, which is identified in *Xenopus* eggs, has also been characterized as a major regulator of MT plus end growth[20]. These proteins stabilize and promote MT polymerization such as rescue, or inhibit MT depolymerization such as catastrophe. In addition, since the γ-tubulin ring complex (γ-TuRC) acts as a scaffold for tubulin to begin polymerization in an initiation point called MT nucleation, γ-TuRC plays the role in promoting MT assembly[21,22]. Recent work has shown that most plus-end-biding proteins (+TIPs), including CLIP (cytoplasmic linker protein)-170 and EB1 (end-binding 1), promote MT plus end growth[23]. On the other hand, MT destabilizing proteins include stathmin/oncoprotein 18 (Op18), Kin (kinesin with an internal catalytic domain) I, spastin and katanin. Stathmin/Op18 interacts with free tubulin and negatively regulates its assembly in MTs[24]. The 3D structure of complex between tubulin and stathmin-like domain was determined by X-ray crystallography to 3.5 Å resolutions[25]. Kin I, a kind of kinesin motor protein, promotes MT catastrophe[26]. Spastin and katanin are well known as MT-severing factors.



FIGURE 4. **Some examples of MT stabilizing factors and destabilizing factors.**

## Katanin, MT-severing enzyme

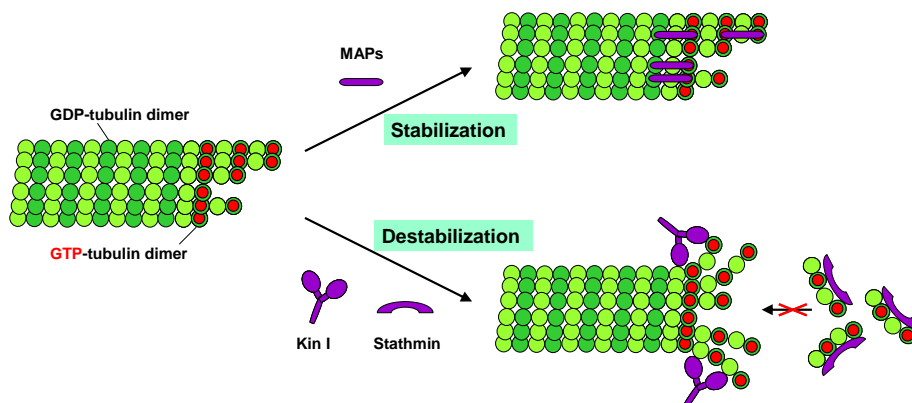MT-severing enzymes regulate MT disassembly by breaking the middle point of MTs. There are three major MT-severing enzymes, spastin, katanin, and fidgetin, all of which belong to AAA (ATPases associated with various cellular activities) ATPases[27,28,29]. AAA ATPases[30,31] are involved in diverse cellular activities, including cell cycle regulation, membrane fusion, protein transport, and protein degradation. AAA ATPases contain one (type I) or two (type II) conserved AAA domains that defines a large protein superfamily. In many cases, AAA domains assemble into hexameric rings that are likely to change their shape during the ATPase cycle. This ATP-dependent conformational change may apply tension to bound proteins and thereby allow AAA ATPases to unfold polypeptides and dissociate protein–protein interactions. On the other hand, their $NH_2$-terminal regions are unique sequences and may determine the specificities to their substrates and/or adaptors. Above three MT-severing enzymes play key roles in diverse cellular dynamic event of MTs, including formation and maintenance of cell, formation of spindle pole, cell division, intracellular transport, and neurite outgrowth, through disassembling MTs and regulating lengths of polymers at the optimal length in an ATP-dependent manner.

Katanin was originally purified from sea urchin eggs[32]. Katanin was shown to sever MTs and hence was named "katanin" from katana, the Japanese word for samurai sword. Katanin is a heterodimer, which is composed of a 60 kDa catalytic MT-severing subunit (kp60) and an 80 kDa regulatory subunit (kp80). Both subunits are genetically conserved among many higher eukaryotes, but not in yeast and bacteria. In nematodes (*C. elegans*), MEI-1 and MEI-2 correspond to catalytic and regulatory subunits, respectively[33]. Katanin contributes to the organization and transportation of MT arrays in the cells including neurons, by severing MTs and generating new sites for MT growth[34]. Kp60, a type I AAA ATPase, is known to regulate directly MT-severing in an ATP-dependent manner. On the other hand, kp80 targets kp60 to centrosomes and regulates the MT-severing activity of kp60[35]. An active form of kp60 is believed to an oligomer like other AAA

ATPases[36]. Perhaps, kp60 may disassemble MTs in a hexameric ring suggesting a severing mechanism similar to spastin, which uses its pore to tug on the COOH-terminal tail of tubulin and leads to breakdown of MTs[37]. However, its severing mechanism is still unproven. Here I have focused especially on the mechanism of MT-severing by kp60 and carried out this study through structural biology.

## Bioinformatics—*Domain isolation of katanin p60: CHAPTER 1*

The AAA domains of AAA ATPases are well conserved from prokaryotes to human, while their $NH_2$-terminal regions are unique and are often known to be the binding sites specific for their substrates. Thus, to interpret the molecular mechanisms of specific recognition for MTs in kp60, I have started to analyze the 3D structure and the function of the $NH_2$-terminal regions of kp60. I have first identified a novel structural domain from the $NH_2$-terminal regions of kp60 by bioinformatics techniques. I have further succeeded to optimize the domain boundaries suited for structural determination by the combination of bioinformatics, point mutations in proteins, and NMR techniques. The bioinformatics techniques include database searches, sequence alignments, structural predictions, and so on. These are much variety, highly upgraded, and now essential for protein analyses including the 3D structural analyses.

## Structural biology—*Determination of the 3D structure of katanin p60 $NH_2$-terminal domain and the interface between katanin p60 and tubulin: CHAPTER 2*

I determined the novel structure of the $NH_2$-terminal domain (NTD) of kp60 using $^{13}C/^{15}N$-labeled sample in solution by 3D NMR techniques for the first time. It was shown that the structure of kp60-NTD has resembled the $NH_2$-terminal domain (MIT domain) of Vps4, another member of

type I AAA ATPases. In the next, I found that kp60-NTD binds tubulin and determined its interface with tubulin by biochemical assays. The same results were obtained when the assays were carried out by use of the full-length kp60 protein. Interestingly, both kp60 and Vps4 have been similar in the molecular mechanisms of how the enzymes disassemble their macromolecular substrates. Finally, I proposed a model for kp60–MT complex based on the interface between Vps4-MIT and its substrate.

The biochemical techniques used here are the pull-down assays, by which the binding partners are searched for using the recombinant proteins (tagged proteins) bound to an affinity ligand. The pull-down assays is an *in vitro* method used to determine a physical interaction between two or more proteins. Protein–protein interactions can be visualized by sodium dodecyl sulfate-polyacrylamide gel electrophoresis (SDS-PAGE) and associated detection methods, including gel staining and Western blotting detection. SDS-PAGE is a technique widely used in biochemistry and molecular biology to separate proteins according to their electrophoretic mobility such as molecular weight.

## Biochemistry—*Regulatory function of katanin p60: CHAPTER 3*

I identified the minimum structural domain of the COOH-terminal domain (CTD) of kp80. My studies suggested that this minimum region of kp80-CTD interacts with the surface of kp60-NTD at the opposite interface between kp60-NTD and tubulin. Thus, I assumed that kp60-NTD may bind both tubulin and kp80-CTD using its distinct interfaces. I also focused on the regulatory role of kp60-NTD to the ATPase activity that is energy of ATP hydrolysis. In the result, I found that $Ca^{2+}$ ion cancels out the enhancement of ATPase activity of kp60 in the presence of the substrate (MT) and/or adaptor (kp80-CTD) and inhibits the MT-severing activity of kp60. $Ca^{2+}$ acts as a regulator of many biological processes. The concentration change of $Ca^{2+}$ occurs as a response to

various signals, resulting neural excitement, secretion, muscle contraction, fertilization, cell division, and other phenomena. Furthermore, I showed that $Ca^{2+}$ binds kp60-NTD at the edge of domain by NMR titration experiments. On the basis of a model of kp60–MT complex in CHAPTER 2, I predicted that $Ca^{2+}$ binding site becomes close to the putative interface between kp60-NTD and the AAA domain of kp60 in an ATPase activate state. Finally, I hypothesized that $Ca^{2+}$ and a spatial rearrangement of the NTD relative to the AAA domain regulate the ATPase activity of kp60 in the presence of the substrate and/or adaptor.

NMR titration experiment is a powerful technique to map the interacting site of a $^{15}$N-labeled protein with its binding partner such as other protein and a metal ion. Changes in chemical shifts in $^{1}$H-$^{15}$N HSQC spectra demonstrate exchanges of magnetic environments. These exchanges are thought to be due to two phenomena: the interaction between $^{15}$N-labeled protein and its binding partner will change magnetic environments around the interface; the addition of the partner may induce structural change or conformational change in the $^{15}$N-labeled protein.

# References

1. Gurrath, M. (2001) Peptide-binding G protein-coupled receptors: new opportunities for drug design. *Curr. Med. Chem.* **8**, 1605-1648.

2. Jordan, A., Hadfield, J. A., Lawrence, N. J. & McGown, A. T. (1998) Tubulin as a target for anticancer drugs: agents which interact with the mitotic spindle. *Med. Res. Rev.* **18**, 259-296.

3. Corbo, C. P. & Alonso Adel, C. (2011) Therapeutic targets in Alzheimer's disease and related tauopathies. Prog *Mol. Biol. Transl. Sci.* **98**, 47-83.

4. Frixione, E. (2000) Recurring views on the structure and function of the cytoskeleton: a 300-year epic. *Cell Motil. Cytoskeleton* **46**, 73-94.

5. Shih, Y. L. & Rothfield, L. (2006) The bacterial cytoskeleton. *Microbiol. Mol. Biol. Rev.* **70**, 729-754.

6. Karsenti, E. & Vernos, I. (2001) The mitotic spindle: a self-made machine. *Science* **294**, 543-547.

7. Scholey, J. M. (2003) Intraflagellar transport. *Annu. Rev. Cell Dev. Biol.* **19**, 423-443.

8. Hirokawa, N. (1998) Kinesin and dynein superfamily proteins and the mechanism of organelle transport. *Science* **279**, 519-526.

9. Hirokawa, N. & Takemura, R. (2005) Molecular motors and mechanisms of directional transport in neurons. *Nat. Rev. Neurosci.* **6**, 201-214.

10. Rodionov, V. I., Gyoeva, F. K. & Gelfand, V. I. (1991) Kinesin is responsible for centrifugal movement of pigment granules in melanophores. *Proc. Natl. Acad. Sci. U S A* **88**, 4956-4960.

11. Desai, A. & Mitchison, T. J. (1997) Microtubule polymerization dynamics. *Annu. Rev. Cell Dev. Biol.* **13**, 83-117.

12. Nogales, E. (2001) Structural insight into microtubule function. *Annu. Rev. Biophys. Biomol. Struct.* **30**, 397-420.

13. Nogales, E., Wolf, S. G. & Downing, K. H. (1998) Structure of the alpha beta tubulin dimer by electron crystallography. *Nature* **391**, 199-203.

14. Nogales, E., Whittaker, M., Milligan, R. A. & Downing, K. H. (1999) High-resolution model of the microtubule. *Cell* **96**, 79-88.

15. Burns, R. G. (1991) Alpha-, beta-, and gamma-tubulins: sequence comparisons and structural constraints. *Cell Motil. Cytoskeleton* **20**, 181-189.

16. Mitchison, T. & Kirschner, M. (1984) Dynamic instability of microtubule growth. *Nature* **312**, 237-242.

17. Inoué, S. & Salmon, E. D. (1995) Force generation by microtubule assembly/disassembly in mitosis and related movements. *Mol. Biol. Cell* **6**, 1619-1640.

18. Vallee, R. B. (1982) A taxol-dependent procedure for the isolation of microtubules and microtubule-associated proteins (MAPs). *J. Cell Biol.* **92**, 435-442.

19. Tokuraku, K., Katsuki, M. & Kotani, S. (2002) Structural and functional analyses of microtubule-associated protein 4. *Recent Res. Devel. Biochem.* **3**, 315–333.

20. Vasquez, R. J., Gard, D. L. & Cassimeris, L. (1994) XMAP from Xenopus eggs promotes rapid plus end assembly of microtubules and rapid microtubule polymer turnover. *J. Cell Biol.* **127**, 985-993.

21. Wiese, C. & Zheng, Y. (2000) A new function for the gamma-tubulin ring complex as a microtubule minus-end cap. *Nat. Cell Biol.* **2**, 358-364.

22. Moritz, M., Braunfeld, M. B., Guénebaut, V., Heuser, J. & Agard, D. A. (2000) Structure of the gamma-tubulin ring complex: a template for microtubule nucleation. *Nat. Cell Biol.* **2**, 365-370.

23. Schuyler, S. C. & Pellman, D. (2001) Microtubule "plus-end-tracking proteins": The end is just the beginning. *Cell* **105**, 421-424.

24. Cassimeris, L. (2002) The oncoprotein 18/stathmin family of microtubule destabilizers. *Curr. Opin. Cell Biol.* **14**, 18-24.

25. Ravelli, R. B., Gigant, B., Curmi, P. A., Jourdain, I., Lachkar, S., Sobel, A. & Knossow, M. (2004) Insight into tubulin regulation from a complex with colchicine and a stathmin-like domain. *Nature* **428**, 198-202.

26. Desai, A., Verma, S., Mitchison, T. J. & Walczak, C. E. (1999) Kin I kinesins are microtubule-destabilizing enzymes. *Cell* **96**, 69-78.

27. Errico, A., Ballabio, A. & Rugarli, E. I. (2002) Spastin, the protein mutated in autosomal dominant hereditary spastic paraplegia, is involved in microtubule dynamics. *Hum. Mol. Genet.* **11**, 153-163.

28. Cox, G. A., Mahaffey, C. L., Nystuen, A., Letts, V. A. & Frankel, W. N. (2000) The mouse fidgetin gene defines a new role for AAA family proteins in mammalian development. *Nat. Genet.* **26**, 198-202.

29. Frickey, T. & Lupas, A. N. (2004) Phylogenetic analysis of AAA proteins. *J. Struct. Biol.* **146**, 2-10.

30. Ogura, T. & Wilkinson, A. J. (2001) AAA$^+$ superfamily ATPases: common structure–diverse function. *Genes Cells* **6**, 575-597.

31. Vale, R. D. (2000) AAA proteins: Lords of the ring. *J. Cell Biol.* **150**, F13-9.

32. McNally, F. J. & Vale, R. D. (1993) Identification of katanin, an ATPase that severs and disassembles stable microtubules. *Cell* **75**, 419-429.

33. Srayko, M., Buster, D. W., Bazirgan, O. A., McNally, F. J. & Mains, P. E. (2000) MEI-1/MEI-2 katanin-like microtubule severing activity is required for Caenorhabditis elegans meiosis. *Genes Dev.* **14**, 1072-1084.

34. Roll-Mecak, A. & Vale, R. D. (2006) Making more microtubules by severing: a common theme of noncentrosomal microtubule arrays? *J. Cell Biol.* **175**, 849-851.

35. McNally, K. P., Bazirgan, O. A. & McNally, F. J. (2000) Two domains of p80 katanin regulate microtubule severing and spindle pole targeting by p60 katanin. *J. Cell Sci.* **113**, 1623-1633.

36. Hartman, J. J. & Vale, R. D. (1999) Microtubule disassembly by ATP-dependent oligomerization of the AAA enzyme katanin. *Science* **286**, 782-785.

37. Roll-Mecak, A & Vale, R. D. (2008) Structural basis of microtubule severing by the hereditary spastic paraplegia protein spastin. *Nature* **451**, 363-367.

# PART II


# MOLECULAR MECHANISM OF MICROTUBULE-SEVERING BY KATANIN P60

# CHAPTER 1

# Fine-tuning of Protein Domain Boundary by Minimizing Potential Coiled coil Regions

## Abstract

Structural determination of individual protein domains isolated from multidomain proteins is a common approach in the post-genomic era. Novel and thus uncharacterized domains liberated from intact proteins often self-associate due to incorrectly defined domain boundaries. Self-association results in missing signals, poor signal dispersion and a low signal-to-noise ratio in $^1$H–$^{15}$N HSQC spectra. We have found that a putative, non-canonical coiled coil region close to a domain boundary can cause transient hydrophobic selfassociation and monomer–dimer equilibrium in solution. Here we propose a rational method to predict putative coiled coil regions adjacent to the globular core domain using the program COILS. Except for the amino acid sequence, no preexisting knowledge concerning the domain is required. A small number of mutant proteins with a minimized coiled coil region have been rationally designed and tested. The engineered domains exhibit decreased self-association as assessed by $^1$H–$^{15}$N HSQC spectra with improved peak dispersion and sharper cross peaks. Two successful examples of isolating novel N-terminal domains from AAA-ATPases are demonstrated. Our method is useful for the experimental determination of domain boundaries suited for structural genomics studies.

## Introduction

An enormous amount of sequence information has been generated from numerous genome sequencing projects[1] (also see http://www.ncbi.nlm.nih.gov/). The next major challenge is to focus on the genome-wide analysis of protein structure/function relationships[2-4]. A sequence comparison of proteins from various genome sets has provided information concerning individual domains, which constitute an evolutionarily conserved stretch of 50–300 amino acids capable of folding autonomously. Although many proteins are still annotated as ''function unknown'', an analysis of mammalian genomes shows that >70% of proteins are in fact ''multidomain proteins'', which harbor more than one protein domains[5]. Genetic dissection of genes encoding large proteins in order to obtain individual domains for structural studies is a key methodology in this field. Two major technical problems of working with individual domains in isolation from the parent protein have emerged: (i) the isolated domain tends to precipitate and is not well expressed in the cytosol of bacterial expression systems, and (ii) the isolated domain may form a soluble multimeric aggregate by nonspecific self-association. Both problems make the NMR analysis of novel protein domains difficult. When using solution NMR techniques, the first criterion of a promising protein domain for structure determination is to give a good HSQC spectrum. However, there is currently no rational approach to avoid self-association of uncharacterized protein domains.

In order to minimize self-association, we focused on regions of the target protein likely to form a coiled coil structure, which may act as a site for protein-protein interaction. Coiled coil structures are widely observed in proteins, and have been classified as one of the common supersecondary structures for protein-protein interactions[6,7]. Two to six amphipathic right-handed α-helices interact and wrap together to form a left-handed twist structure[8-10]. The periodic repeat of hydrophobic residues in an α-helical context is important for forming a coiled coil structure. Because seven amino acid residues form two rounds of each α-helix strand, the motif has a

representative heptad repeat sequence with the amino acid residues designated *a* to *g* according to their position. Studies involving artificially designed coiled coils show that the *a*- and the *d*- positions are particularly important for inter-helical interactions and structural uniqueness. For example, the coiled coil without the structural uniqueness was found to be an ensemble of sub-optimal structures, resulting in a broadened NMR spectrum[11]. The arrangement of the packing structure in the protein interior is an important *de novo* design target. According to these concepts, many successful designs for the control of the orientation[12] and the selective assembly of peptide fragments of coiled coils have been reported[13-15]. For example, the improved packing of the protein structure could lead to an increase in thermal stability[16]. By contrast, substitution of one or more hydrophobic residues for small or charged residues can cause instability of a coiled coil structure as well as loss of structural uniqueness. This strategy can easily be used to eliminate predicted coiled coil regions of proteins, in which mutations are introduced to destabilize such packing.

Herein, we propose a simple prediction and design method to minimize protein self-association by destabilizing the putative coiled coil regions in the target protein in order to improve the HSQC signal with a minimum of experimental effort. Potential coiled coil regions are simply predicted by the program COILS (version 2.1) with the ''–mtidk'' option and weighting of hydrophobic residues[17]. The program takes the periodicity of hydrophobic amino acid residues in a heptad repeat into account for prediction. Using the ''–mtidk'' option, the program is more sensitive to the detection of non-canonical coiled coils. The putative coiled coil region is sometimes hidden in one domain region of the target protein. Since the program uses only the amino acid sequence as an input, we can virtually design any mutant sequence to avoid forming a coiled coil. Virtual mutants with deletion(s) and/or amino acid substitution(s) are first analyzed by COILS. A limited number of sequences for further study are then selected by using the COILS score as a guide. Using this approach, we have successfully isolated two N-terminal domains derived from the AAA-ATPases.

## Experimental procedures

### *Protein techniques*

Vectors for the heterologous expression of GST fusion proteins of the N-terminal domains from both mouse and human katanin p60 (residues 1–90, denoted as $kp60_{1-90}$) and nuclear VCP-like protein 2 (residues 1–93, denoted as $NVL2_{1-93}$) were constructed using PRESAT-vector methodology, derived from pGEX-4T3 vector (Amersham Biosciences, Piscataway, NJ)[18]. Truncated constructs and the L73R mutant of mouse $kp60_{1-90}$ were prepared by site directed mutagenesis using Gene-Editor (Promega, La Jolla, CA) according to the manufacturer's instructions. The solubility of GST-fusion proteins was assayed by the CDNB colorimetric assays according to the manufacturer's instructions (Amersham Biosciences). The $^{15}$N-labeled recombinant proteins for NMR spectroscopy were generated in *E. coli* BL21(DE3) from a 1.0 l M9 minimal medium culture grown in the presence of $^{15}NH_4Cl$ as the sole nitrogen source at 30°C. The cell lysate after sonication was cleared by centrifugation and then applied to a DEAE-Sepharose column (Amersham Biosciences), and then affinity purified by Glutathione Sepharose (Amersham Biosciences) chromatography. The GST tag was removed by thrombin ''on-beads'', and the protease was trapped using benzamidine Sepharose (Amersham Biosciences) and then dialyzed.

### *NMR Spectroscopy*

Samples for NMR spectroscopy contained mouse kp60 N-terminal domains at a concentration of approximately 0.1 mM in 5% $D_2O$–95% $H_2O$, 20 mM sodium phosphate buffer (pH 7.5) and 1% CHAPS. Samples for NMR spectroscopy contained mouse NVL2 N-terminal domains at a concentration of approximately 0.1 mM in 5% $D_2O$–95% $H_2O$ and 25 mM sodium phosphate buffer (pH 6.4). $^1H$–$^{15}N$ HSQC spectra for kp60 N-terminal domains were recorded on a 500 MHz Bruker DRX NMR spectrometer equipped with a cryogenic probe at 25°C. $^1H$–$^{15}N$ HSQC

spectra for NVL2 domains were recorded on a 800 MHz Bruker *Avance* NMR spectrometer equipped with a cryogenic probe at 25°C. Data were processed by using NMRPipe[19].

## *CD and fluorescence spectroscopy*

CD spectra of mouse kp60 N-terminal domains were measured in 0.1-cm path length cuvettes at 25°C using a JASCO J-720W spectropolarimeter (JASCO, Co, Tokyo). 10 μM of each protein was dissolved in buffer containing 1 mM EDTA and 50 mM Tris–HCl (pH 7.5). Fluorescence spectra of 8-ANS bound to mouse kp60 N-terminal domains and bovine α-lactalbumin were measured in a 1-cm path length cuvette at 25°C using a Shimadzu RF-5300PC spectrofluorophotometer (Kyoto, Japan). An excitation wavelength of 370 nm was used and emission from 400 to 600 nm measured. Fluorescence enhancement experiments were done by measuring the difference spectra of fluorescence emission from various concentrations of 8-ANS (0–100 μM) with and without 4 μM of protein in buffer containing 1 mM EDTA and 50 mM Tris–HCl (pH 7.5), except α-lactalbumin (pH 2.0). Because the unit of fluorescence intensity is arbitrary, α-lactalbumin at pH 2.0 was used as a reference of fluorescence enhancement of a molten globule protein.

## *Analytical ultracentrifugation*

Sedimentation velocity experiments were carried out using an Optima XL-I analytical ultracentrifuge (Beckman Coulter, Fullerton, CA) with a Beckman An-50 Ti rotor. For sedimentation velocity experiments, cells with a standard Epon two-channel centerpiece and sapphire windows were used. Sample (400 μl) and reference buffer (420 μl) were loaded into cells. The rotor temperature was equilibrated at 20°C in the vacuum chamber for 1–2 h prior to start-up. Absorbance ($OD_{280}$) scans were collected at 10 min intervals during sedimentation at $50 \times 10^3$ rpm. The sedimentation velocity experiments for kp60 N-terminal domains were conducted at

concentrations of between 0.17 and 0.4 mg/ml. Partial specific volume of the protein, solvent density and solvent viscosity were calculated from standard tables using the program SEDNTERP, version 1.08[20]. The resulting scans were analyzed using the continuous distribution ($c(s)$) analysis module in the program SEDFIT version 9.3[21]. Sedimentation coefficient increments of 50 or 100 were used in the appropriate range for each sample, and the frictional coefficient was allowed to float during fitting. The weight average sedimentation coefficient was obtained by integrating the range of sedimentation coefficients in which peaks were present.

Sedimentation equilibrium experiments were also carried out in cells with six channel centerpiece and quartz windows. The sample concentrations were 0.17, 0.29 and 0.4 mg/ml. The absorbance wavelength was set at 280 nm, and data was acquired at 20°C. Data were obtained at 15, 20, 25, and 30 x $10^3$ rpm. A total equilibration time of 14 h was used for each speed, with a scan taken at 12 h to ensure equilibrium had been reached. Data analysis was performed by global analysis of data sets obtained at different loading concentrations and rotor speeds using XL-A/XL-I Data Analysis Software Version 4.0.

## Results


*Initial NMR assessment of N-terminal domains from AAA ATPases*

We have analyzed members of the AAA-ATPase family of proteins[22,23]; katanin p60 (kp60) and nuclear VCP-like protein 2 (NVL2). We anticipated that the N-terminal region of AAA-ATPases may possess modular domains responsible for specific substrate and/or adaptor binding regions. Our recent success in determining the structure of the N-terminal domain(s) from PEX1 ATPase[24] encouraged us to apply such an approach to the AAA proteins. Figure 1 shows a sequence alignment of the N-terminal 100 amino acid region of kp60 and NVL2. Starting from the full length sequence of mammalian proteins of both kp60 and NVL2, orthologous sequences were retrieved from the nr (non-redundant) protein sequence database using PSI-BLAST. Although there had been no indication of the presence of an isolatable domain at the N-terminus of either protein at the starting point of this research, the initial domain boundaries were defined as residues 1−90 and 1−93 for mouse kp60 and mouse NVL2, respectively, because these positions are less conserved among their orthologs (Fig. 1). Note that the newer version of fold recognition servers (e.g. FORTE and FUGUE) have been enabled to detect a MIT-domain like region at the N-terminus of kp60, after the structures of MIT domain were reported[25-27]. GST-fusion expression vectors for both domains of mouse and human orthologs were constructed, and the domains were expressed in *Escherichia coli* BL21(DE3). Preliminary experiments showed that mouse kp60$_{1-90}$ and mouse NVL2$_{1-93}$ were more soluble than the human orthologs (data not shown). Thus, the recombinant mouse proteins were selected for further investigation.
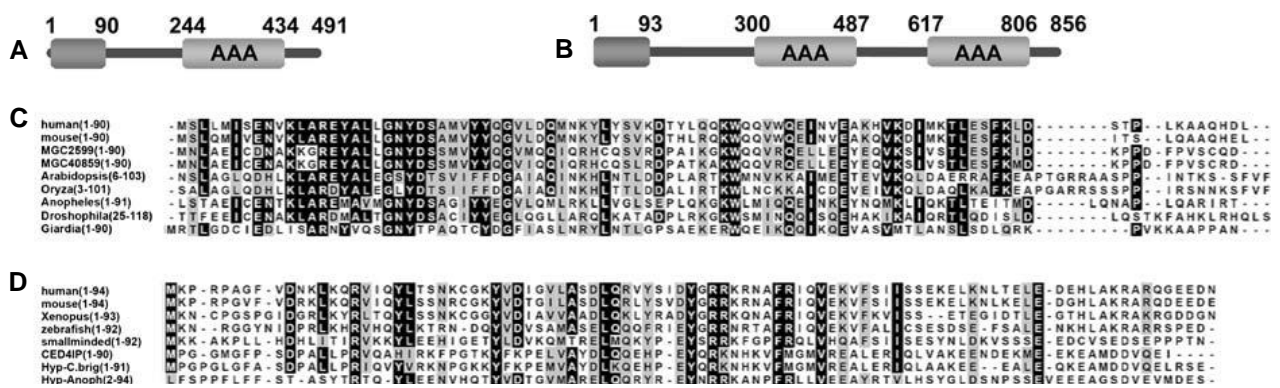
FIGURE 1. **Multiple alignment of protein sequences used in this study.** (A) Domain architectures of mouse katanin p60 (kp60). (B) Domain architectures of mouse nuclear VCP-like protein 2 (NVL2). (C) Multiple alignment of the N-terminal region of kp60 orthologs; human (UniProtKB accession no. O75449) and mouse (Q9WV86) katanins, human (MGC2599; Q9BW62) and mouse (MGC40859; Q8K0T4) hypothetical proteins, *Arabidopsis* (Q9SEX2), *Oryza* (Q8S118), *Anopheles* (Q7PY77, fragment), *Drosophila* (Q9VN89) and *Giardia* (Q7R5W7) katanin p60. (D) Multiple alignment of the N-terminal region of NVL2 orthologs; human (O15381), mouse (Q9DBY8), *Xenopus* (Q7ZXI4), zebrafish (Q803I9), *Drosophila* (smallminded; P91638), *C. elegans* CED4IP (Q9U8K0), *C. briggsae* (CBG20797; Q60SQ4) and *Anopheles* (ENSANGP00000024422; Q7PID7) hypothetical proteins. Residue numbers are in parentheses. The sequence alignments were generated by ClustalX

The $^1$H–$^{15}$N HSQC spectrum of mouse kp60$_{1–90}$ is shown in Fig. 2E. We anticipated a total of 95 main chain amide signals for kp60$_{1–90}$ (including six additional vector-derived signals), but only about 60 signals were obtained. The dispersion of observed signals was similar to that of a typical HSQC pattern for a folded molecule, suggesting certain parts of the domain were folded. We performed an extensive search of different buffer conditions for NMR measurements of kp60$_{1–90}$ according to standard practice[28], by varying pH (5.5–7.5) and ionic strength (0–0.5 M), prior to applying the method described below (Fig. 3). Because the quality of HSQC spectra was largely independent of salt conditions, self-association appeared to be hydrophobic in nature. Nevertheless, more than 30 cross peaks were still missing. Thus, we attempted to improve the spectral quality of these protein domains using an alternative approach such as introducing mutations.
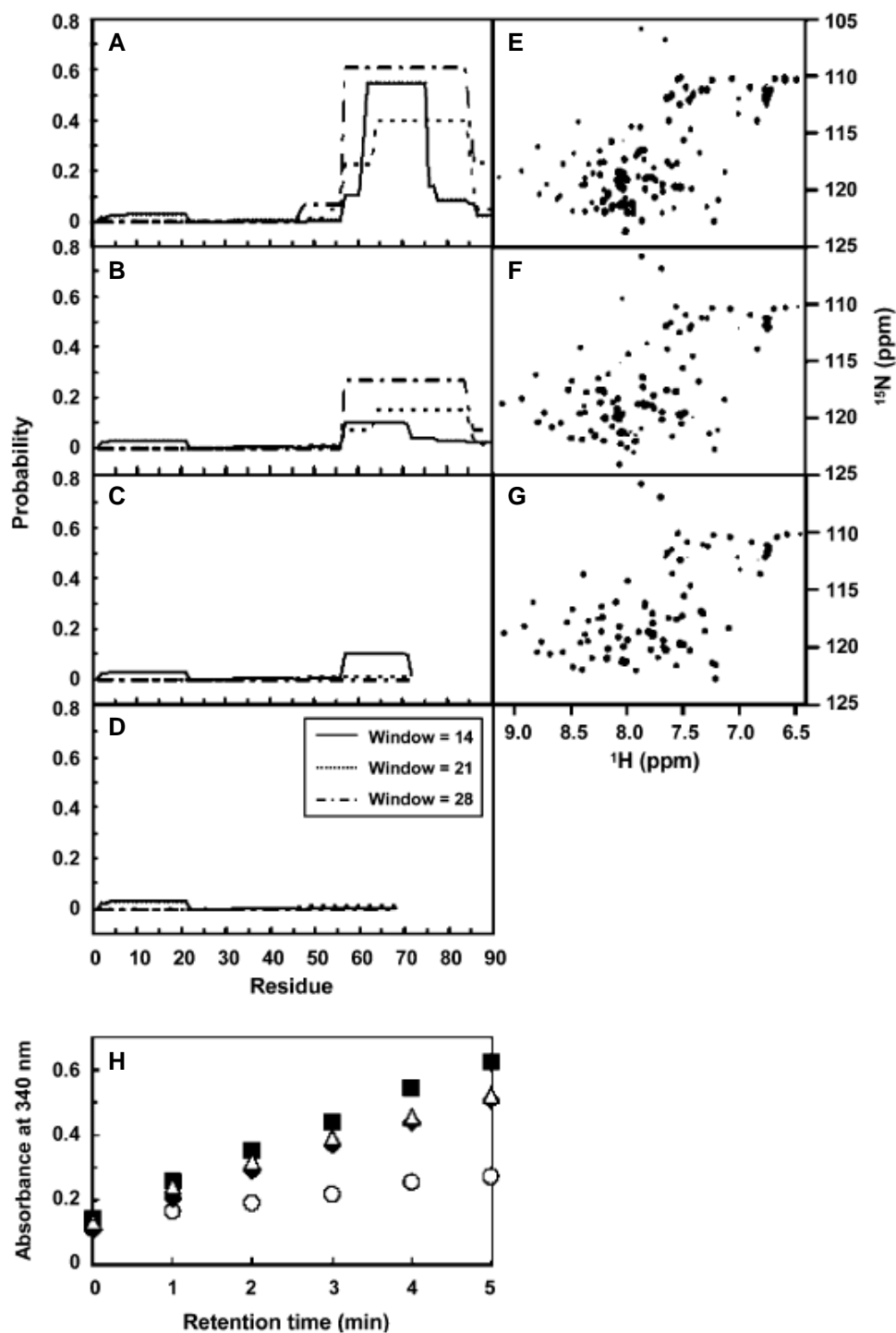
FIGURE 2. **Correlation of coiled coil propensity and $^1H$–$^{15}N$ HSQC spectral dispersion for the N-terminal regions of katanin p60.** (A–D) Coiled coil propensity calculated by the program COILS. A: kp60$_{1-90}$, B: kp60$_{1-90}$ (L73R), C: kp60$_{1-72}$, D: kp60$_{1-68}$, solid, dotted and dashed lines indicate window sizes of 14, 21 and 28 residues, respectively. (E–G) $^1H$–$^{15}N$ HSQC spectra. E: kp60$_{1-90}$, F: kp60$_{1-90}$ (L73R), G: kp60$_{1-72}$. (H) Solubility of GST-tagged katanin p60 Nterminal regions monitored by CDNB colorimetric assays. Filled diamond: kp60$_{1-90}$, filled box: kp60$_{1-90}$ (L73R), open triangle: kp60$_{1-72}$, open circle: kp60$_{1-68}$
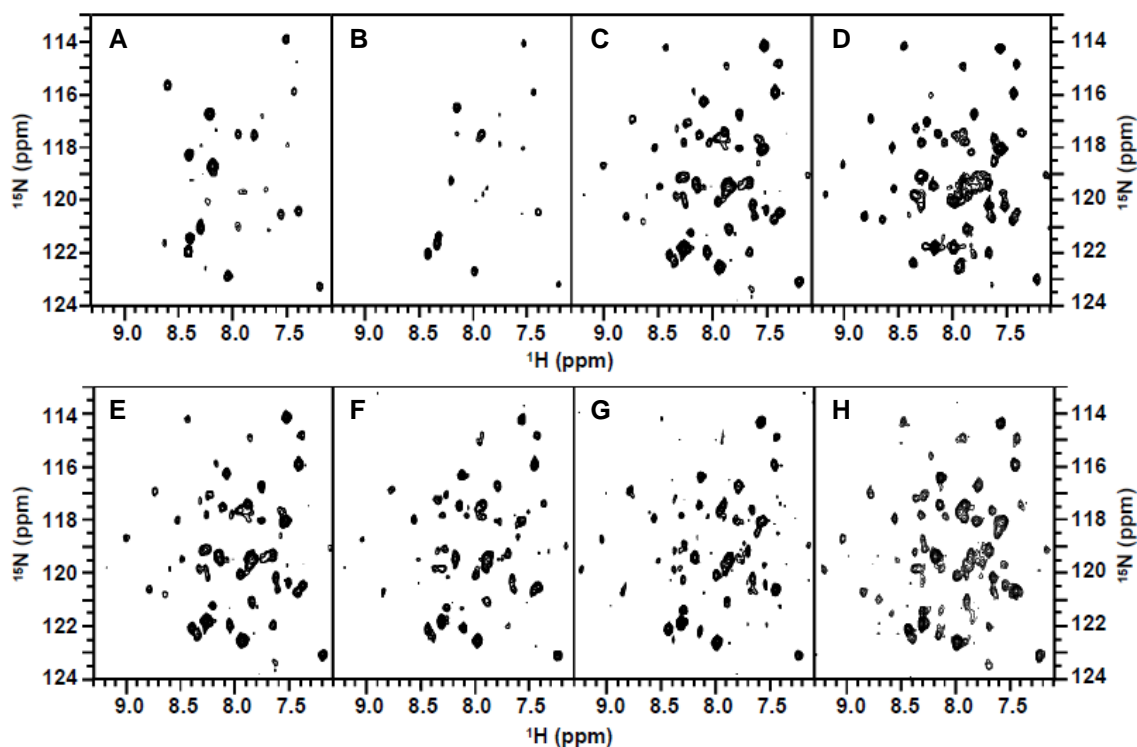
FIGURE 3. **Optimization of NMR conditions of kp60$_{1-90}$ according to the standard practice.** (A-D) $^1$H-$^{15}$N HSQC spectra of kp60$_{1-90}$ in various pH at fixed NaCl concentration of 0 mM. A: pH 4.3, B: pH 5.5, C: pH 6.5, D: pH 7.5. (E-H) $^1$H-$^{15}$N HSQC spectra of kp60$_{1-90}$ at various NaCl concentrations at fixed pH 6.5. E: 0 mM, F: 50 mM, G: 150 mM, H: 250 mM.

*Fine-tuning of boundaries of mouse kp60 N-terminal domain by destabilizing putative coiled coil region*

The sequences of mouse and human kp60$_{1-90}$ were analyzed by the program COILS with window sizes of 14, 21 and 28 residues. These are the default values of the size of gliding window to calculate the coiled-coil propensity[17]. In all cases, approximately 30 amino acid residues at the C-terminal region of the putative domain showed a coiled coil propensity of greater than 50% (Fig. 2A). Thus far, however, the predicted coiled coil region has not been ascribed any biological function. The length of the predicted coiled coil region was consistent with the number of missing cross peaks in the HSQC spectra (Fig. 2E). We therefore assumed that the missing signals on the HSQC spectrum originated from the region of the predicted coiled coil.

We designed several virtual mutants for the putative N-terminal domain of kp60. The virtual sequences for the N-terminal domain of kp60 were as follows: $kp60_{1-90}$ (I69R), $kp60_{1-90}$ (I80R), $kp60_{1-90}$ (L73R), $kp60_{1-90}$ (L78R), $kp60_{1-90}$ (V66R), $kp60_{1-75}$, $kp60_{1-72}$ and $kp60_{1-68}$. It is known that increasing the number of heptad repeats dramatically stabilizes the coiled coil in two-, three-and four-stranded coiled coils[29], and vice versa. It is known that partial digestion by endogenous trypsin-like protease in *E. coli* often generates products with Lys or Arg as the C-terminal residue. Thus, we considered several truncated mutants with Lys or Arg at the C-terminus, which may avoid the heterogeneity of the C-terminal residues. The substitution mutants involved replacing a hydrophobic residue with an arginine, which was expected to increase solubility. In general, hydrophobic residues, such as Ile, Val, Leu, Met, Phe, Tyr and Trp, can be substituted by either charged (Arg, Lys, Asp, Glu) or small (Ser, Gly) residues. All the sequences were subjected to COILS analysis, and those that gave a substantial reduction of coiled coil propensity ($kp60_{1-90}$ (L73R), $kp60_{1-72}$, $kp60_{1-68}$) were chosen for further study (Fig. 2B–D).

The three candidate proteins were engineered for expression and purified. The shortest construct $kp60_{1-68}$ tended to precipitate during protein expression and purification. The solubility of the kp60 N-terminal domains was semi-quantitatively assessed by CDNB colorimetric assays of GST activity (Fig. 2H). Interestingly, the $kp60_{1-90}$ (L73R) mutant exhibited greater solubility than intact $kp60_{1-90}$. The $kp60_{1-90}$ (L73R) and $kp60_{1-72}$ mutants were soluble, and were further analyzed by $^1H$–$^{15}N$ HSQC (Fig. 2F and G, respectively; expansions of these spectra are available in Fig. 4). More than 60 NH signals were detected, which were essentially identical among all three constructs. However, the intensities in $kp60_{1-72}$ were more uniform than those of $kp60_{1-90}$ and $kp60_{1-90}$ (L73R). As a result, $kp60_{1-72}$ was chosen for further NMR structural determination studies. By further optimization of the solvent conditions for $kp60_{1-72}$, 98% completeness of the HSQC signal data was achieved (Fig. 5). Using this data, we were able to identify the missing signals in the spectra of $kp60_{1-90}$. The signals originating from 73 to 90 and additional seven signals (Y22, E62, A63, Q65,

V66, K67 and I69) were absent, and six out of the seven missing signals were originating from the helical region adjacent to the residues 73–90. These residues are thought to be involved in the self-association interface, which is consistent with our initial assumption.
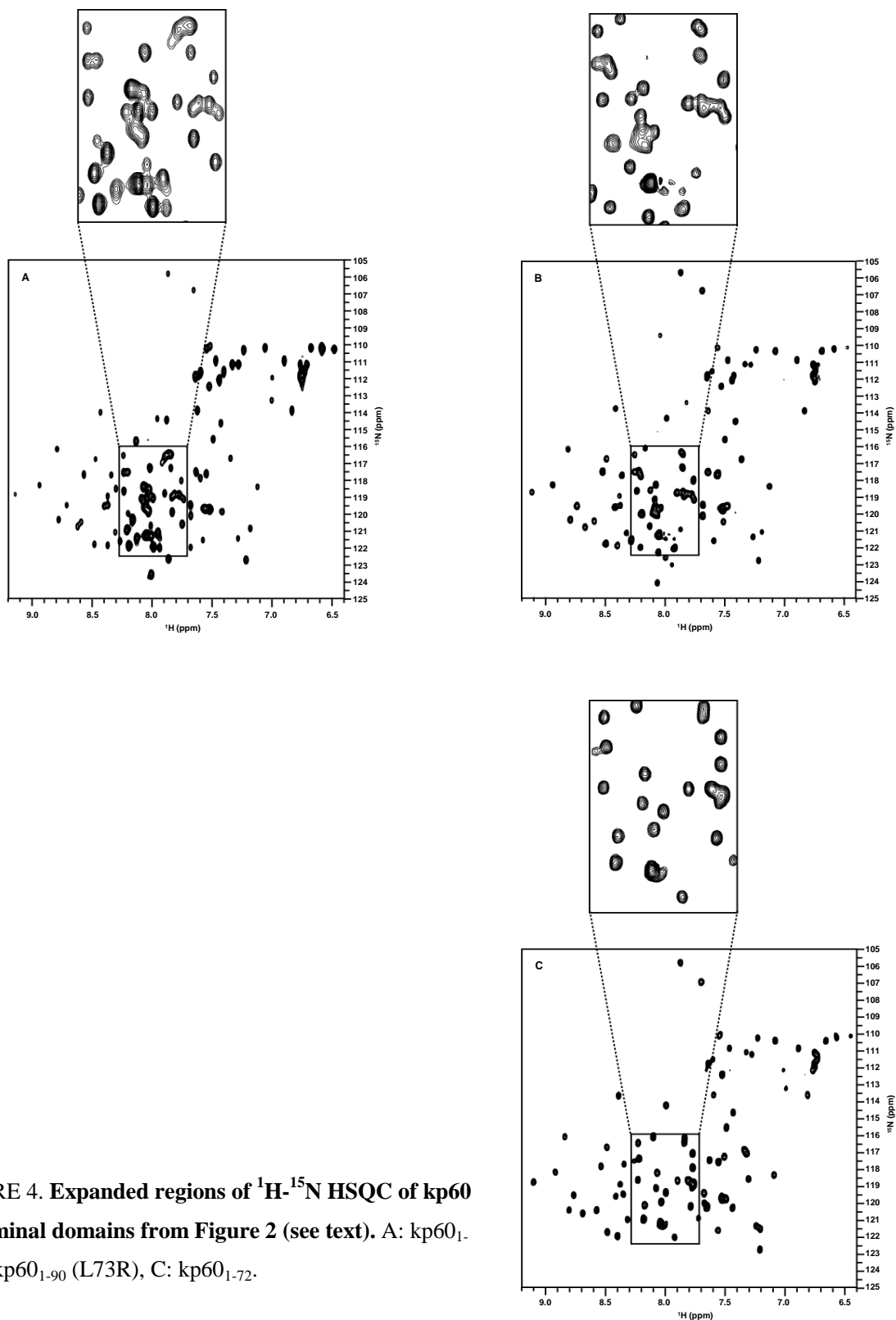


FIGURE 4. **Expanded regions of $^1$H-$^{15}$N HSQC of kp60 N-terminal domains from Figure 2 (see text).** A: kp60$_{1-90}$, B: kp60$_{1-90}$ (L73R), C: kp60$_{1-72}$.

FIGURE 5. **$^1$H-$^{15}$N HSQC of kp60$_{1-72}$ in the optimized buffer condition, containing 1 mM EDTA and 20 mM sodium phosphate buffer (pH 6.5).** 71 amide proton peaks out of 72 expected were observed and assigned, except the six signals from the additional amino acids derived from the expression vector. The sequential assignments were achieved by using a combination of the 3D spectra, HNCA, HNCOCA, CBCACONH and HNCACB. The signal pairs of Gln and Asn side chain amide protons were indicated by lines. The spectra were obtained by 500 MHz Bruker *Avance* NMR spectrometers equipped with a cryogenic probe at 25 °C.
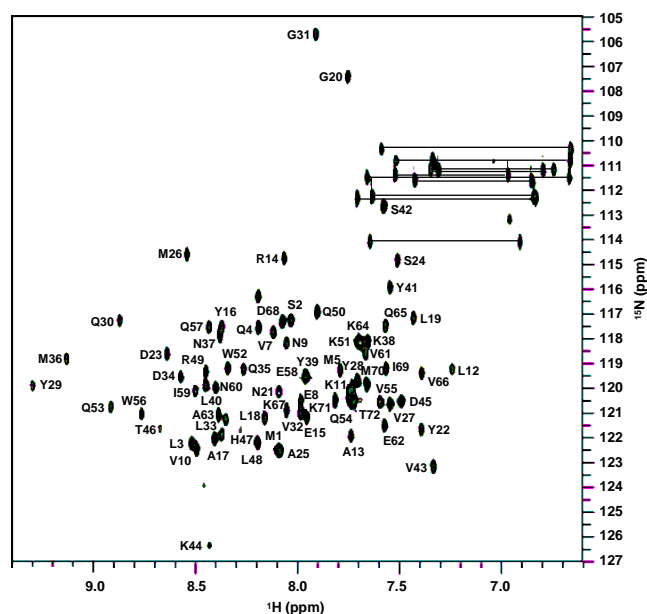


## The putative coiled coil region adopts a α-helix, but is not sensitive to 8-ANS

On the basis of the good signal dispersion of the HSQC spectra, it is likely that kp60$_{1-72}$ is the core folded domain. Thus, we assessed whether the truncated region, residues 73–90, adopts a α-helical conformation as predicted. The CD spectra of kp60$_{1-90}$ and kp60$_{1-90}$ (L73R) showed a substantial increase of α-helicity compared to that of kp60$_{1-72}$ (Fig. 6), suggesting the presence of a helix within the putative coiled coil region. The mutant kp60$_{1-90}$ (L73R) exhibited reduced self-association whilst retaining the helical structure in the residues 73–90. In contrast, the spectra of kp60$_{1-68}$ showed a drastic loss of helical content, suggesting that the deletion of only four terminal residues introduced disturbance of the proper folding of the core domain. Interestingly, the GST-fusion form of kp60$_{1-68}$ was less soluble, which may reflect decreased stability.
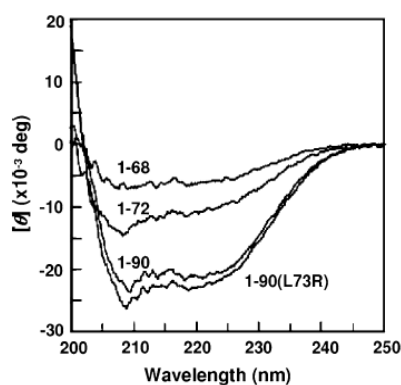
FIGURE 6. **Comparison of CD spectra of kp60 N-terminal domains.** N-terminal domain variants are shown in the panel. Each 10 μM of protein were dissolved in buffer containing 1 mM EDTA and 50 mM Tris–HCl (pH 7.5)

It is known that a protein in a molten-globule state often shows broadening or elimination of signals in $^1$H–$^{15}$N HSQC spectra, probably because of chemical exchange between conformationally heterogeneous sub-optimal species[30]. Since the signals originating from residues 73–90 were not fully observed, kp60$_{1-90}$ may fit this criterion. Proteins in a molten-globule state are known to be sensitive to 8-ANS and increase their fluorescence. Thus, we examined whether the observed weak self-association of kp60$_{1-90}$ through the putative coiled coil region is observable in the 8-ANS fluorescence enhancement assay (Fig. 7). We measured 8-ANS fluorescence of various concentrations (0–100 μM) in the presence of 4 μM kp60 N-terminal domains. The same experiment was performed with α-lactalbumin instead of kp60 N-terminal domains as a positive control for a molten globule protein. Nevertheless, as shown in Fig. 7, only a small fluorescence enhancement of kp60$_{1-90}$ as well as kp60$_{1-90}$ (L73R) was observed. This shows that the completeness and the signal dispersion of $^1$H–$^{15}$N HSQC spectra of the protein of interest is a better diagnostic fingerprint for the degree of transient self-association than hydrophobic fluorescent probes.
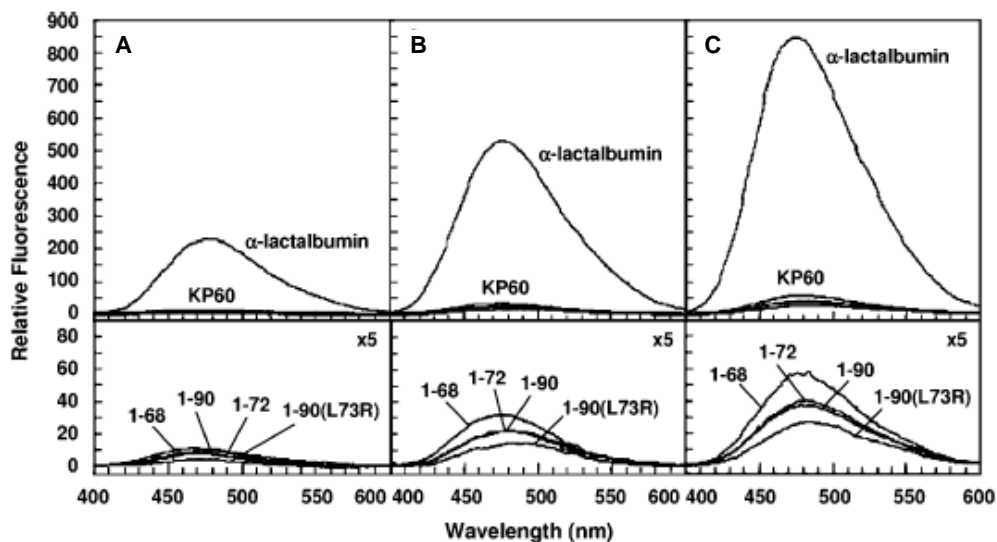
FIGURE 7. **Fluorescence enhancement experiments of 8-ANS bound to kp60 N-terminal domains and α-lactalbumin.** The difference spectra of fluorescence emission between ANS with and without the protein are shown. (A) 10 μM, (B) 20 μM, (C) 40 μM of ANS were added to 4 μM of protein in buffer containing 1 mM EDTA and 50 mM Tris–HCl (pH 7.5), except α-lactalbumin (pH 2.0). Lower panel is x 5 magnification of upper panel. kp60 N-terminal domain variants are shown in the spectra

### *The putative coiled coil region caused monomer–dimer equilibrium in solution*

Sedimentation velocity provides hydrodynamic information about the sample and establishes the size distribution of proteins due to their different rates of migration in the centrifugal field. We analyzed the sedimentation velocity of $kp60_{1-90}$, $kp60_{1-90}$ (L73R) and $kp60_{1-72}$ at three different protein concentrations (0.17, 0.29 and 0.4 mg/ml) in order to assess whether self-association was also concentration-dependent. We analyzed continuous distribution $c(s)$ versus sedimentation coefficient for each data set by using the program SEDFIT, because $c(s)$ distributions provide excellent sensitivity and resolution, enabling a clear distinction between different sedimenting species.

Figure 8 shows the distributions of sedimentation coefficients on kp60 N-terminal domains at the concentration of 0.4 mg/ml. First, we confirmed that $kp60_{1-72}$ was a monomer. The $c(s)$ distribution of $kp60_{1-72}$ shows the presence of a single species in the solution with a sedimentation

coefficient (*s*) of 1.2 (± 0.1) *S*. The *c*(*s*) distribution of kp60$_{1-72}$ did not show any significant change

upon varied protein concentration. The molecular mass of kp60$_{1-72}$ was determined to be 9.7 (± 0.1)

kDa by the sedimentation equilibrium experiments (Fig. 9), which agreed very well with the

theoretical value (9.35 kDa) based on the amino acid sequence.
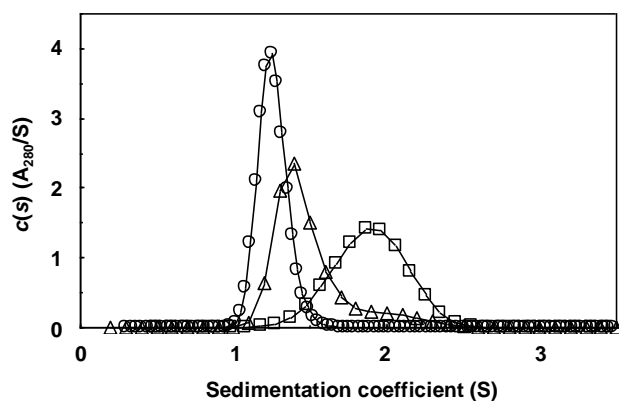


FIGURE 8. **Distribution of sedimentation coefficients [*c*(*s*)] for kp60 N-terminal domains.** Calculated *c*(*s*) is plotted versus sedimentation coefficient (*s*). Open box: kp60$_{1-90}$, open triangle: kp60$_{1-90}$ (L73R), open circle: kp60$_{1-72}$. Experiments were conducted at an initial protein concentration of 0.4 mg/ml in 1 mM EDTA, 100 mM NaCl and 20 mM sodium phosphate buffer (pH 7.5, 20°C) and a rotor speed of 50 x 10$^3$ rpm, and data was collected at time intervals of 10 min. The calculated values for the weight-average sedimentation coefficient (*s*) are *s* = 1.9 S, 1.4 S and 1.2 S for kp60$_{1-90}$, kp60$_{1-90}$ (L73R) and kp60$_{1-72}$, respectively

However, the *c*(*s*) distribution of kp60$_{1-90}$ and kp60$_{1-90}$ (L73R) showed that they were not

simple monomeric proteins. kp60$_{1-90}$ gave a single peak, but the shape was much broader and the

peak position much larger compared to that of kp60$_{1-72}$ (Fig. 8). At increased protein concentration

(0.17, 0.29 and 0.4 mg/ml), the weight average of the peak increased (1.7, 1.8 and 1.9 S, data not

shown). These results are consistent with a relatively rapid reversible equilibrium between the

monomer and oligomer species, which was previously assumed from NMR spectra. To further

examine the oligomerization status of kp60$_{1-90}$, we performed sedimentation equilibrium

experiments (Fig. 9). Sedimentation equilibrium is a good indication of a thermodynamic

equilibrium of the self-association systems and can be used to determine the dissociation

constants[31,32]. We applied several models for fitting. A simple monomeric model gave an estimated

molecular mass of 20.1($\pm$ 0.2) kDa, which was greater than the theoretical value of 11.4 kDa. In the

case of kp60$_{1-90}$ (L73R), $c(s)$ distribution profiles also showed protein concentration-dependent

peaks at positions between that of kp60$_{1-72}$ and kp60$_{1-90}$. The profile has a main peak relatively

close to the peak for kp60$_{1-72}$, with a larger S-value component as a shoulder (Fig. 8). Upon

increasing protein concentration the shoulder became larger. Thus, we conclude that kp60$_{1-90}$

(L73R) exists as a monomer–dimer (or oligomer) equilibrium, although the level of oligomerization

was much less than observed for kp60$_{1-90}$.
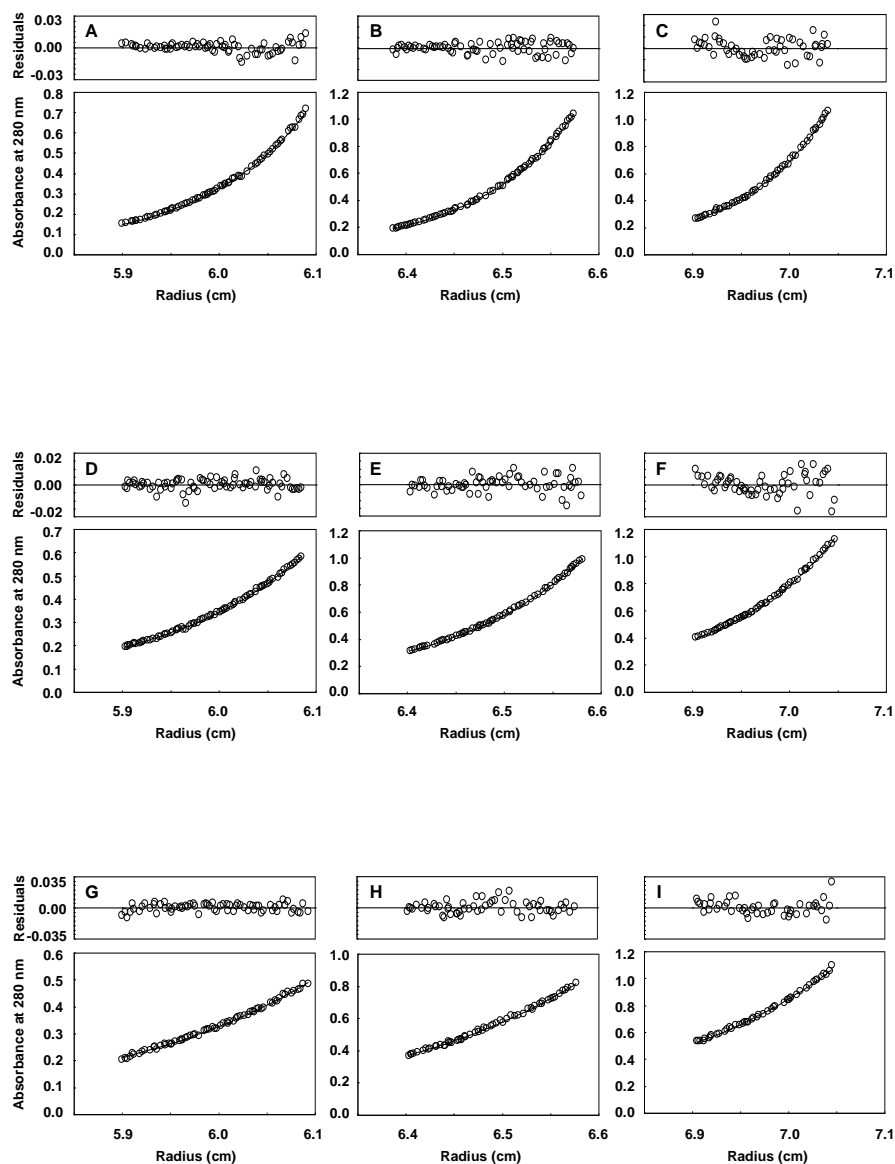


FIGURE 9. **Sedimentation equilibrium analysis for kp60 N-terminal domains.** Measurements were performed at three different protein concentrations (0.17, 0.29 and 0.4 mg/ml) in 1 mM EDTA, 100 mM NaCl and 20 mM sodium phosphate buffer (pH 7.5, 20°C) and a rotor speed of 25 x 103 rpm. (A-C): kp60$_{1-90}$. A: 0.17, B: 0.29, C: 0.4 mg/ml. (D-F): kp60$_{1-90}$ (L73R). D: 0.17, E: 0.29, F: 0.4 mg/ml. (G-I): kp60$_{1-72}$. G: 0.17, H: 0.29, I: 0.4 mg/ml. The data for kp60$_{1-90}$ and kp60$_{1-90}$ (L73R) were fit to a monomer-dimer equilibrium model and the data for kp60$_{1-72}$ was fit to a single ideal species model. The residuals for kp60$_{1-72}$ are random and centered around zero, indicating that kp60$_{1-72}$ sediments as a single homogeneous species.

*Application of the COILS method for fine-tuning of boundaries of mouse NVL2 N-terminal domain*

The successful determination of the domain boundary for kp60 encouraged us to apply the same approach to another case, NVL2. $^1$H–$^{15}$N HSQC spectra of mouse NVL2$_{1–93}$ are shown in Fig. 10E. As with kp60, only about 50 signals were obtained from an expected total of 94 amide signals for NVL2$_{1–93}$ (including four additional vector-derived signals). The sequence of NVL2$_{1–93}$ was analyzed by the program COILS (Fig. 10A). Improved constructs for the N-terminal domain of NVL2 were designed using a similar approach to that described for kp60. The sequences NVL2$_{1–82}$, NVL2$_{1–77}$ and NVL2$_{1–74}$ were analyzed by COILS (Fig. 10B–D). In this case we only focused on deletion of the predicted coiled coil region, and the three constructs were engineered for expression and purified. HSQC data for all these mutant proteins showed a dramatic improvement in terms of either the number of observed peaks or the line widths compared to that of NVL2$_{1–93}$ (Fig. 10E–H; expansions of these spectra are available in Fig. 11). Interestingly, several weaker and sharper signals for NVL2$_{1–82}$ and NVL2$_{1–77}$, within the range of $^1$H chemical shift of 7.6-8.4, were not observed in the spectra for NVL2$_{1–93}$ and NVL2$_{1–74}$. These signals were presumably from the C-terminal region, which exists as a random coil, rather than as a result of self-association. Therefore it would appear that removal of residues 83–93 is sufficient to hinder self-association.
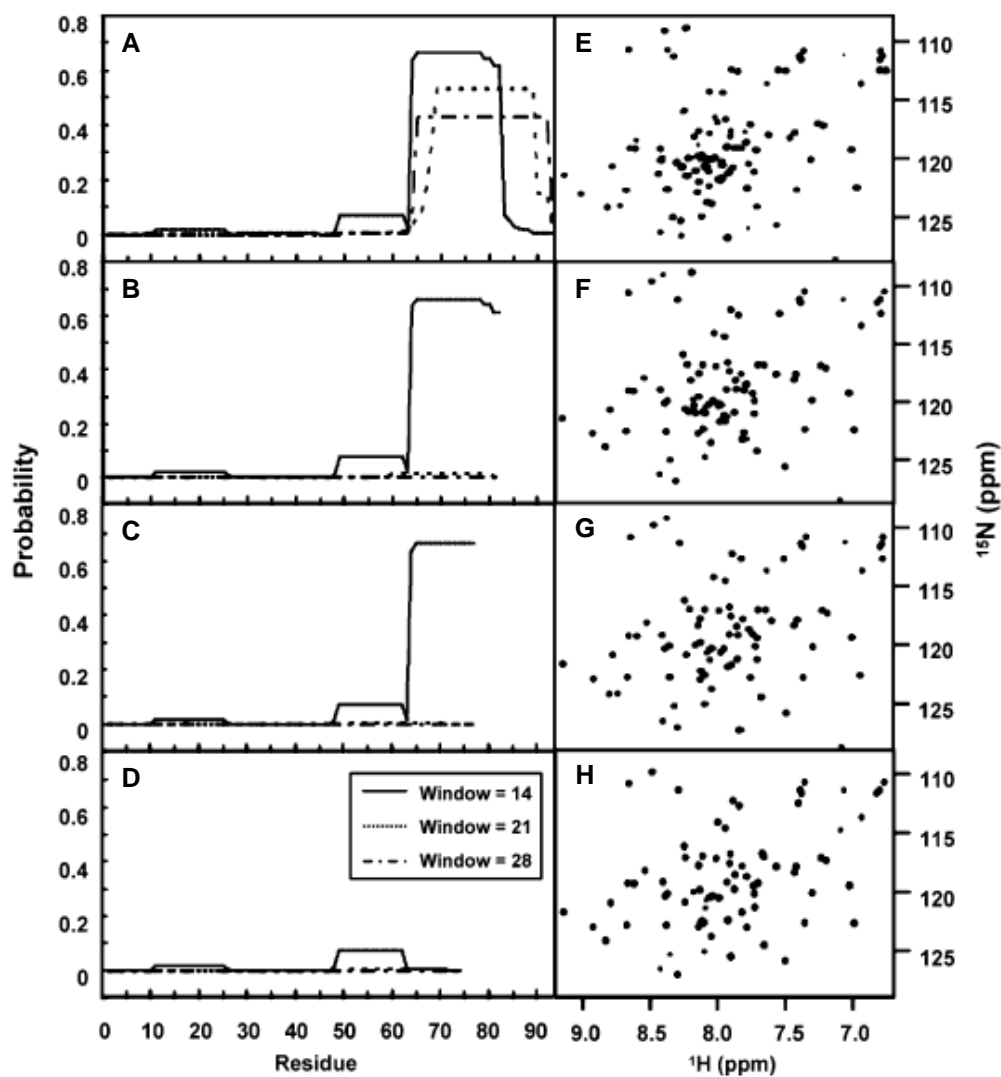
FIGURE 10. **Correlation of coiled coil propensity and $^{1}H$–$^{15}N$ HSQC spectral dispersion for the N-terminal regions of nuclear VCP-like protein 2.** (A–D) Coiled coil propensity calculated by the program COILS. A: $NVL2_{1-93}$, B: $NVL2_{1-82}$, C: $NVL2_{1-77}$, D: $NVL2_{1-74}$, solid, dotted and dashed lines indicate window sizes of 14, 21 and 28 residues, respectively. (E–H) $^{1}H$–$^{15}N$ HSQC spectra. E: $NVL2_{1-93}$, F: $NVL2_{1-82}$, G: $NVL2_{1-77}$, H: $NVL2_{1-74}$

38
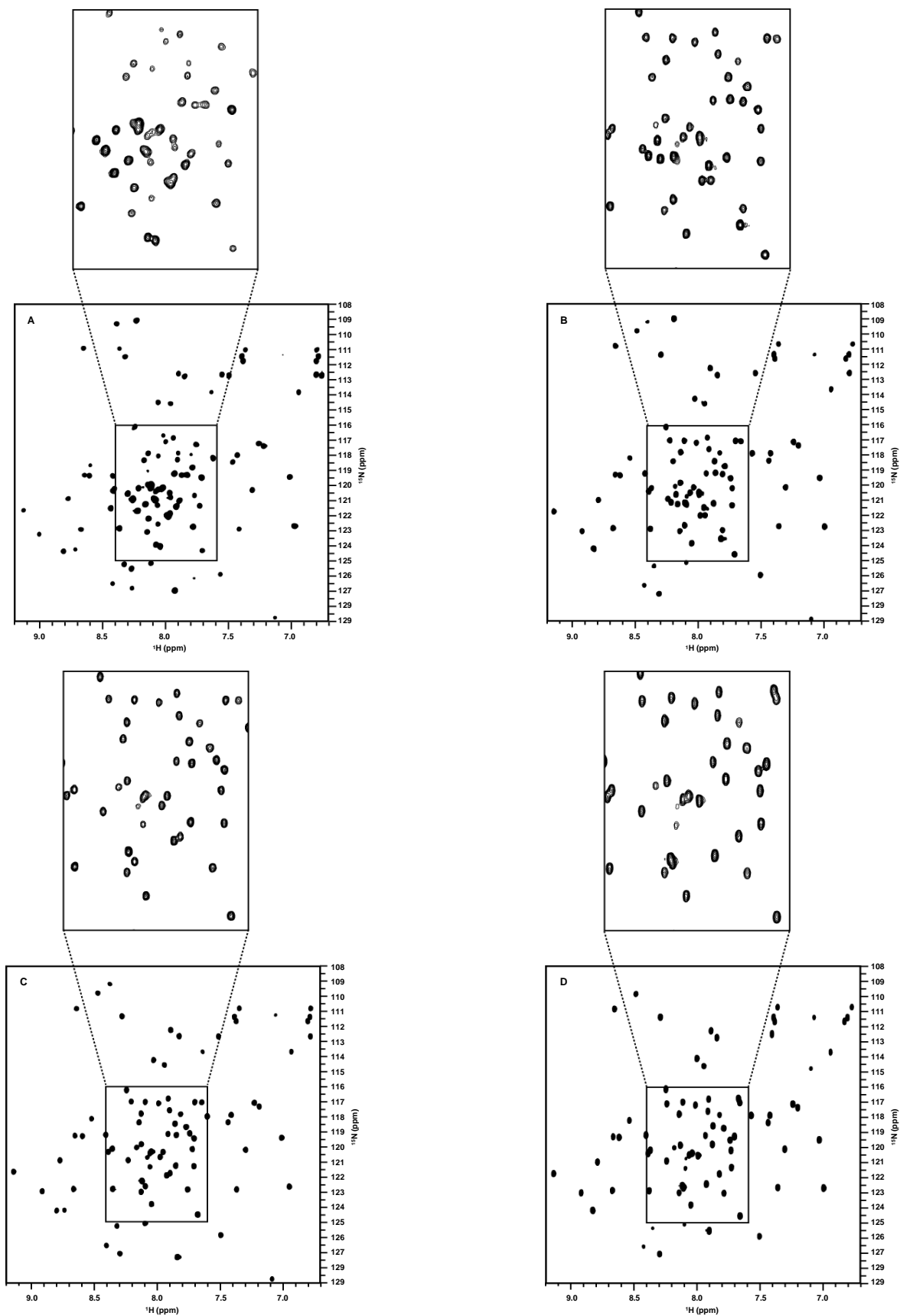
FIGURE 11. **Expanded regions of $^1$H-$^{15}$N HSQC of NVL2 N-terminal domains from Figure 10 (see text).** A: NVL2$_{1-93}$, B: NVL2$_{1-82}$, C: NVL2$_{1-77}$, D: NVL2$_{1-74}$.

## Discussion

We have shown two successful examples of rational fine-tuning of protein domain boundaries, kp60 and NVL2, excised from multidomain proteins, in which the initial HSQC assessment of the domains was poor. Our methodology circumvents the laborious practice of improving the protein characteristics, which usually involves engineering and screening large numbers of mutants in order to obtain a promising HSQC signal. This process is simplified by identifying residues likely to cause self-association prior to mutant design. We have employed a primitive bioinformatics approach to help eliminate the problem of self-association.

The putative N-terminal domains of kp60 and NVL2 gave $^1$H–$^{15}$N HSQC spectra typical of proteins displaying a tendency to self-associate. The disappearance of approximately 30 amide proton signals originating from interfacial residues upon oligomerization was attributed to exchange broadening at equilibrium. Interestingly, although the signals arising from the interfacial residues disappeared, there was no substantial line-broadening of other signals, suggesting that the coiled coil segments are connected to the core of the folded domain via a flexible segment. The proteins may have been in equilibrium between a monomer and oligomer with an uncertain association number. If a monomer–dimer self-association equilibrium model is applied, the dissociation constant of the equilibrium can be obtained from the analytical ultracentrifugation data. The molecular mass was constrained to the theoretical value and the dissociation constant was allowed to float during fitting. The fits were good (Fig. 9) and the dissociation constants were calculated to be $(10^{-5} \sim 10^{-6})$ M and $(10^{-3} \sim 10^{-4})$ M for kp60$_{1-90}$ and kp60$_{1-90}$ (L73R), respectively. This means that when the protein concentration is set to 0.1 mM as in an NMR sample, the monomer–dimmer ratio of the samples was approximately 1:2~7 and 1:0.1~0.5, respectively. Thus, the dimer species is dominant for kp60$_{1-90}$ in the NMR conditions, whereas the monomer is dominant for kp60$_{1-90}$ (L73R). In both cases, chemical exchange between monomer and dimer spoiled the HSQC spectra.

The result obtained from both NMR and analytical ultracentrifugation was consistent with the proposed monomer–dimer equilibrium.

Although analytical ultracentrifugation studies showed the molecular weight average of $kp60_{1-90}$ was close to that of a dimer, we do not rule out the potential formation of oligomers. Amino acid residues occurring in the (*a*–/*d*–) positions of the predicted coiled coil regions are different from the ideal amino acids for a homotypic coiled coil formation. Specifically, either (Leu/Leu) or (Ile/Leu) in the (*a*–/*d*–) positions respectively, form a dimeric coiled coil and the combination of (Ile/Ile) or (Leu/Ile) affords trimer or tetramer formation, respectively[29]. Since neither the sequences of kp60 and NVL2 met these criteria, the oligomerization through the putative coiled coil regions is probably promiscuous.

Comparison of the HSQC spectra of the putative coiled coil-containing domains with those of the pruned domains show that the peak positions of dispersed amide proton signals are essentially identical. This supported the conclusion that the putative coiled coil regions are only engaged in inter-molecular interactions rather than internal contacts. The putative coiled coil regions of $kp60_{1-90}$ (L73R) adopt a α-helical conformation (Fig. 6), with decreased selfassociation (Fig. 8). The truncated constructs appear to encode the minimal core structural domains, which are monomeric in nature and therefore useful for further structure determination.

Based on the two successful examples of this study, we propose a flow diagram for obtaining a protein domain suitable for structural NMR studies (Fig. 12). Firstly, the boundaries of putative globular domains are identified by several bioinformatics techniques. The highly conserved region among the orthologs is tentatively defined as a domain. In addition, sequences likely to fall outside the putative domain are predicted as either disordered regions (e.g., disopred2)[33]or ''linker''-like regions (e.g., DomCut)[34]. Alternatively, if the target protein exhibits high or substantial similarity to known protein domains, the initial domain boundary is defined according to the known example by using the PSI-BLAST[35], Pfam[36], SMART[37] or ProDom[38] servers. In addition,

fold recognition algorithms, such as FORTE[39] and FUGUE[40], are equally helpful because they are highly sensitive in finding distant homologs. Secondly, the sequence is subjected to the program COILS with the ''-mtidk'' option. In most cases, a putative coiled coil region is found at the N- or C-termini of the prototype domain. Protein sequences with either deletion or amino acid substitution at the coiled coil region are then virtually generated. The virtually generated sequences are analyzed by COILS, and coiled coil propensity is calculated. It is better to monitor all the scores from window sizes of 14, 21, and 28 residues, because the sensitivities may differ. Thirdly, the expression plasmids with the designed domain boundaries are constructed, by using high-throughput PRESAT-vector methodology[18]. A limited number of candidate target domains are cloned in parallel and incorporated into a bacterial expression vector, such as a GST-fusion vector. Amino acid substitution may also be introduced. Finally, only the most soluble proteins are subjected to $^{15}$N-labeling studies to obtain $^1$H–$^{15}$N HSQC spectra. In this study, we performed the initial HSQC assessment for both the prototypical domains of kp60 and NVL2 according to standard practice. However, we propose the COILS analysis could be performed prior to the assessment by HSQC spectra (Fig. 12).
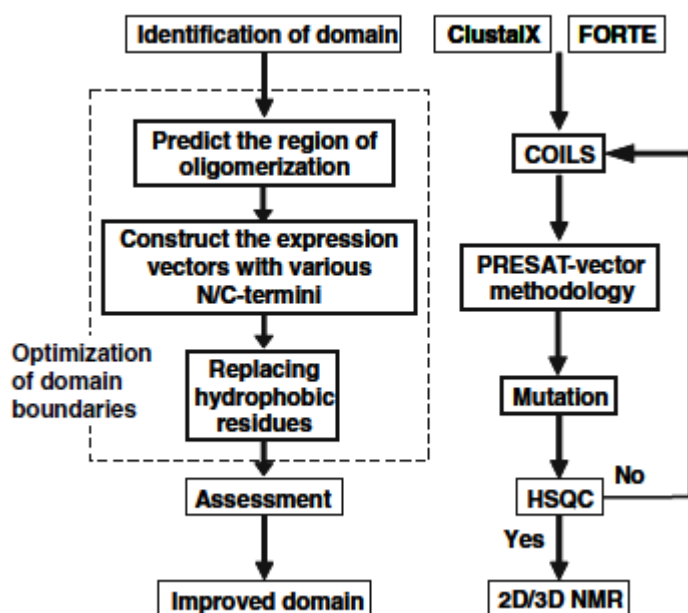


FIGURE 12. **Flow-chart for optimizing domain boundaries by minimizing coiled coil propensity.** The steps drawn by bold lines are skipped if an initial HSQC assessment is attempted first

Ideally, a protein sample for 3D-structure determination should be stable, highly soluble and should not undergo self-association. The development of high-throughput structural genomics requires the adoption of novel strategies to obtain suitable protein samples. Examples include parallel construction of different fusion proteins[41], cell-free expression systems using PCR-amplified DNA fragments[42], and parallel *E. coli* protein expression in a 96-well plate format[43]. These candidate proteins were isotopically-labeled and subjected to HSQC measurements. Finally, a ''go or no-go'' decision of the selected protein as a target for structure determination is made based on the quality of the HSQC spectra. Constructs giving the best quality HSQC spectral data are ranked for further analysis. Such a strategy is suited to maximize throughput for genome-wide structural studies[44]. In contrast, our strategy is a rational method that proposes to improve protein behavior in solution using ''negative design'' of potential coiled coils. Additionally, we have launched an automatic web-based server for this design method (available at http://www.mbs.cbrc.jp/coiled-coil/). Adoption of our strategy might avoid discarding biologically important protein samples with less promising HSQC spectra at an early stage. Furthermore, this design approach could be useful for preparing protein constructs for X-ray crystallography, because the putative coiled coil regions may prevent crystallization. In conclusion, it is useful to examine the existence of putative coiled coil regions associated with the target protein domain, when the initial HSQC spectrum is poor, or even before measuring the initial HSQC. Furthermore, our method is widely applicable because it does not require any preexisting knowledge of a ''not-yet-characterized'' domain.

# References

1. Wakeland, E. K. & Wandstrat, A. E. (2002) Analyzing genomes: current realities and future possibilities. *Curr. Opin. Immunol.* **14**, 622–626.

2. Burley, S. K. & Bonanno, J. B. (2003) Structural genomics. *Methods Biochem. Anal.* **44**, 591–612.

3. Yokoyama, S., Hirota, H., Kigawa, T., Yabuki, T., Shirouzu, M., Terada, T., Ito, Y., Matsuo, Y., Kuroda, Y., Nishimura, Y., Kyogoku, Y., Miki, K., Masui, R. & Kuramitsu, S. (2000) Structural genomics projects in Japan. *Nat. Struct. Biol.* **7**, Suppl. 943–945.

4. Phizicky, E., Bastiaens, P. I., Zhu, H., Snyder, M. & Fields, S. (2003) Protein analysis on a proteomic scale. *Nature* **422**, 208–215.

5. Vogel, C., Berzuini, C., Bashton, M., Gough, J. & Teichmann, S. A. (2004) Supra-domains: evolutionary units larger than single protein domains. *J. Mol. Biol.* **336**, 809–823.

6. Yu, Y. B. (2002) Coiled-coils: stability, specificity, and drug delivery potential. *Adv. Drug Deliv. Rev.* **54**, 1113–1129.

7. Burkhard, P., Stetefeld, J. & Strelkov, S. V. (2001) Coiled coils: a highly versatile protein folding motif. *Trends Cell Biol.* **11**, 82–88.

8. Apic, G., Gough, J. & Teichmann, S. A. (2001) Domain combinations in archaeal, eubacterial and eukaryotic proteomes. *J. Mol. Biol.* **310**, 311–325.

9. Cohen, C. & Parry, D. A. (1990) Alpha-helical coiled coils and bundles: how to design an alpha-helical protein. *Proteins* **7**, 1–15.

10. Sanishvili, R., Pennycooke, M., Gu, J., Xu, X., Joachimiak, A., Edwards, A. M. & Christendat, D. (2004) Crystal structure of the hypothetical protein TA1238 from Thermoplasma acidophilum: a new type of helical super-bundle. *J. Struct. Funct. Genom* **5**, 231–240.

11. Lumb, K. J. & Kim, P. S. (1995) A buried polar interaction imparts structural uniqueness in a designed heterodimeric coiled coil. *Biochemistry* **34**, 8642–8648.

12. Oakley, M. G. & Kim, P. S. (1998) A buried polar interaction can direct the relative orientation of helices in a coiled coil. *Biochemistry* **37**, 12603–12610.

13. Kiyokawa, T., Kanaori, K., Tajima, K. & Tanaka, T. (2000) Engineering of the hydrophobic core of an alpha-helical coiled coil. *Biopolymers* **55**, 407–414.

14. Schnarr, N. A. & Kennan, A. J. (2003) Specific control of peptide assembly with combined hydrophilic and hydrophobic interfaces. *J. Am. Chem. Soc.* **125**, 667–671.

15. Kashiwada, A., Hiroaki, H., Kohda, D., Nango, M. & Tanaka, T. (2000) Design of a Heterotrimeric α-Helical Bundle by Hydrophobic Core Engineering. *J. Am. Chem. Soc.* **122**, 212–215,

16. Sandberg, W.S. & Terwilliger, T. C. (1989) Influence of interior packing and hydrophobicity on the stability of a protein. *Science* **245**, 54–57.

17. Lupas, A., Van Dyke, M. & Stock, J. (1991) Predicting coiled coils from protein sequences. *Science* **252**, 1162–1164.

18. Goda, N., Tenno, T., Takasu, H., Hiroaki, H. & Shirakawa, M. (2004) The PRESAT-vector: asymmetric T-vector for high-throughput screening of soluble protein domains for structural proteomics. *Protein Sci.* **13**, 652–658.

19. Delaglio, F., Grzesiek, S., Vuister, G. W., Zhu, G., Pfeifer, J. & Bax, A. (1995) NMRPipe: a multidimensional spectral processing system based on UNIX pipes. *J. Biomol. NMR* **6**, 277–293.

20. Laue, T. M., Shah, B. D., Ridgeway, T. M. & Pelletier, S. L. (1992) Computer-aided interpretation of analytical sedimentation data for proteins. In *Analytical Ultracentrifugation in Biochemistry and Polymer Science*. (eds. Harding, S. E., Rowe, A. J. & Horton J. C.), pp. 90-125. TheRoyal Society of Chemistry, Cambridge.

21. Schuck, P., Perugini, M. A., Gonzales, N. R., Howlett, G. J. & Schubert, D. (2002) Size-distribution analysis of proteins by analytical ultracentrifugation: strategies and application to model systems. *Biophys J.* **82**, 1096–1111.

22. Beyer, A. (1997) Sequence analysis of the AAA protein family. *Protein Sci.* **6**, 2043–2058.

23. Lupas, A. N. & Martin, J. (2002) AAA proteins. *Curr. Opin. Struct. Biol.* **12**, 746–753.

24. Shiozawa, K., Maita, N., Tomii, K., Seto, A., Goda, N., Akiyama, Y., Shimizu, T., Shirakawa, M. & Hiroaki, H. (2004) Structure of the N-terminal domain of PEX1 AAA-ATPase. Characterization of a putative adaptor-binding domain. *J. Biol. Chem.* **279**, 50060–50068.

25. Ciccarelli, F. D., Proukakis, C., Patel, H., Cross, H., Azam, S., Patton, M. A., Bork, P. & Crosby, A. H. (2003) The identification of a conserved domain in both spartin and spastin, mutated in hereditary spastic paraplegia. *Genomics* **81**, 437–441.

26. Scott, A., Gaspar, J., Stuchell-Brereton, M. D., Alam, S. L., Skalicky, J. J. & Sundquist, W. I. (2005) Structure and ESCRT-III protein interactions of the MIT domain of human VPS4A. *Proc. Natl. Acad. Sci. USA* **102**, 13813–13818.

27. Takasu, H., Jee, J. G., Ohno, A., Goda, N., Fujiwara, K., Tochio, H., Shirakawa, M. & Hiroaki, H. (2005) Structural characterization of the MIT domain from human Vps4b. *Biochem. Biophys. Res. Commun.* **334**, 460–465.

28. Kremer, W. & Kalbitzer, H. R. (2001) Physiological conditions and practicality for protein nuclear magnetic resonance spectroscopy: experimental methodologies and theoretical background. *Methods Enzymol.* **339**, 3–19.

29. Harbury, P. B., Zhang, T., Kim, P. S. & Alber, T. (1993) A switch between two-, three-, and four-stranded coiled coils in GCN4 leucine zipper mutants. *Science* **262**, 1401–1407.

30. Schulman, B. A., Kim, P. S., Dobson, C. M. & Redfield, C. (1997) A residue-specific NMR view of the non-cooperative unfolding of a molten globule. *Nat. Struct. Biol.* **4**, 630–634.

31. Lebowitz, J., Lewis, M. S. & Schuck, P. (2002) Modern analytical ultracentrifugation in protein science: a tutorial review. *Protein Sci.* **11**, 2067–2079.

32. Laue, T. M. & Stafford, W. F. (1999) Modern applications of analytical ultracentrifugation. *Annu. Rev. Biophys. Biomol. Struct.* **28**, 75–100.

33. Ward, J. J., McGuffin, L. J., Bryson, K., Buxton, B. F. & Jones, D. T. (2004) The DISOPRED server for the prediction of protein disorder. *Bioinformatics* **20**, 2138–2139.

34. Suyama, M. & Ohara, O. (2003) DomCut: prediction of inter-domain linker regions in amino acid sequences. *Bioinformatics* **19**, 673–674.

35. Altschul, S. F., Madden, T. L., Schaffer, A. A., Zhang, J., Zhang, Z., Miller, W. & Lipman, D. J. (1997) Gapped BLAST and PSI-BLAST: a new generation of protein database search programs. *Nucleic Acids Res.* **25**, 3389–3402.

36. Bateman, A., Birney, E., Cerruti, L., Durbin, R., Etwiller, L., Eddy, S. R., Griffiths-Jones, S., Howe, K. L., Marshall, M. & Sonnhammer, E. L. (2002) The Pfam protein families database. *Nucleic Acids Res.* **30**, 276–280.

37. Schultz, J., Milpetz, F., Bork, P. & Ponting, C. P. (1998) SMART, a simple modular architecture research tool: identification of signaling domains. *Proc. Natl. Acad. Sci. USA* **95**, 5857–5864.

38. Bru, C., Courcelle, E., Carrere, S., Beausse, Y., Dalmar, S. & Kahn, D. (2005) The ProDom database of protein domain families: more emphasis on 3D. *Nucleic Acids Res* **33**, Database Issue: D212–D215.

39. Tomii, K. & Akiyama, Y. (2004) FORTE: a profile-profile comparison tool for protein fold recognition. *Bioinformatics* **20**, 594–595.

40. Shi, J., Blundell, T. L. & Mizuguchi, K. (2001) FUGUE: sequence-structure homology recognition using environment-specific substitution tables and structure-dependent gap penalties. *J. Mol. Biol.* **310**, 243–257.

41. Hammarstrom, M., Hellgren, N., van Den Berg, S., Berglund, H. & Hard, T. (2002) Rapid screening for improved solubility of small human proteins produced as fusion proteins in Escherichia coli. *Protein Sci.* **11**, 313–321.

42. Sawasaki, T., Ogasawara, T., Morishita, R. & Endo, Y. (2002) A cell-free protein synthesis system for high-throughput proteomics. *Proc. Natl. Acad. Sci. USA* **99**, 14652–14657.

43. Shih, Y. P., Kung, W. M., Chen, J. C., Yeh, C. H., Wang, A. H. & Wang, T. F. (2002) High-throughput screening of soluble recombinant proteins. *Protein Sci.* **11**, 1714–1719.

44. Christendat, D., Yee, A., Dharamsi, A., Kluger, Y., Gerstein, M., Arrowsmith, C. H. & Edwards, A. M. (2000) Structural proteomics: prospects for high throughput sample preparation. *Prog. Biophys. Mol. Biol.* **73**, 339–345.

# CHAPTER 2


# A Common Substrate Recognition Mode Conserved between Katanin p60 and VPS4 Governs Microtubule Severing and Membrane Skeleton Reorganization

## Abstract

Katanin p60 (kp60), a microtubule severing enzyme, plays a key role in cytoskeletal reorganization during various cellular events in an ATP-dependent manner. We show that a single domain isolated from the N-terminus of mouse katanin p60 (kp60-NTD) binds to tubulin. The solution structure of kp60-NTD was determined by NMR. Although their sequence similarities were as low as 20%, the structure of kp60-NTD revealed a striking similarity to those of the microtubule interacting and trafficking (MIT) domains, which adopt anti-parallel three-stranded helix bundle. In particular, the arrangement of helices 2 and 3 is well conserved between kp60-NTD and the MIT domain from Vps4, which is a homologous protein that promotes disassembly of the endosomal sorting complexes required for transport (ESCRT)-III membrane skeleton complex. Mutation studies revealed that the positively charged surface formed by helices 2 and 3 binds tubulin. This binding mode resembles the interaction between the MIT domain of Vps4 and Vps2/CHMP1a, a component of ESCRT-III. Our results show that both the molecular architecture and the binding modes are conserved between two AAA-ATPases: kp60 and Vps4. A common mechanism is evolutionarily conserved between two distinct cellular events, one which drives microtubule severing and the other involving membrane skeletal reorganization.

## Introduction

Microtubules (MTs) are polymers of $\alpha$ and $\beta$ tubulin heterodimers. MTs exist as networks that dynamically and rapidly reorganize during different phases of the cell cycle. Spontaneous growth as well as shortening at the ends is indispensable for functional rearrangement. For example, they form the mitotic spindle during M phase, which mediates chromosome segregation during cell division based on the nature of dynamic rearrangement of MTs[1,2]. Many cellular events involving MTs are driven not only by tubulin's autonomous polymerization and dissociation, but also by MT-severing enzymes. These enzymes disassemble the MTs to promote large changes in the cytoskeleton in an ATP-dependent manner[3].

There are three known MT-severing enzymes, katanin, spastin, and fidgetin, all of which belong to type I AAA-ATPases[4-7]. Katanin was first identified from sea urchin cytosol[8], and consists of 2 subunits: a 60 KDa catalytic subunit (kp60) containing a single AAA domain and an 80 KDa regulatory subunit (kp80)[9,10]. Both the subunits are genetically conserved among many higher eukaryotes. Katanin localizes at the centrosomes in an MT-dependent manner[11], which is probably required for recycling and for the poleward flux of tubulin in the spindle by disassembling MTs at their minus ends[12,13]. Kp60 homologs are also found in plants, insects, and nematodes, but not in yeasts.

Kp60 has a common domain organization typical of a type I AAA-ATPase, which consists of an N-terminal substrate binding region followed by a single AAA domain at the C-terminus. In general, AAA-ATPases are believed to act as protein unfoldases that promote various cellular events, including dissociation of protein complexes, MT severing, protein degradation, protein translocation across organelle membranes, vesicle fusions, and multivesicular body formation[14,15].

Hartman and Vale[13] demonstrated that the N-terminal half of kp60 contains an MT binding region, although the presence of a structural MT binding domain was not proved. The importance of

the N-terminal MT binding region of a plant kp60 ortholog has been recently reported[16]. In our previous study, we successfully isolated a folded structural domain from the kp60 N-terminal region (termed kp60-NTD)[17]. Although standard bioinformatics tools (*e.g.* PSI-BLAST[18], Pfam[19,20], and SMART[21] failed to detect any similarity between kp60-NTD and other known domains, more sensitive bioinformatics techniques (*e.g.* FORTE[22] and FUGUE[23] can detect substantial similarities between kp60-NTD and MIT domains. MIT domains are small helical domains involved in protein-protein interactions that are conserved among Vps4, spartin, spastin, and some other proteins[24].

In this study, we present the solution structure of kp60-NTD. We show that this structure is closely related to that of the MIT domain. In this context, the overall molecular architecture of kp60 resembles other MIT domain-containing type I AAA-ATPases, such as the MT-severing enzyme spastin and the ESCRT-III disassembling enzyme Vps4 (Fig. 1A). Because the isolated kp60-NTD solely binds tubulin *in vitro*, the domain is a novel tubulin binding domain. Finally, the key residues of kp60-NTD for binding tubulin were determined. A model for MT binding is further discussed, which allows us to propose a model for the mechanism of MT severing by katanin.

## Experimental procedures

### *Protein Techniques*

Expression vectors for the recombinant GST-tagged form of kp60-NTDs of human and mouse were constructed using PRESAT vector methodology[17,25]. The fusion proteins were expressed in *Escherichia coli* BL21 (DE3), followed by affinity purification on glutathione-Sepharose (GE Healthcare), and were dialyzed. These fusion proteins were used for tubulin binding assays. For NMR spectroscopy, 2 liters of culture was incubated with [$^{15}$N]ammonium chloride and [$^{13}$C]glucose as the sole nitrogen and carbon sources, respectively, following a standard fermentation protocol at 25 °C. Divalent cation was present as a trace mineral during fermentation. Purification of $^{15}$N- and $^{13}$C-/$^{15}$N-labeled kp60-NTDs was achieved by glutathione-Sepharose affinity chromatography followed by thrombin digestion, benzamidine-Sepharose chromatography, cation exchange chromatography using a SP-Sepharose column, and gel filtration using Superdex 75 column (GE Healthcare).

### *NMR Spectroscopy*

Samples for NMR spectroscopy contained either $^{15}$N- or $^{13}$C-/$^{15}$N-labeled kp60-NTD at concentrations of 0.5–0.9 mM in 5% $D_2O$, 95% $H_2O$, 20 mM sodium phosphate, and 1 mM EDTA with 50 mM NaCl/without NaCl (pH 6.5). Backbone and side chain assignments were obtained from $^{15}$N-heteronuclear single quantum coherence spectroscopy, $^{13}$C-heteronuclear single quantum coherence spectroscopy, HNCA, HNCO, HNCACB, CBCACONH, HCC(CO)NH, CC(CO)NH, and HCCH-total correlation spectroscopy spectra recorded at 25 °C, using Bruker Avance spectrometers (500 and 800 MHz, Avance; Bruker Biospin, Germany) equipped with cryomagnetic probes[26,27]. Data were processed using NMRPipe[28] and SPARKY[29] software. Interproton distances were obtained from three-dimensional $^{13}$C- and $^{15}$N-edited nuclear Overhauser effect spectroscopy

spectra recorded with a 100-ms mixing time. Structures were calculated using a standard seven iteration cycle protocol of the program CYANA version 2.0.17[30,31]. All nuclear Overhauser effect cross-peaks were selected manually using SPARKY. In total, 1723 meaningful nuclear Overhauser effect upper distance restraints were obtained, including 304 long range distances. Dihedral angle restraints were calculated on the basis of backbone atom chemical shifts[32] using the TALOS program. The 20 structures with the lowest restraint energies were selected and analyzed using MOLMOL[33] and PROCHECK-NMR software (Table 1)[34]. No distance restraint was violated by more than 0.3 Å and no torsional restraint by more than 5.0°. All the figures were prepared using MOLMOL and PyMOL. The atomic coordinates of the 20 best kp60-NTD NMR structures have been deposited in the Protein Data Bank under accession code 2rpa. Chemical shift assignments have been deposited in the BioMagResBank under accession code 11075.

TABLE 1. **Experimental restraints and statistics for 20 structures of kp60-NTD.**

| | |
|---|---|
| **Distance restraints** | |
| Total no. of restraints | 1723 |
| Intraresidue | Unused |
| Sequential restraints ($|i - j| = 1$) | 831 |
| Medium range restraints ($1 < |i - j| \leq 4$) | 462 |
| Long range restraints ($|i - j| > 4$) | 304 |
| Dihedral angle restraints | 126 |
| $\phi/\psi/\chi$ | 63/63/0 |
| Hydrogen bond restraints | 0 |
| **Statistics used for and obtained from the structure calculations** | |
| Final Statistics (20/100) | |
| Cutoffs, distance (0.3 Å) and angle (3.0°) | |
| Maximum target function | 0.06 |
| Maximum violations | |
| Distance violation | 0.21 Å |
| Angle violation | 9.15° |
| Coordinate precision (residues 4–68) | |
| Backbone r.m.s.d. | 0.33 Å |
| Heavy atom r.m.s.d. | 0.83 Å |
| Ramachandran plot statistics (%) (all residues) | |
| Residues in most favored regions | 92.2 |
| Residues in additionally allowed regions | 7.1 |
| Residues in generously allowed regions | 0.1 |
| Residues in disallowed regions | 0.0 |

*Mutation Studies and Tubulin Binding Assays*

Ala-substituted mutants were prepared by PCR amplification of the entire expression plasmid for kp60-NTD (residues 1–72) according to a standard PCR mutagenesis method using QuikChange sitedirected mutagenesis kit (Stratagene). Two complementary oligonucleotides with mutated sequences for each mutant were used as primers (Table 2). The resulting kp60-NTD genes were sequenced to confirm the mutations. All proteins were purified with glutathione-Sepharose (GE Healthcare) and dialyzed against a buffer containing 50 mM Tris-HCl and 150 mM NaCl (pH 7.5). For pulldown assay, 80 pmol of GST (negative control) or GST fusion proteins were mixed with 10 μl of glutathione-Sepharose 4B (GE Healthcare) in 100 μl of binding buffer containing 80 mM PIPES-KOH (pH 6.8), 0.5 mM EGTA, and 2 mM $MgCl_2$ for 1 h at 4 °C. After washing the beads, 182 pmol (10 μg) of porcine tubulin (Cytoskeleton) was mixed in 200 μl of binding buffer for 2 h at 4 °C. The beads were washed three times, and the associated proteins were eluted with 50 mM Tris-HCl and 10 mM reduced glutathione (pH 7.5). The eluted proteins were resolved by SDS-PAGE and stained with silver.

TABLE 2. **Oligonucleotides used as primers for Ala substitution.**

| Primer | Sequence |
|--------|----------|
| Q35A_F | CAGGGAGTTCTTGAC**GCC**ATGAACAAGTACCTGTACTCAGTC |
| Q35A_R | GACTGAGTACAGGTACTTGTTCAT**GGC**GTCAAGAACTCCCTG |
| N37A_F | CAGGGAGTTCTTGACCAAATG**GCC**AAGTACCTGTACTCAGTC |
| N37A_R | GACTGAGTACAGGTACTT**GGC**CATTTGGTCAAGAACTCCCTG |
| D45A_F | CTGTACTCAGTCAAA**GCC**ACACACCTCCGTCAGAAATGG |
| D45A_R | CCATTTCTGACGGAGGTGTGT**GGC**TTTGACTGAGTACAG |
| R49A_F | GTCAAAGATACACACCTC**GCC**CAGAAATGGCAACAG |
| R49A_R | CTGTTGCCATTTCTG**GGC**GAGGTGTGTATCTTTGAC |
| Q53A_F | CTCCGTCAGAAATGG**GCC**CAGGTTTGGCAGGAAATAAATGTG |
| Q53A_R | CACATTTATTTCCTGCCAAACCTG**GGC**CCATTTCTGACGGAG |
| V55A_F | CTCCGTCAGAAATGGCAACAG**GCC**TGGCAGGAAATAAATGTG |
| V55A_R | CACATTTATTTCCTGCCA**GGC**CTGTTGCCATTTCTGACGGAG |
| E58A_F | CAGAAATGGCAACAGGTTTGGCAG**GCC**ATAAATGTGGAAGCTAAG |
| E58A_R | CTTAGCTTCCACATTTAT**GGC**CTGCCAAACCTGTTGCCATTTCTG |
| K64A_F | GTTTGGCAGGAAATAAATGTGGAAGCT**GCC**CAAGTTAAGGATATCATG |
| K64A_R | CATGATATCCTTAACTTG**GGC**AGCTTCCACATTTATTTCCTGCCAAAC |
| K67A_F | GTGGAAGCTAAGCAAGTT**GCC**GATATCATGAAAACATAATAGAGC |
| K67A_R | GCTCTATTATGTTTTCATGATATC**GGC**AACTTGCTTAGCTTCCAC |
| D68A_F | GTGGAAGCTAAGCAAGTTAAG**GCC**ATCATGAAAACATAATAGAGC |
| D68A_R | GCTCTATTATGTTTTCATGAT**GGC**CTTAACTTGCTTAGCTTCCAC |

## *Model Building*

A molecular model of the complex of kp60-NTD with a tubulin tetramer was constructed manually using MOLMOL[33] on the basis of the complex between Vps4a-MIT and CHMP1a (PDB code 2jq9). First, the kp60-NTD structure determined in this study was superimposed onto the corresponding position of Vps4a-MIT. Then the tubulin tetramer, taken from PDB code 3du7, was superimposed onto the C-terminal helix of CHMP1a with the best one position selected out of the eight candidate positions of tubulin.

## *Production of Full-length kp60*

Expression vector for the recombinant GST-tagged full-length kp60 of mouse was constructed by standard protocol using PCR, and ligated into *BamHI-SalI* sites of pGEX-6P3 (GE Healthcare Bioscience). Ala-substituted mutants were engineered with QuikChange site-directed mutagenesis kit (Stratagene). The fusion proteins were produced in *E. coli* JM109. Expression was induced with 0.1 mM IPTG, and LB cultures were grown overnight at 20 °C. For pull-down assays, GST-tagged proteins were bound to glutathione-Sepharose 4B (GE Healthcare Bioscience) and washed with the storage buffer (20 mM Tris-HCl, pH 7.5, 150 mM NaCl, 1 mM $MgCl_2$, and 0.1 mM ATP) supplemented with EDTA-free protease inhibitor cocktail (Nacali tesque Inc, Kyoto, Japan) on column. GST-kp60s bound to glutathione-Sepharose were eluted with the elution buffer (50 mM Tris-HCl, 100 mM NaCl, 40 mM reduced glutathione, pH 8.0, and 5% glycerol). The eluents were further used for ATPase assays.

## *ATPase assays*

ATPase activity was measured using an ATP regenerating system. The reaction mixture containing 50 mM Tris-HCl, pH 7.5, 50 mM KCl, 2 mM MgCl2, 2 mM phosphoenolpyruvate, 1 mM ATP, 50 µg/ml pyruvate kinase, 50 µg/ml lactate dehydrogenase, and 0.2 mM NADH was used.

The reactions were initiated by the addition of GST-kp60s (0.5 μM), and the activities were measured by monitoring the decrease of NADH absorption at 340 nm at room temperature using UV-Vis spectrophotometer, UV mini-1240 (Shimadzu, Tokyo, Japan). The data were normalized for further analysis.

### *Tubulin Binding Assays of full-length kp60*

5 μg of GST-proteins bound to glutathione-Sepharose 4B (20 μl) were incubated with 10 μg of tubulin in the binding buffer (80 mM PIPES, pH 7.0, 1 mM MgCl$_2$ and 1 mM EGTA) for 30 min at 4°C. The beads were washed four times in the wash buffer (4.3 mM Na$_2$HPO$_4$, 1.47 mM KH$_2$PO$_4$, 137 mM NaCl, 2.7 mM KCl, pH 7.3, and 5% glycerol). The associated proteins were eluted in the elution buffer (50 mM Tris-HCl, 100 mM NaCl, 50 mM reduced glutathione, pH 8.0, and 5% glycerol). The eluted proteins were analyzed by SDS-PAGE and Western blotting.

### *Western Blotting*

Proteins were resolved in SDS-PAGE and blotted onto a PVDF membrane. We detected tubulin using 1/2000 diluted anti-α-tubulin antibody (Siguma-Aldrich) followed by HRP-conjugated anti-mouse IgG secondary antibody (Promega). The proteins were visualized using an ECL-Plus kit (GE Healthcare Bioscience) and detected using LAS-1000 detector (Fuji Film, Tokyo, Japan).

### *Model building of full-length kp60*

A molecular model of the complex of kp60-NTD with a tubulin tetramer was constructed based on the complex between spastin-MIT and CHMP1b (PDB: 3eab). The kp60-NTD structure and the tubulin tetramer (3du7) were superimposed onto the corresponding position of spastin-MIT and the C-terminal helix of CHMP1b (174-193), respectively. The best model fully overrided on

helices with binding sites was selected considering steric crash and complementary charge interactions between structures. A hexameric ring model of AAA ATPase domains of kp60 was generated by superimposing the C$\alpha$ atoms of kp60 onto those of the hexameric ring structure of p97 D1 (PDB: 1s3s) using MODELLER (version 9v6) (http://salilab.org/modeller/). Finally, the complex model structure of hexameric full-length kp60 with tubulin oligomer was constructed using MOLMOL[33] by joining the components manually.

## Results


### *Structural Prediction and Sequence Analysis of kp60-NTD*

Prior to structural determination, we extensively analyzed residues 1–90 of the N-terminal sequences of mouse and human kp60, which represent the sequences preceding the AAA domains, by both bioinformatics and biophysical methods[17]. In brief, we found that these regions are genetically conserved only within a single subfamily of type I AAA-ATPase, corresponding to kp60 orthologs (Fig. 1B). Members of this family are found in mammals, other vertebrates, plants, insects, urchins, and nematodes, but not in yeasts or bacteria. It should be noted that some archaeal kp60s (*e.g.* gi: 13814089 and 223478990) that lack this N-terminal region are less well related to other kp60s, although a strong relationship is found for Vps4 orthologs. Thus, these archaeal kp60s may be better annotated as Vps4 homologs[35].

Focusing upon the AAA-ATPase domain and analyzing the domain level phylogenetic tree, the type I AAA-ATPases, including kp60, spastin, and Vps4, form a single cluster[7,36]. The kp60 orthologs with a conserved N-terminal region form a small subfamily, which is different from the Vps4 subfamily (Fig. 2). In some mammalian genomes (*e.g.* mouse, rat, and human), kp60-like A1s (katanal1s) are also conserved (Fig. 1). Katanal1s are very similar kp60 paralogs (~67% sequence identity over the entire chain). Moreover, this region (residues 1–90) can be further divided into two parts as follows: a well conserved core region (residues 1–72) and the following less-conserved region (~18 residues). The latter was a putative coiled-coil region, and the N-terminal region (residues 1–90) may form a dimer[17], whereas the first 72 residues behaved as an ideal "NMR ready" monomer. We call this region (residues 1–72) the core N-terminal domain (denoted kp60-NTD) and used it for further analysis.
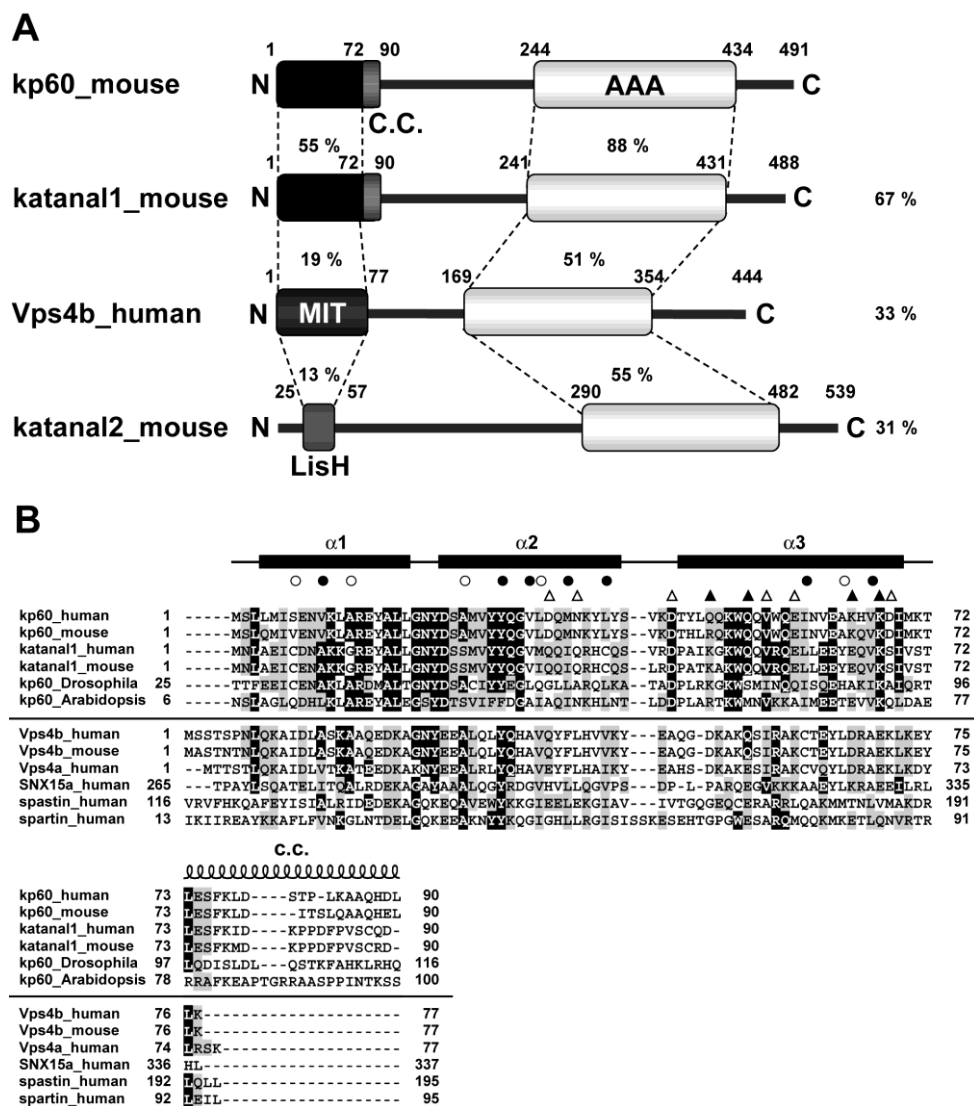
FIGURE 1. **Domain architectures and multiple sequence alignment of kp60s and proteins containing MIT domains.** (A) Domain architectures of mouse kp60, katanal1 and -2, and human Vps4b. The amino acid identities of each domain and full-length proteins between kp60 and other proteins are indicated. *C.C.*, coiled-coil; *MIT*, MIT domain; *LisH*, LIS1 homology domain; *AAA*, AAA domain. (B) Multiple sequence alignment of kp60-NTDs and related proteins with secondary structure elements of kp60-NTD. The secondary structure elements are shown at the *top* of the figure. The α-helices (α1–3) are represented as *thick lines* and the *C.C.* region as a coil. *Filled* and *open circles above* the alignments indicate well conserved and less conserved core residues, respectively (see Fig. 3A). *Triangles* indicate residues substituted with Ala for examining tubulin binding. (*Filled triangle*, involved in tubulin binding; *open triangle*, not involved.) Protein names and UniProtKB accession numbers are as follows: kp60 human (O75449); kp60 mouse (Q9WV86); kp60 *Drosophila* (Q9VN89); kp60 *Arabidopsis* (Q9SEX2); katanal1 human (Q9BW62); katanal1 mouse (Q8K0T4); Vps4b human (O75351); Vps4b mouse (P46467); Vps4a human (Q9UN37); SNX15a human (Q9NRS6); spartin human (Q8N0X7); and spastin human (Q9UBP0). The sequence alignment was generated by ClustalX[62].
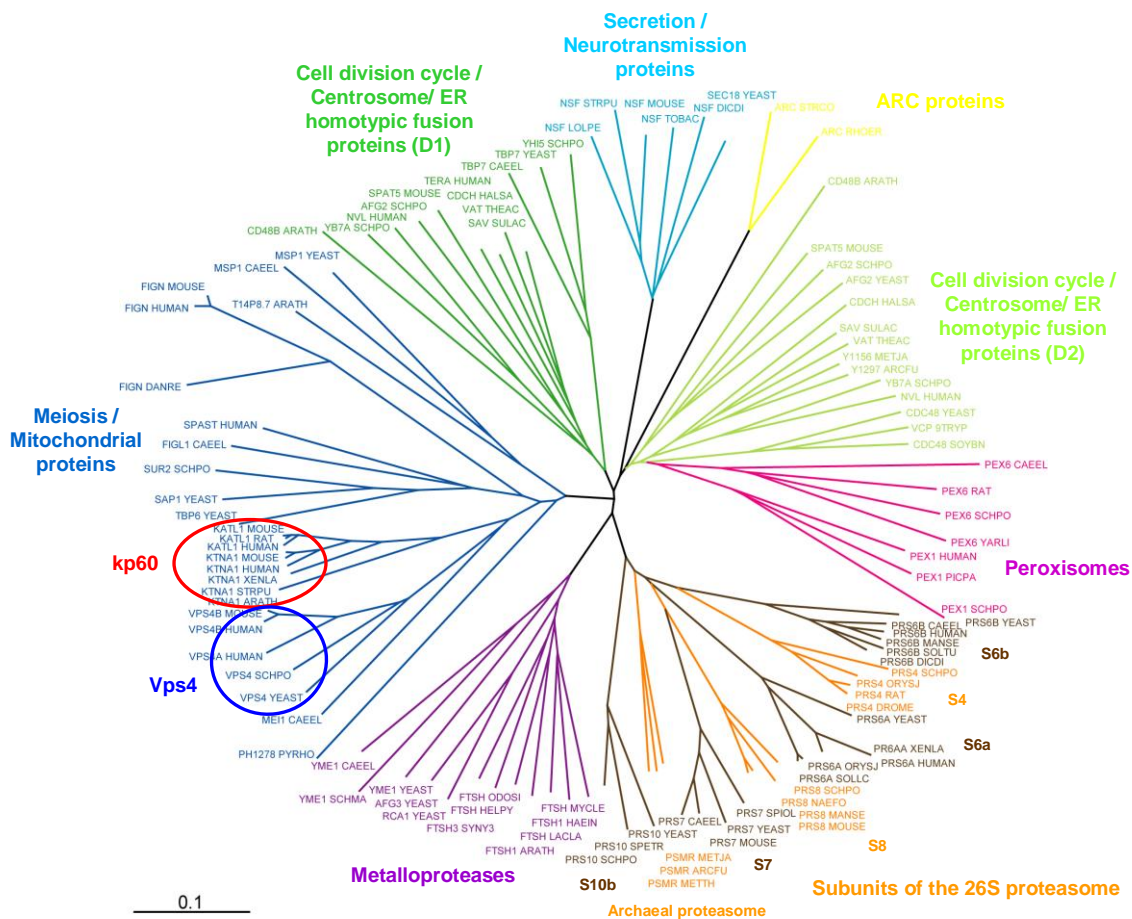
FIGURE 2. **Phylogenetic tree of the AAA protein superfamily.** Red circle, kp60 subfamily; Blue circle, Vps4 subfamily. The tree data were calculated by ClustalX[62] and the tree was drawn with TreeView (http://taxonomy.zoology.gla.ac.uk/rod/treeview.html).

### *Structure of kp60-NTD*

kp60-NTD was analyzed by standard solution NMR techniques. All of the backbone and 96% of the nonexchangeable protons of the side chain signals were assigned. An ensemble of 20 structures with low CYANA target functions (Fig. 3A) was generated from 1723 experimental NMR constraints. These 20 structures satisfy the experimental constraints very well (Table 1). The stereochemical quality of the ensemble members is good, with all backbone $\phi/\psi$ angles occupying the most favored or additionally allowed regions of the Ramachandran plot (Table 1; Fig. 4). Excluding the disordered regions, *i.e.* the N-terminal region (residues 1–3 plus the preceding extra

six residues of the tag) and the C-terminal region (residues 69–72), the r.m.s.d. values were 0.33 Å

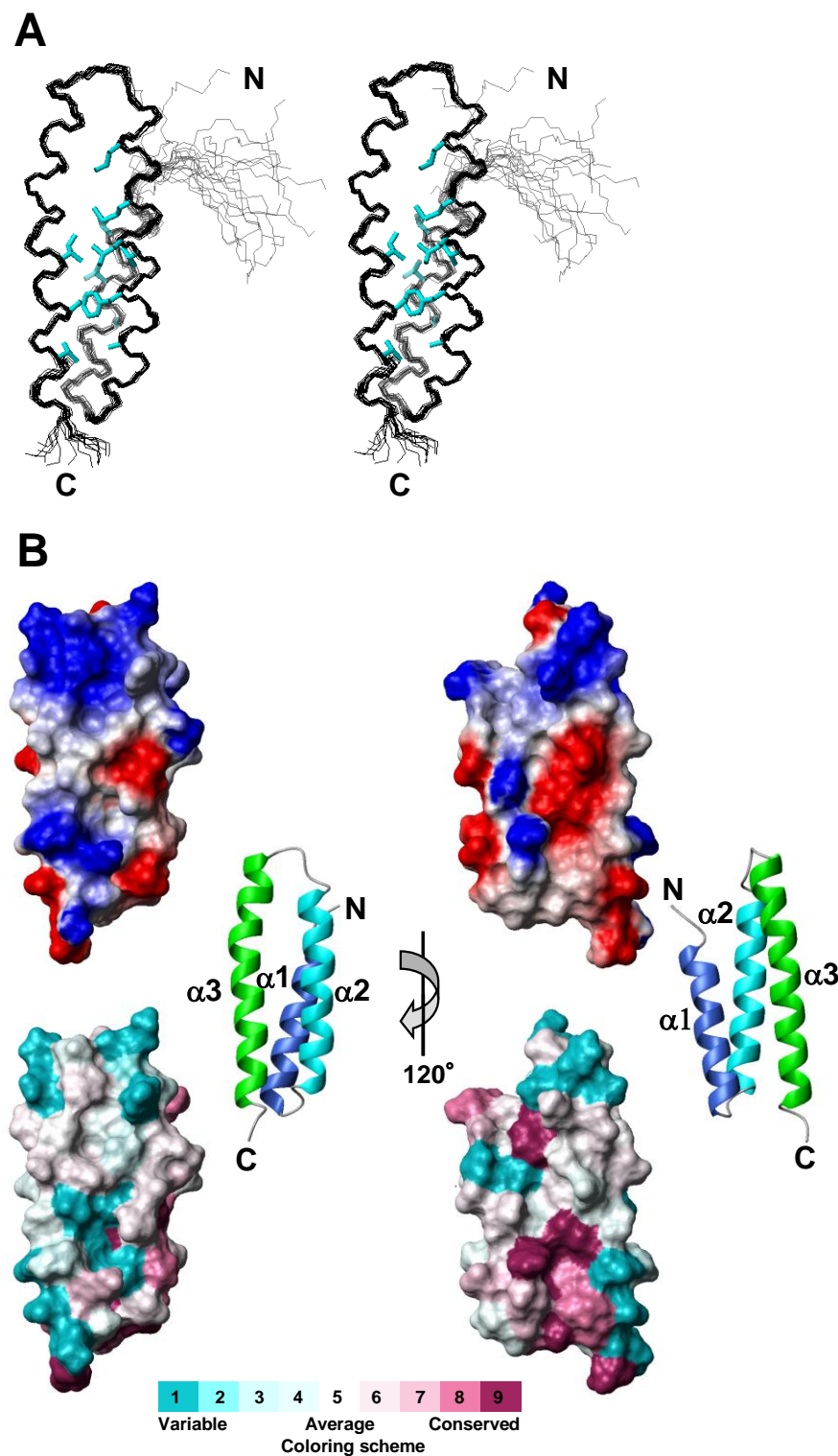for backbone heavy atoms and 0.83 Å for all heavy atoms.



FIGURE 3. **Solution structure of kp60-NTD.** (A) Stereo view of the best fit superposition of the 20 structures with lowest target functions. Side chains of buried residues with solvent accessibility less than 10% are shown (*cyan*). (B) *Top,* electrostatic surface potential mapped onto a van der Waals surface diagram. The color scale ranges between $-20\ k_BT$ (*red*) to $-20\ k_BT$ (*blue*), where $kB$ is Boltzmann's constant and $T$ is temperature. *Bottom,* sequence conservation among the kp60-NTDs is mapped on the surface. Conservative and variable residues are colored *purple* and *cyan*, respectively. The color codes were produced by ConSurf[63]. Ribbon diagrams of the kp60-NTDs are shown in the *middle*. The surface composed of helices 2 and 3 is shown as the front view (*left*) and the rear view (*right*).
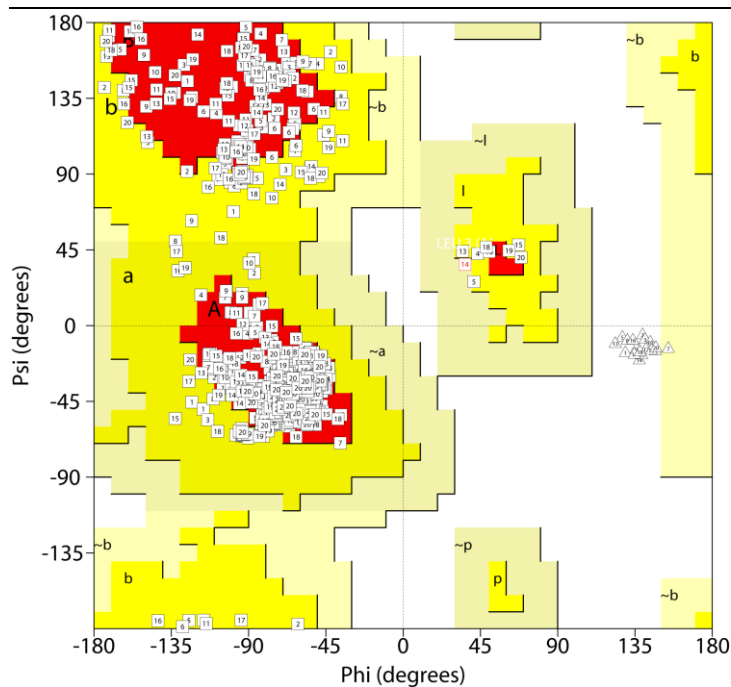
FIGURE 4. **Ramachandran plot for the phi-psi values of the final 20 structures of kp60-NTD.** This figure was produced using PROCHECK-NMR[34].

As shown in Fig. 3B, kp60-NTD is organized into antiparallel three-helix bundle that consists of helix 1 (4–19), helix 2 (23–41), and helix 3 (46–69). The secondary structure is shown in Fig. 1B along with its amino acid sequence. Helices 1 and 2 are connected by a very tight three-residue turn, whereas helices 2 and 3 are connected by a more flexible four-residue loop. Helices 2 and 3 are longer than helix 1, thereby exposing a large protrusion formed by helix 2 C-terminus and helix 3 N-terminus. These three helices are packed against one another nearly in parallel. The packing angles between the helices are similar as follows: 19.3° between 1 and 2, 21.1° between 2 and 3, and 26.1° between 1 and 3. Interhelical contacts mainly include hydrophobic side chain-side chain interactions. Core residues employed in these contacts are shown in Fig. 3A as well as in Fig. 1B. A total of 12 nonpolar contacts between helices 1 and 2, 17 between helices 2 and 3, and 5 between helices 1 and 3 were observed. The spatial arrangement of these three helices is nearly symmetric. The interhelical distances between helices 1 and 2 (5.0 Å) and helices 2 and 3 (5.5 Å) were shorter than that between helices 1 and 3 (6.5 Å). We found no obvious crevices or pockets on the surface of kp60-NTD. The kp60-NTD surface is highly charged (Fig. 3B).

### *Structural Similarities of kp60-NTD with MIT Domains and Other Tetratricopeptide Repeat Proteins*

When the structure of kp60-NTD was subjected to DALI search[37], several MIT domains were first retrieved with Z-scores higher than 7.0, including NRBF-2 (PDB code 2crb, Z-score of 9.6, and r.m.s.d. of 1.6 Å), Vps4b (PDB code 1wr0, Z-score of 8.9, and r.m.s.d. of 2.7 Å), Vta1 (PDB code 2rkk, Z-score of 7.4, and r.m.s.d. of 2.4 Å), spastin (PDB code 3eab, Z-score of 7.2, and r.m.s.d. of 2.2 Å), and spartin (PDB code 2dl1, Z-score of 7.1, and r.m.s.d. of 2.4 Å). Thus, we first compared the structure of kp60-NTD with those of the MIT domains. Fig. 5 shows the structural comparisons between kp60-NTD and each of the MIT domains along with their sequence identity and structural fitness. Despite a low sequence similarity (10–19%), the kp60-NTD fold resembles those of the MIT domains, as shown by backbone r.m.s.d. of 2.2–2.7 Å for more than 67 residues from the secondary structural regions. Among these, spastin is the product of SPG4, which is mutated in the most common form of hereditary spastic paraplegia[4], and is involved with MT maintenance in axons[38,39]. Thus, the MIT domain of spastin is one of the closest homolog of kp60-NTD with regard to its physiological relevance to MT severing.

After comparing the structures in detail, all the helices were well superimposed, although the loop between helices 2 and 3 was not (Fig. 5E). The structures of the kp60 tubulin-binding site, kp60-NTD, and the MIT domain were strikingly similar, although their sequence similarity was very low (~19%). Thus, kp60-NTD is classified as a variant MIT domain. Because some of the MIT domains (*e.g.* spastin and spartin) are considered to bind microtubule (and/or tubulin), this structural similarity is not surprising.

One of the most characteristic features of the MIT domain is its unique hydrophobic core formed by conserved Ala residues, referred to as the "Ala zipper"[40,41]. These are thus identified as the key residues for the MIT domain signature (Ala-Xaa$_6$-Ala-Xaa$_{11}$-Ala-Xaa$_6$-Ala). These conserved Ala residues are present along the buried surfaces of helices 1–3 facing each other,

thereby forming a hydrophobic core. In kp60 and its closely related homologs, these key Ala residues are only partly conserved. For example, Ile-6 and Val-32 in mouse kp60-NTD correspond to the zipper-forming Ala residues (Ala-9 and Ala-35) in the human Vps4a-MIT domain. Although the MIT domain signature is not conserved in kp60-NTD, this domain is obviously a close variant of the MIT domain. This imperfect conservation of the MIT-domain signature may explain why methods such as PSI-BLAST[18] and HMMER[19] could not predict the structural similarity between kp60-NTD and the MIT domain. In the DALI search, we also found other proteins containing either twisted α-helical hairpins or tetratricopeptide repeat motifs with Z-scores higher than 5.0. For example, partial structures of glycine-tRNA synthetase α-chain (PDB code 1j5w, Z-score of 8.7, and r.m.s.d. of 2.2 Å), 14-3-3 protein Tau (PDB code 2btp, Z-score of 8.2, and r.m.s.d. of 2.4 Å), cyclophilin 40 (PDB code 1ihg, Z-score of 8.1, and r.m.s.d. of 2.7 Å), α-E-catenin (PDB code 1l7c, Z-score of 7.9, and r.m.s.d. of 2.0 Å), fkbp52 (PDB code 1p5q, Z-score of 7.5, and r.m.s.d. of 3.0 Å), invertase inhibitor Nt-CIF (PDB code 1rj1, Z-score of 6.3, and r.m.s.d. of 2.1 Å), and Hop (PDB code 1elr, Z-score of 5.2, and r.m.s.d. of 3.7 Å) were shown to resemble kp60-NTD (data not shown).

| | | | | |
|---|---|---|---|---|
| **A** | **B** | **C** | **D** | **E** |

| Identity (%) | - | 19 | 10 | 14 |
|---|---|---|---|---|
| rmsd (Å) | - | 2.7 | 2.2 | 2.4 |

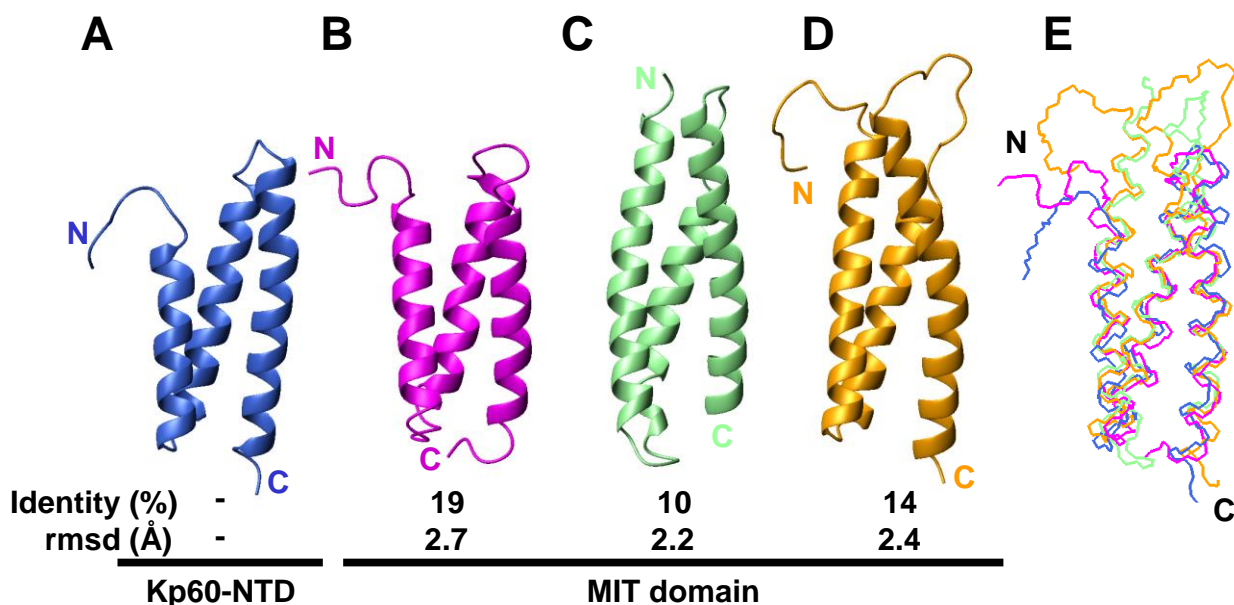| Kp60-NTD | MIT domain | | |
|---|---|---|---|

FIGURE 3. **Structural comparisons of kp60-NTD with MIT domains.** Ribbon diagrams of the proteins are as follows: (A) kp60 (PDB code 2rpa); (B) Vps4b (PDB code 1wr0); (C) spastin (PDB code 3eab); (D) spartin (PDB code 2dl1). Identity (*top*, %) and r.m.s.d. (*bottom*, Å) between kp60-NTD and the MIT domains are also presented. (E) Superposition of kp60-NTD (*blue*), Vps4b-MIT (*magenta*), spastin-MIT (*pale green*), and spartin-MIT (*orange*).

*Tubulin Binding by kp60-NTDs*

To examine the molecular function of kp60-NTD as an MT binding domain, we performed *in vitro* MT binding assays using polymerized MTs. Contrary to our expectation, we found that the amount of kp60-NTD co-sedimented with MTs was very low, at the limit of detectability (Fig. 6) (data not shown). However, kp60-NTD co-sedimented with medium size MTs (Fig. 6D).

These results suggested that kp60-NTD might bind to oligomeric tubulin and/or MT fragments rather than enormous polymerized MTs. Thus, we did a pulldown assay using GST-tagged kp60-NTD with unpolymerized tubulin. *In vitro* tubulin binding activity of kp60-NTD was observed (Fig. 7A, *lane 5*).
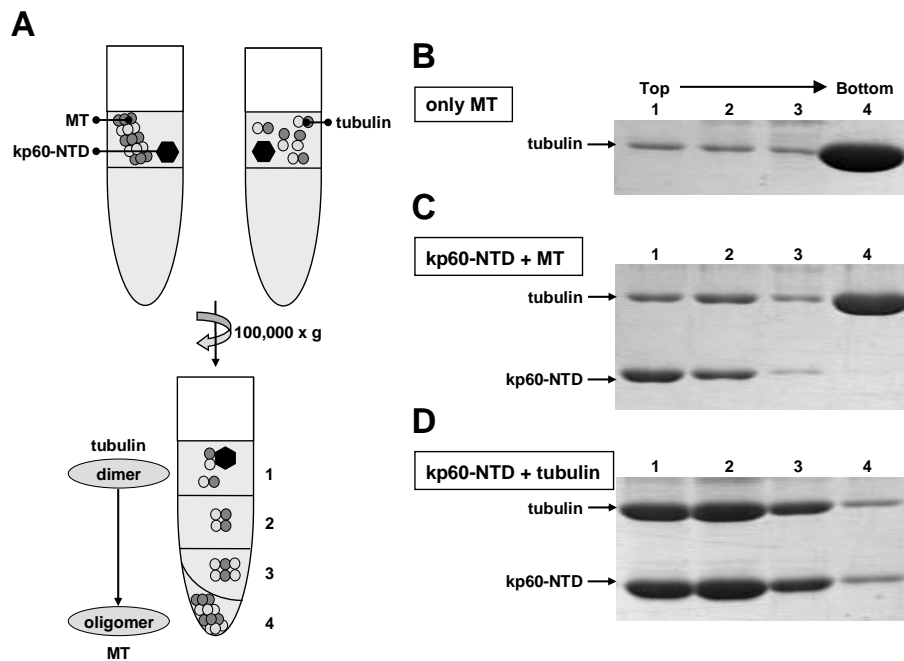
FIGURE 6. **Interactions between kp60-NTD and MTs/tubulin dimer.** (A) Schematic diagram of pull-down assay using Microtubule binding protein spin down assay kit, BK029 (Cytoskeleton) to assess interactions between GST-tagged kp60-NTD and MTs/tubulin *in vitro*. GST-tagged kp60-NTD was mixed with a reaction solution after (upper left) and before (upper right) tubulin polymerization reaction, then ultracentrifuged. Tubulin was separated by molecular weight; polymerized MTs were sedimented at the bottom of tubes, non-polymerized tubulin migrated to the top of the solution (lower panel). Reaction solutions were divided into four fractions (from top to bottom) and each fraction was analyzed by SDS-PAGE. GST-tagged kp60-NTD co-sedimented with non-polymerized tubulin. (B) The reaction solution after polymerization of only tubulin was ultracentrifuged and analyzed as a control. Lanes 1–4 correspond to fractions from top to bottom, indicated in the lower panels of A. (C) Pull-down assay for kp60-NTD mixed after tubulin polymerization reaction. kp60-NTD may possibly bind with a tubulin dimer rather than MTs. (D) Pull-down assays of the GST-tagged kp60-NTD mixed before tubulin polymerization reaction. SDS-PAGEs are Coomassie-stained.

This tubulin binding activity varied with the length of the N-terminal domain. kp60-NTD (residues 1–72) binds tubulin, whereas kp60-NTD (residues 1–90) does not (Fig. 7A, *lane 6*). In our previous report, we showed that kp60-NTD (residues 1–90) formed a dimer using the coiled-coil region (residues 73–90)[17]. Thus, dimer formation may hide the interface of kp60-NTD from tubulin.

In addition, we found that the Vps4b-MIT domain (residues 1–77) did not bind tubulin (Fig. 7A, *lane 17*). Thus, the observed tubulin binding activity is specific for kp60-NTD.

### *Tubulin-binding Site of kp60 NTD*

To determine the interfacial residues on kp60-NTD involved with tubulin recognition, we carried out mutagenesis experiments. Prior to these experiments, we attempted to identify the tubulin-interacting residues on kp60-NTD by NMR titration experiments and failed. We observed unexpected severe signal broadening even at very low tubulin concentration, which made further NMR analysis difficult (data not shown). Then, 10 residues from kp60-NTD (Gln-35, Asn-37, Asp-45, Arg-49, Gln-53, Val-55, Glu-58, Lys-64, Lys-67, and Asp-68) were selected, and each was substituted with Ala. These residues were carefully selected from the surface residues located on helices 2 and 3. The binding activities of mutants were examined by pulldown experiments (Fig. 7A, *lanes 7–16*).

The most significant effects were observed in mutations of residues on helix 3 as follows: Arg-49, Gln-53, Lys-64, and Lys-67. All of these side chains are hydrophilic and are exposed to the surface composed of helices 2 and 3 (Fig. 7, B and C). In addition, three of the four key residues are positively charged, suggesting an electrostatic interaction between kp60-NTD and tubulin. These residues were not conserved in the Vps4b-MIT domain as well as in the other MIT domains, such as spastin and spartin (Fig. 1B). This result is partially consistent with the inability of Vps4b-MIT to bind tubulin (Fig. 7A, *lane 17*). Because spastin and spartin can bind or regulate MTs[42,43], this might indicate that these proteins bind MTs using regions other than the MIT domains. In contrast, mutants V55A, E58A, and D68A retained substantial tubulin binding activities (Fig. 7A, *lanes 12, 13,* and *16*). These residues are also on helix 3, but are exposed to the surface composed of helices 1 and 3 or outside of helix 3 (Fig. 7, B and C). Similarly, residues in helix 2 (Gln-35 and Asn-37) and loop 2 (Asp-45) were not involved in tubulin binding (Fig. 7A, *lanes 7–9*).
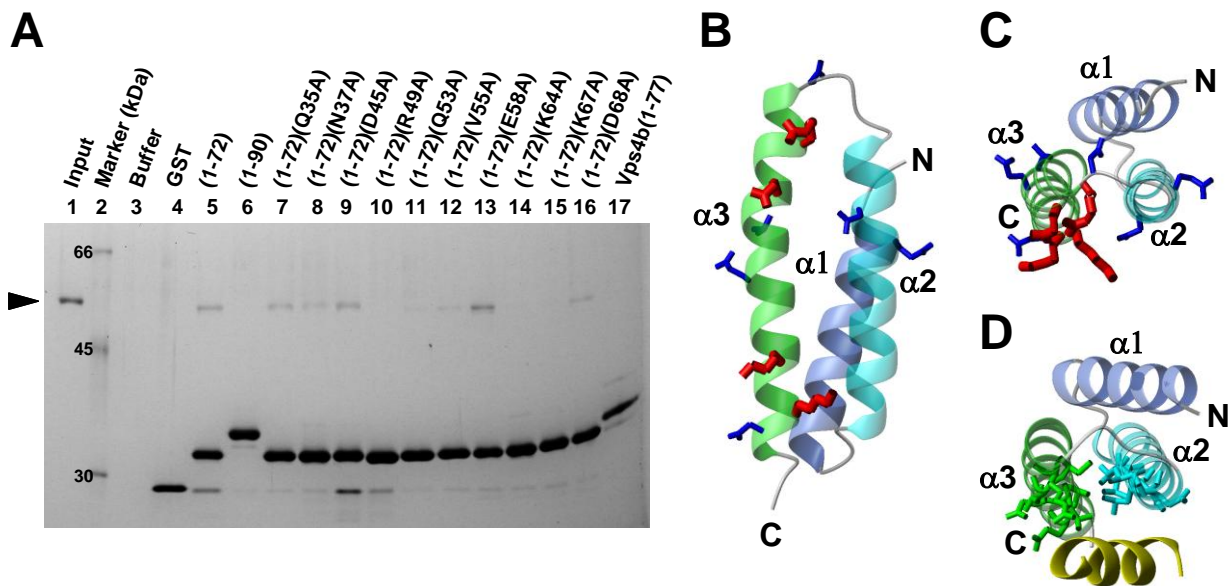
FIGURE 4. **Interactions of kp60-NTD with tubulin.** (A) Pulldown assays of tubulin with GST-tagged kp60-NTDs of wild type and Ala mutants and Vps4b-MIT *in vitro*. Tubulin was used as the input. Molecular size is shown in *lane 2*. Only the buffer and the GST tag used as negative controls are shown in *lanes 3* and *4*. Recombinant proteins used for pulldown are indicated at the top of the gel. SDS-PAGE was silver-stained. (B) and (C) Side and top views of the ribbon diagram of kp60-NTD, respectively. Side chains of residues that were substituted with Ala are shown. In the pulldown assay, residues that were affected and unaffected by Ala mutations for tubulin binding are colored *red* and *blue*, respectively. (D) Top view of the ribbon diagram of the complex between Vps4-MIT and CHMP1a (*yellow*) (PDB code 2jq9). Side chains of the residues interacting between Vps4 and CHMP1a are indicated.

We further examined whether full-length kp60s with or without mutation in the N-terminal domain bind tubulin. We generated GST-tagged full-length kp60 in *E. coli*. Prior to the binding assay, we confirmed that the recombinant full-length kp60s had ATPase activity, according to the protocol in the recent paper (Fig. 8A)[16]. We then performed pulldown experiments using mutants R49A and K67A of full-length kp60. The full-length kp60 (wild type) bound tubulin, whereas the mutants lacked tubulin binding activities, as expected by the results of kp60-NTDs (Fig. 8B; Fig. 7A).
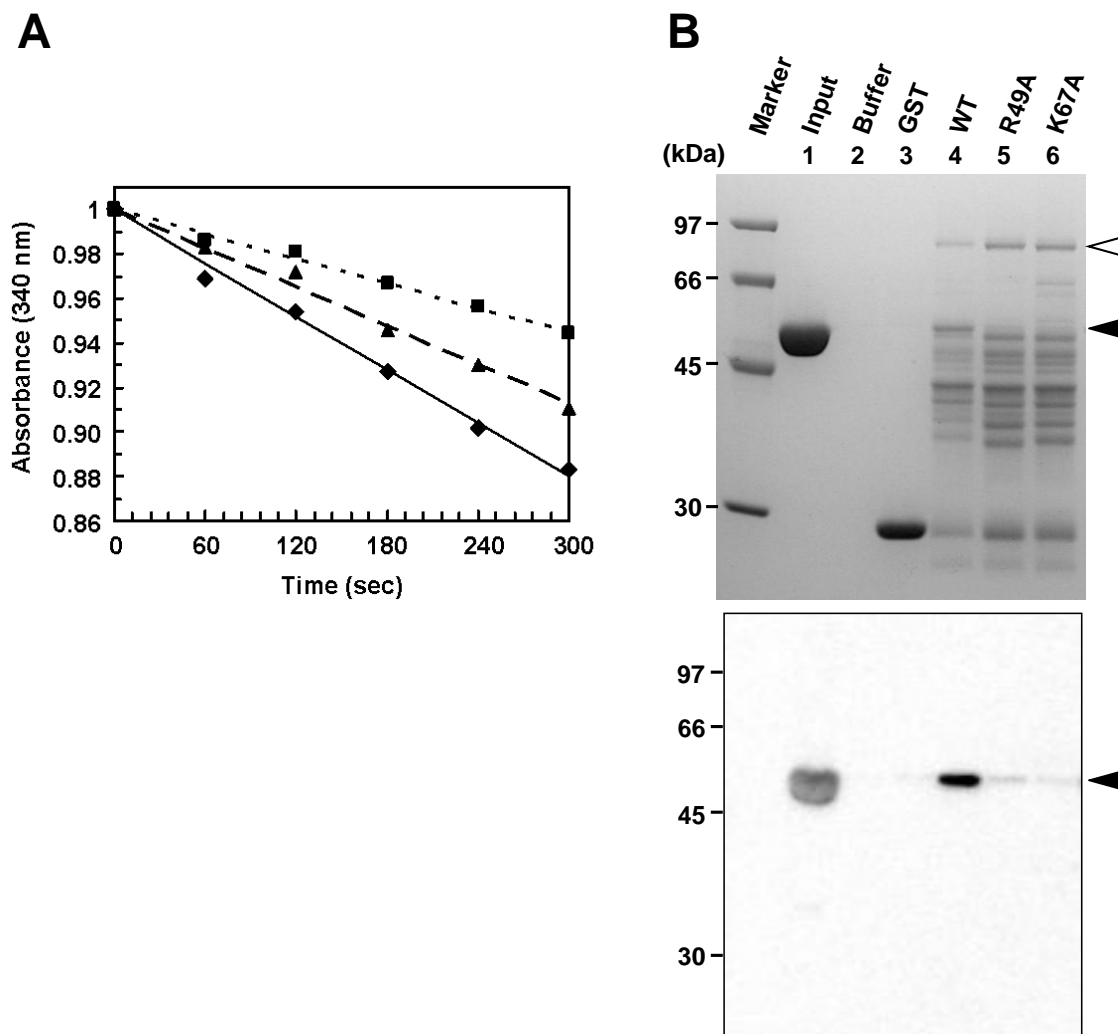
FIGURE 8. **ATPase activity of full-length kp60 and interactions of kp60 with tubulin.** (A) ATPase activities of kp60s (0.5 μM) at 340 nm. Filled diamond (continuous line): wild type, filled box (dotted line): R49A, filled triangle (broken line): K67A. (B) Pull-down assays of tubulin with wild type (WT) of GST-kp60 and Ala mutants *in vitro*. Molecular size is shown in the left. Tubulin was used as the input. Only the buffer and the GST-tag mixed with tubulin as negative controls are shown in lanes 2 and 3. Recombinant proteins used for pull-down are indicated at the top of the gel. Filled and open arrowheads show tubulin and full-length kp60s, respectively. SDS-PAGE was Coomassie-stained (upper panel). Western blotting analysis of tubulin bound to full-length kp60s was visualized by ECL (lower panel).

# Discussion

### *Structural and Functional Comparisons with Other Tubulin Binding Domains*

In this study, we have determined the structure of a novel tubulin binding domain derived from the conserved region of kp60, which was classified as a variant MIT domain. To our knowledge, this is the first experimental evidence for the direct interaction between an isolated MIT domain and tubulin.

To date, structures of many MT and/or tubulin binding domains have been determined (Fig. 9)[44–49]. Interestingly, all-α-helical protein domains are dominant in these with solved structures, which might be advantageous for interactions with MT and/or tubulin. In the MT structure, the only accessible surface of tubulin includes helices 11 and 12 and the C-terminal tail[49–51]. Thus, for one of tubulin recognition, helix-helix interactions of tubulin binding domains are suggested, although there are many structures of the known MT-interacting proteins left unsolved.

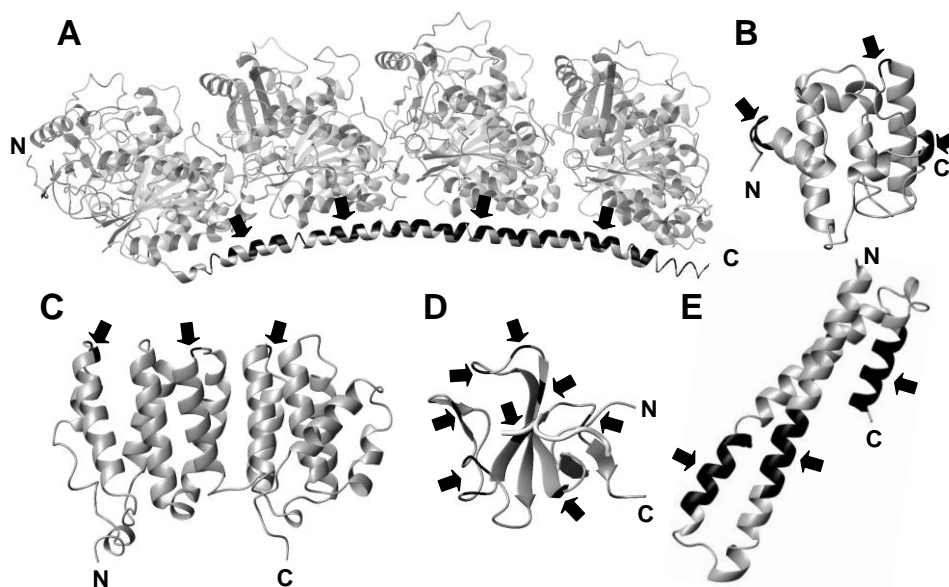FIGURE 9. **Comparison of structures and tubulin binding interfaces with other tubulin binding domains.** Tubulin binding interfaces are indicated by black and arrows. (A) stathmin-like domain bound to the tubulin (white) (PDB: 1sa1); (B) EB1 CH domain (2qjz); (C) Msps TOG2 domain (2qk2); (D) CAP-Gly domain bound to the tubulin peptide (white) (2e4h), and (E) tubulin-specific chaperone cofactor A (1h7c).

### *Structural and Functional Similarities to Vps4*

We identified the tubulin-binding interface of kp60-NTD, which is on the surface comprising helices 2 and 3 (Fig. 7B). This result is consistent with the studies by Stoppin-Mellet, in which a truncation mutant of *Arabidopsis* kp60 (*At*KSS) that lacked the N-terminal 15 residues corresponding to helix 1 still retained MT severing activity[16]. Surprisingly, the tubulin binding interface is very similar to the substrate (Vps2 and CHMP1a)-binding interfaces of the MIT domains of Vps4 (Fig. 7, C and D)[35,52,53]. In other words, the common substrate-binding interfaces appear to be preserved between MT severing and membrane skeletal reorganization.

In studies of Vps4-MIT complexed with C-terminal regions of Vps2 or CHMP1a, the MIT domains use helices 2 and 3 as the interface for the α-helical peptides[35, 52]. The residues involved with kp60-NTD-tubulin interaction are relatively conserved among kp60 orthologs (Fig. 1B), but they are not conserved between kp60-NTD and the other MIT domains, thus explaining why Vps4-MIT did not bind tubulin (Fig. 7A, *lane 17*). In contrast, another interface of Vps4-MIT for CHMPs has been reported, in which Vps4-MIT uses a shallow cleft between helices 1 and 3 for binding a proline-rich, CHMP6-derived peptide named MIT-interacting motif 2 (MIM2)[53]. In the structure of kp60-NTD, there was no correspondence between helices 1 and 3, as the interhelical distance was substantially narrower (6.5 Å) than that of Vps4-MIT. We do not rule out the possibility that the interface composed of helices 1–3 serves as the binding site of other factors, such as katanin p80 and NDEL1[54], both of which regulate the subcellular localization of kp60.

### *Conserved Macromolecular Disassembling Mechanisms between Vps4 and Kp60*

Our findings indicate that the molecular architectures of kp60 and Vps4 are very similar in the following points: domain organization, structures of the N-terminal domains, and the relative locations of the interfaces for target proteins. Here, we propose some common features of the molecular mechanisms in different biological processes, MT severing and late endosomal luminal

membrane budding, driven by kp60 and Vps4, respectively.

First, both the enzymes disassemble polymeric macromolecular complexes known as cytoskeleton and membrane skeleton. Second, these enzymes release protomers from macromolecular complexes (MT and ESCRT-III) in the cytoplasm depending on ATP hydrolysis. Finally, their N-terminal domains serve as adaptors to the protomers. The similarities of these mechanisms are illustrated in Fig. 10.

The ESCRT-III complex is composed of self-associating coiled-coil proteins (CHMP1–6), which form filamentous circular structures on the membrane surface[55]. When Vps4 interacts with ESCRT-III filaments, it pulls out CHMP protomers from the filamentous circular structure. The residual filaments of ESCRT-III then reorganize into a smaller circular structure by self-association. Vps4 continues to pull protomers away, and the circular structure shrinks into a smaller wheel. Finally, this downsizing of the ESCRT-III circle results in membrane budding with concomitant alterations of the membrane structure. This model is known as the "concentric circle model"[56].

We propose that the early stage of MT severing might have a similar mechanism. kp60 pulls a tubulin α/β-dimer away from MT in an ATP-dependent manner. However, contrary to the ESCRT-III polymer, polymerization of tubulin dimers is restricted to the plus end of MT as well as to the GTP form of tubulin, whereas polymerization at the minus end is extremely slow[1,57]. It is expected that once tubulin is pulled away by kp60, it can no longer fill the gap on MT. If two or more tubulin dimers are pulled away from this gap, then MT may start severing, resulting in a catastrophe. The structural similarities between kp60 and Vps4 revealed in this study encourage us to propose a model for the molecular mechanism of MT severing.
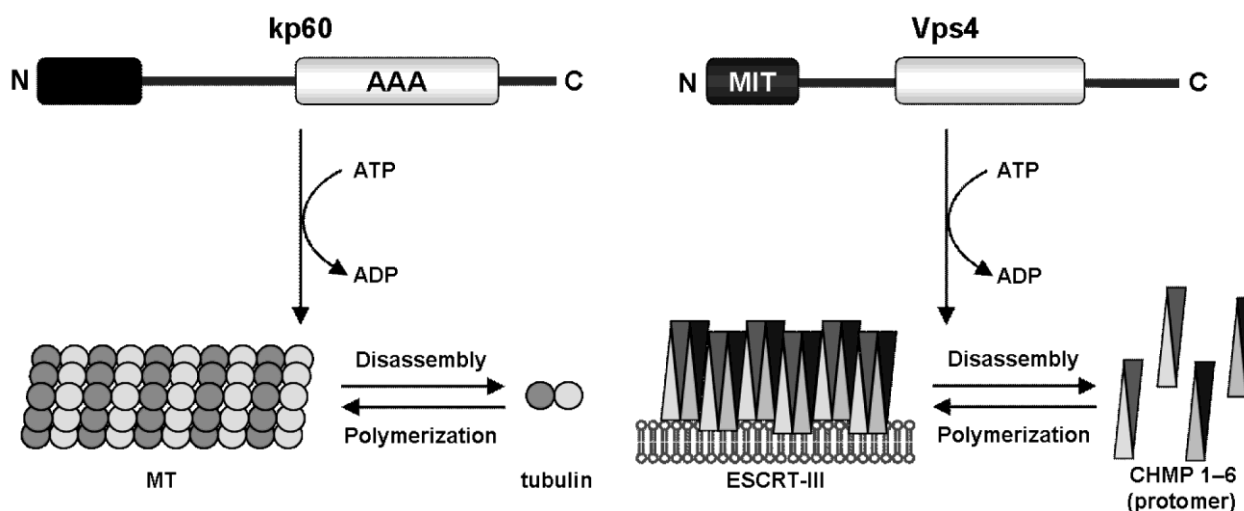
FIGURE 10. **Schematic diagram of architecture and molecular function similarities between kp60 and Vps4.** kp60 catalyzes the disassembly of MT via N-terminal domain binding, which results in MT severing. Vps4 catalyzes the release of the ESCRT-III protomer via the MIT domain binding, which results in endosomal membrane invagination. For both biological events, the N-terminal domains serve as adaptors for the polymeric macromolecules, thereby disassembling either the cytoskeleton or the membrane skeleton in an ATP-dependent manner.

### *Model for kp60-NTD Binding to Tubulin Oligomer*

To assess the detailed mechanism of MT severing, we constructed a model for the complex between kp60-NTD and a tubulin tetramer (Fig. 11). Our study is confined to the interface of the kp60 N-terminal adaptor domain to its tubulin substrate, as we did not identify the kp60-binding site on tubulin. Nevertheless, numerous literature resources provide a basis for model construction as follows. As discussed previously, the major candidates of the structural elements of tubulin that are accessible from outside MT are helices 11 and 12[49–51]. Next, the similarity between the interfaces of kp60-NTD with tubulin and that of Vps4-MIT with CHMP1a suggests that a helix on tubulin, which is similar to the CHMP1a helix (residues 115–127) bound to Vps4-MIT[52], may serve as the binding site of kp60. Taking all the information into account, we propose a model for the tubulin + kp60-NTD complex (Fig. 11).
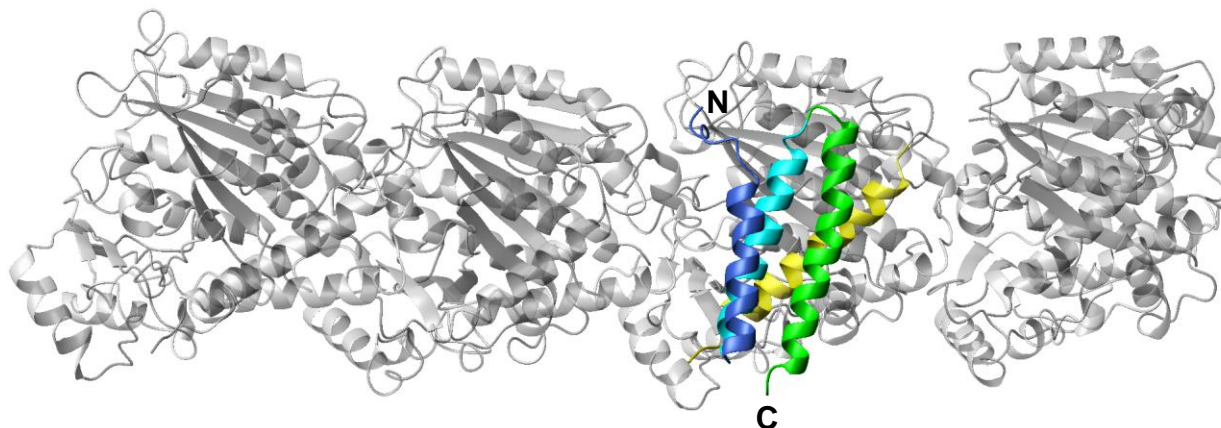
FIGURE 11. **Model of α-tubulin binding with kp60-NTD.** Ribbon diagram of a model complex between kp60-NTD and a tubulin tetramer (*gray*) is shown. α-Tubulin helix 12, a putative interface of kp60-NTD, is colored *yellow*.

While constructing the model, the following points were hypothesized: (i) one of the last helices (helix 11 or 12) makes contact with kp60-NTD at its helix 2/3 interface; (ii) the relative position and orientation between kp60-NTD and one of the tubulin helices mimic those between Vps4-MIT and the CHMP1a helix; (iii) steric crash between kp60-NTD and tubulin should be avoided; and (iv) charge-charge interactions between kp60-NTD and the tubulin helix should be maximized.

As a result, we found the following four candidate positions on tubulin C-terminal helices for kp60-NTD binding: (i) helix 11 (residues 386–396); (ii) helix 11 (residues 390–400); (iii) helix 12 (residues 420–430); and (iv) helix 12 (residues 423–433). All these positions are present on both tubulin-α and tubulin-β. Finally, by assessing complementarity of charge interactions in the model, the final model was selected out of the eight candidate models. Its helix 12 (residues 420–430) of tubulin α3 binds with kp60-NTD by occupying the corresponding position of CHMP1a (residues 115–127) that binds Vps4-MIT (PDB code 2jq9) (Fig. 11; Fig. 12)[52].

FIGURE 12. **Model for α–tubulin helix 12 binding with kp60-NTD.** An electrostatic surface potential diagram (top), a ribbon diagram (middle), and a sequence conservation diagram (bottom) for kp60-NTD were shown. α–Tubulin helix 12 is shown as a transparent cylinder (yellow).
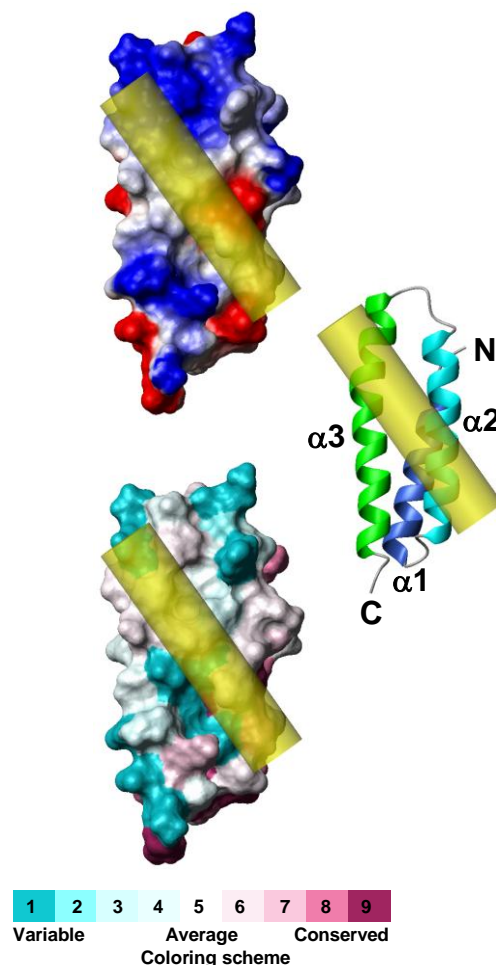
Alternatively, we generated the model of kp60-NTD + tubulin tetramer complex based on the complex between spastin-MIT with CHMP1b (PDB code 3eab) in which spastin-MIT used helices 1 and 3 as the interface to CHMP1b (Fig. 13)[58]. This model is not consistent with our mutation studies (Fig. 7). Consequently, we justified the modeling of helices 2 and 3 as the tubulin-binding site. Because CHMP1b serves as an adaptor of spastin but not a substrate, this alternative model suggests that the helix 1/3 surface of kp60-NTD is a putative binding site for kp80, an adaptor of kp60 to bound MT and/or tubulin.
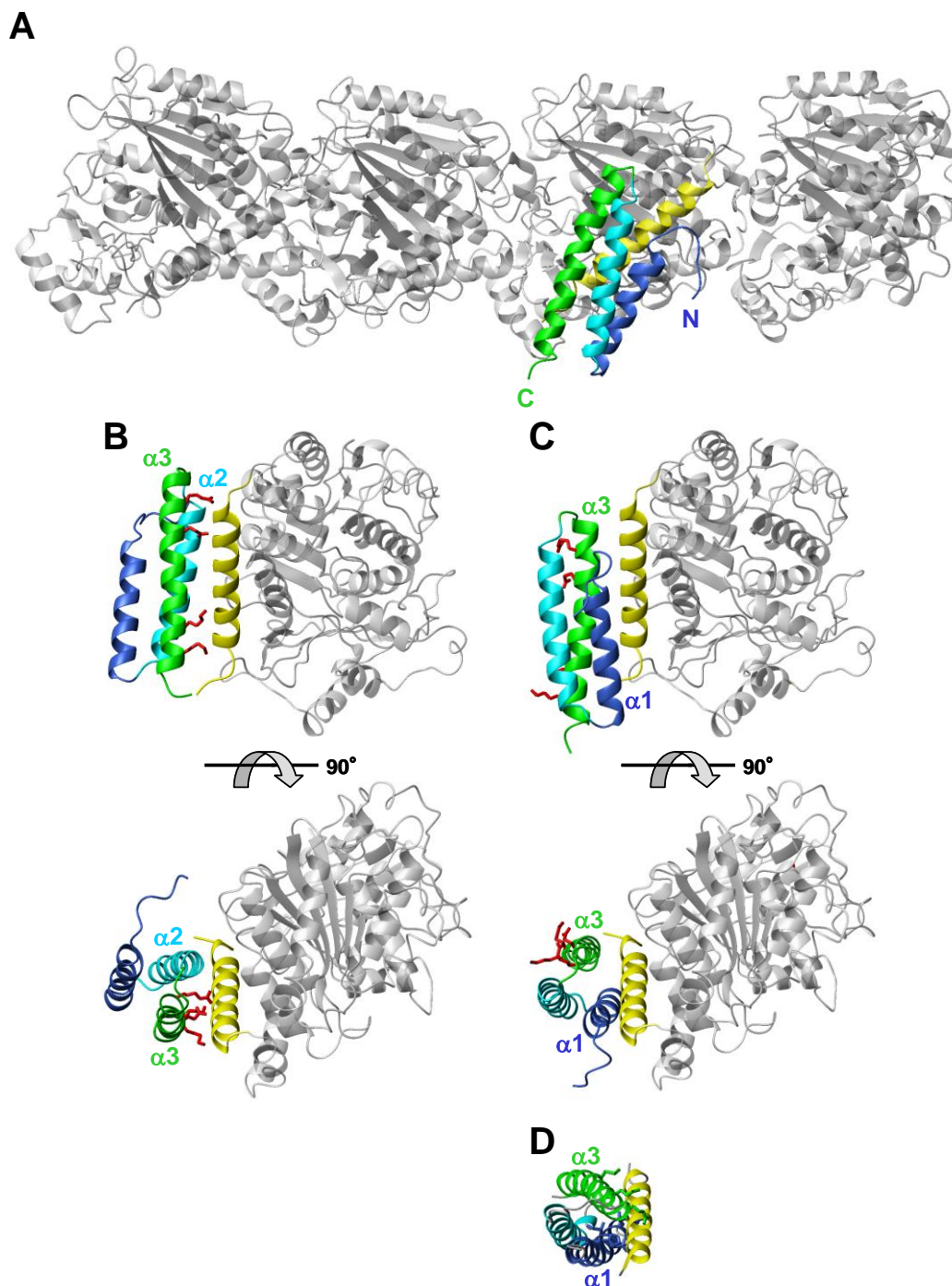
FIGURE 13. **Comparison between model for tubulin binding interfaces of kp60-NTD.** (A) Model of kp60-NTD bound to α–tubulin at the helix 1/3 interface (see text). Ribbon diagram of the model complex between kp60-NTD and α–tubulin tetramer (grey) was constructed based on the complex between spastin-MIT and CHMP1b (PDB: 3eab). α–tubulin helix 12, a putative interface to kp60-NTD, is colored yellow. (B) and (C) Side (top) and top (bottom) views of the ribbon diagram of the complex between kp60-NTD and α–tubulin using the helix 1/3 and helix 2/3 interfaces, respectively. Side chains of key residues for binding tubulin are shown (red). (D) Top view of the ribbon diagram of the complex between spastin-MIT and CHMP1b (yellow) (3eab). Side chains of the residues interacting between spastin and CHMP1b are indicated.

In the model of Fig. 6, the direction of the pore of the hexameric AAA-ATPase domain, which follows C-terminal to kp60-NTD, may approach the C-terminal tail of tubulin. We further confirmed this idea by using the model structure of full-length hexameric kp60 complexes with tubulin (Fig. 14). The location is consistent with the hypothesis that the pore of the AAA domain "sucks in" the tubulin C-terminal tail upon ATP hydrolysis (threading model)[59,60]. In fact, the literature suggests that kp60 function requires its direct interaction with the C-terminal tail of tubulin. This is based on the observation that MT severing activity was abolished when MTs were pretreated with subtilisin[8]. Additional evidence regarding the MT-severing mechanism of spastin, another related AAAATPase, may support this idea. Spastin also recognizes and pulls the tubulin C-terminal tail as an initial binding site that is indispensable for its MT severing activity[42,61]. The hypotheses derived from our complex model require confirmation by additional experimentation.

In conclusion, the structure and key residues of kp60-NTD provide new insights into the molecular mechanisms of how the enzyme severs MT. The similarities of the molecular mechanisms as well as of the domain organizations suggest that these are evolutionarily conserved among type I AAA-ATPases, kp60 and Vps4, whose cellular functions are distinct.
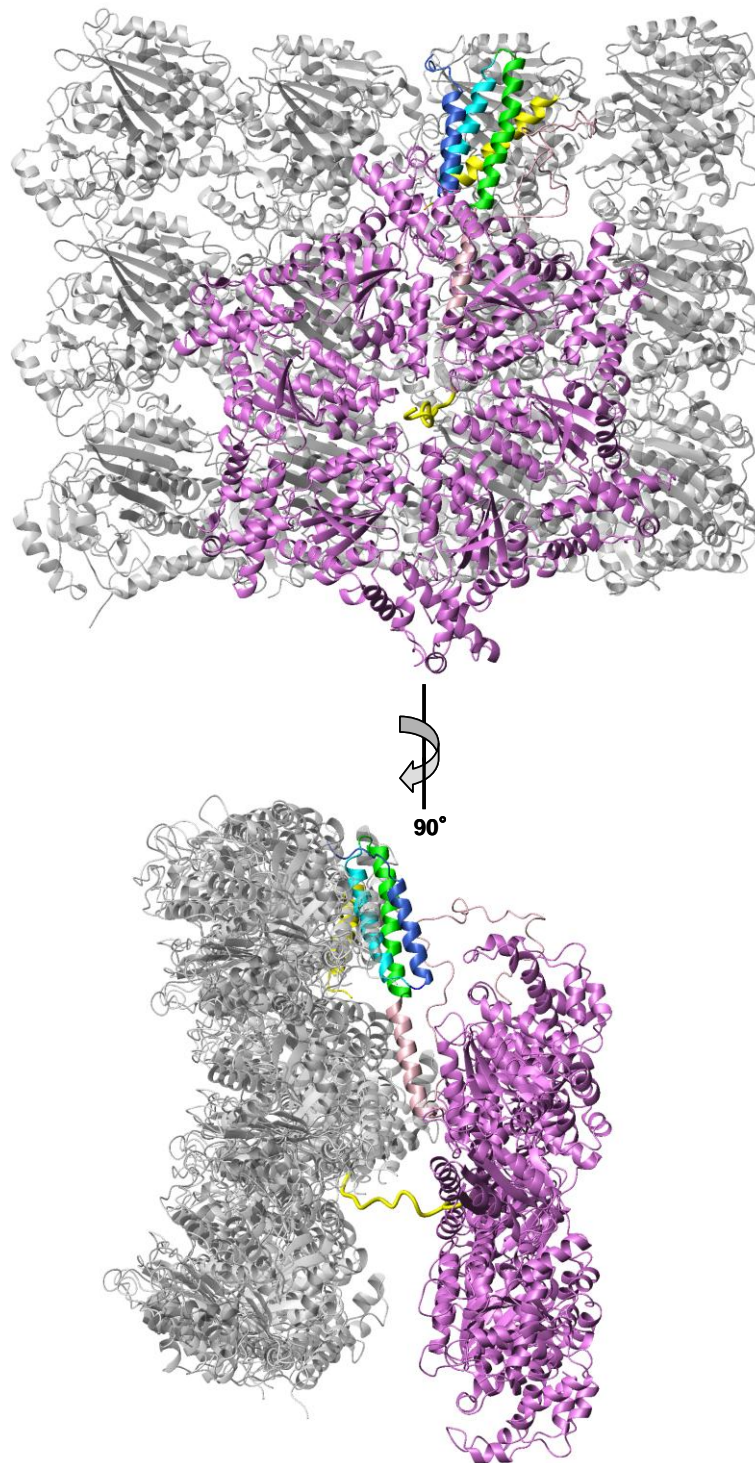
FIGURE 14. **Proposed model for tubulin binding with full-length kp60.** Model complex between tubulin origomer (grey) and hexameric full-length kp60, composed of kp60-NTD and AAA ATPase domain (violet) is shown. AAA ATPase domains form hexameric ring. Five of the six kp60-NTDs on the hexameric AAA ATPase domains were not drawn for clarity. One of the tubulin C-terminal tail is shown in yellow. The tail on the surface of MT may bind to the pore of the hexameric AAA ATPase domain of kp60.

# References

1. Desai, A. & Mitchison, T. J. (1997) Microtubule polymerization dynamics. *Annu. Rev. Cell Dev. Biol.* **13** 83-117.

2. Wittmann, T., Hyman, A. & Desai, A. (2001) The spindle: a dynamic assembly of microtubules and motors. *Nat. Cell Biol.* **3**, E28-34.

3. Zhang, D., Rogers, G. C., Buster, D. W. & Sharp, D. J. (2007) Three microtubule severing enzymes contribute to the "Pacman-flux" machinery that moves chromosomes. *J. Cell Biol.* **177**, 231-242.

4. Hazan, J., Fonknechten, N., Mavel, D., Paternotte, C., Samson, D., Artiguenave, F., Davoine, C. S., Cruaud, C., Durr, A., Wincker, P., Brottier, P., Cattolico, L., Barbe, V., Burgunder, J. M., Prud'homme, J. F., Brice, A., Fontaine, B., Heilig, B. & Weissenbach, J. (1999) Spastin, a new AAA protein, is altered in the most frequent form of autosomal dominant spastic paraplegia. *Nat. Genet.* **23**, 296-303.

5. Errico, A., Ballabio, A. & Rugarli, E. I. (2002) Spastin, the protein mutated in autosomal dominant hereditary spastic paraplegia, is involved in microtubule dynamics. *Hum. Mol. Genet.* **11**, 153-163.

6. Cox, G. A., Mahaffey, C. L., Nystuen, A., Letts, V. A. & Frankel, W. N. (2000) The mouse fidgetin gene defines a new role for AAA family proteins in mammalian development. *Nat. Genet.* **26**, 198-202.

7. Frickey, T. & Lupas, A. N. (2004) Phylogenetic analysis of AAA proteins. *J. Struct. Biol.* **146**, 2-10.

8. McNally, F. J. & Vale, R. D. (1993) Identification of katanin, an ATPase that severs and disassembles stable microtubules. *Cell* **75**, 419-429.

9. Hartman, J. J., Mahr, J., McNally, K., Okawa, K., Iwamatsu, A., Thomas, S., Cheesman, S., Heuser, J., Vale, R. D. & McNally, F. J. (1998) Katanin, a microtubule-severing protein, is a novel AAA ATPase that targets to the centrosome using a WD40-containing subunit. *Cell* **93**, 277-287.

10. McNally, K. P., Bazirgan, O. A. & McNally, F. J. (2000) Two domains of p80 katanin regulate microtubule severing and spindle pole targeting by p60 katanin. *J. Cell Sci.* **113** (Pt 9), 1623-1633.

11. McNally, F. J., Okawa, K., Iwamatsu, A. & Vale, R. D. (1996) Katanin, the microtubule-severing ATPase, is concentrated at centrosomes. *J. Cell Sci.* **109** (Pt 3), 561-567.

12. McNally, F. J. & Thomas, S. (1998) Katanin is responsible for the M-phase microtubule-severing activity in Xenopus eggs. *Mol. Biol. Cell* **9**, 1847-1861.

13. Hartman, J. J. & Vale, R. D. (1999) Microtubule disassembly by ATP-dependent oligomerization of the AAA enzyme katanin. *Science* **286**, 782-785.

14. Lupas, A. N. & Martin, J. (2002) AAA proteins. *Curr. Opin. Struct. Biol.* **12**, 746-753.

15. Ogura, T. & Wilkinson, A. J. (2001) AAA$^+$ superfamily ATPases: common structure–diverse function. *Genes Cells* **6**, 575-597.

16. Stoppin-Mellet, V., Gaillard, J., Timmers, T., Neumann, E., Conway, J. & Vantard, M. (2007) Arabidopsis katanin binds microtubules using a multimeric microtubule-binding domain. *Plant Physiol. Biochem.* **45**, 867-877.

17. Iwaya, N., Goda, N., Unzai, S., Fujiwara, K., Tanaka, T., Tomii, K., Tochio, H., Shirakawa, M. & Hiroaki, H. (2007) Fine-tuning of protein domain boundary by minimizing potential coiled coil regions. *J. Biomol. NMR* **37**, 53-63.

18. Altschul, S. F., Madden, T. L., Schaffer, A. A., Zhang, J., Zhang, Z., Miller, W. & Lipman, D. J. (1997) Gapped BLAST and PSI-BLAST: a new generation of protein database search programs. *Nucleic. Acids Res.* **25**, 3389-3402.

19. Bateman, A., Birney, E., Cerruti, L., Durbin, R., Etwiller, L., Eddy, S. R., Griffiths-Jones, S., Howe, K. L., Marshall, M. & Sonnhammer, E. L. (2002) The Pfam protein families database. *Nucleic. Acids Res.* **30**, 276-280.

20. Bateman, A., Coin, L., Durbin, R., Finn, R. D., Hollich, V., Griffiths-Jones, S., Khanna, A., Marshall, M., Moxon, S., Sonnhammer, E. L., Studholme, D. J., Yeats, C. & Eddy, S. R. (2004) The Pfam protein families database. *Nucleic. Acids Res.* **32** Database issue, D138-D141.

21. Letunic, I., Copley, R. R., Schmidt, S., Ciccarelli, F. D., Doerks, T., Schultz, J., Ponting, C. P. & Bork, P. (2004) SMART 4.0: towards genomic data integration. *Nucleic. Acids Res.* **32** Database issue, D142-D144.

22. Tomii, K. & Akiyama, Y. (2004) FORTE: a profile-profile comparison tool for protein fold recognition. *Bioinformatics* **20**, 594-595.

23. Shi, J., Blundell, T. L. & Mizuguchi, K. (2001) FUGUE: sequence-structure homology recognition using environment-specific substitution tables and structure-dependent gap penalties. *J. Mol. Biol.* **310**, 243-257.

24. Ciccarelli, F. D., Proukakis, C., Patel, H., Cross, H., Azam, S., Patton, M. A., Bork, P. & Crosby, A. H. (2003) The identification of a conserved domain in both spartin and spastin, mutated in hereditary spastic paraplegia. *Genomics* **81**, 437-441.

25. Goda, N., Tenno, T., Takasu, H., Hiroaki, H. & Shirakawa, M. (2004) The PRESAT-vector: asymmetric T-vector for high-throughput screening of soluble protein domains for structural proteomics. *Protein Sci.* **13**, 652-658.

26. Yamazaki, T., Lee, W., Arrowsmith, C. H., Muhandiram, D. R. & Kay, L. E. (1994) A Suite of Triple Resonance NMR Experiments for the Backbone Assignment of $^{15}$N, $^{13}$C, $^{2}$H Labelled Proteins with High Sensitivity. *J. Am. Chem. Soc.* **116**, 11655-11666.

27. Cavanagh, J., Fairbrother, W. J., Palmer, A. G. III. & Skelton, N. J. (1996) *Protein NMR Spectroscopy: Principles and Practice,* Academic Press, San Diego, CA.

28. Delaglio, F., Grzesiek, S., Vuister, G. W., Zhu, G., Pfeifer, J. & Bax, A. (1995) NMRPipe: a multidimensional spectral processing system based on UNIX pipes. *J. Biomol. NMR* **6**, 277-293.

29. Goddard, T. D. & Kneller, D. G. (2004) *SPARKY 3,* University of California, San Francisco, CA.

30. Herrmann, T., Guntert, P. & Wuthrich, K. (2002) Protein NMR structure determination with automated NOE assignment using the new software CANDID and the torsion angle dynamics algorithm DYANA. *J. Mol. Biol.* **319**, 209-227.

31. Guntert, P. (2003) Automated NMR protein structure calculation. *Prog. Nuc. Magn. Reson. Spect.* **43**, 105-125.

32. Cornilescu, G., Delaglio, F. & Bax, A. (1999) Protein backbone angle restraints from searching a database for chemical shift and sequence homology. *J. Biomol. NMR* **13**, 289-302.

33. Koradi, R., Billeter, M. & Wuthrich, K. (1996) MOLMOL: a program for display and analysis of macromolecular structures. *J. Mol. Graph.* **14**, 29-32.

34. Laskowski, R. A., Rullmannn, J. A., MacArthur, M. W., Kaptein, R. & Thornton, J. M. (1996) AQUA and PROCHECK-NMR: programs for checking the quality of protein structures solved by NMR. *J. Biomol. NMR* **8**, 477-486.

35. Obita, T., Saksena, S., Ghazi-Tabatabai, S., Gill, D. J., Perisic, O., Emr, S. D. & Williams, R. L. (2007) Structural basis for selective recognition of ESCRT-III by the AAA ATPase Vps4. *Nature* **449**, 735-739.

36. Frohlich, K. U. (2001) An AAA family tree. *J. Cell Sci.* **114**, 1601-1602.

37. Holm, L. & Sander, C. (1997) Dali/FSSP classification of three-dimensional protein folds. *Nucleic. Acids Res.* **25**, 231-234.

38. Sherwood, N. T., Sun, Q., Xue, M., Zhang, B. & Zinn, K. (2004) Drosophila spastin regulates synaptic microtubule networks and is required for normal motor function. *PLoS. Biol.* **2**, e429.

39. Evans, K. J., Gomes, E. R., Reisenweber, S. M., Gundersen, G. G. & Lauring, B. P. (2005) Linking axonal degeneration to microtubule remodeling by Spastin-mediated microtubule severing. *J. Cell Biol.* **168**, 599-606.

40. Takasu, H., Jee, J. G., Ohno, A., Goda, N., Fujiwara, K., Tochio, H., Shirakawa, M. & Hiroaki, H. (2005) Structural characterization of the MIT domain from human Vps4b. *Biochem. Biophys. Res. Commun.* **334**, 460-465.

41. Scott, A., Gaspar, J., Stuchell-Brereton, M. D., Alam, S. L., Skalicky, J. J. & Sundquist, W. I. (2005) Structure and ESCRT-III protein interactions of the MIT domain of human VPS4A. *Proc. Natl. Acad. Sci. U S A* **102**, 13813-13818.

42. White, S. R., Evans, K. J., Lary, J., Cole, J. L. & Lauring, B. (2007) Recognition of C-terminal amino acids in tubulin by pore loops in Spastin is important for microtubule severing. *J. Cell Biol.* **176**, 995-1005.

43. Patel, H., Cross, H., Proukakis, C., Hershberger, R., Bork, P., Ciccarelli, F. D., Patton, M. A., McKusick, V. A. & Crosby, A. H. (2002) SPG20 is mutated in Troyer syndrome, an hereditary spastic paraplegia. *Nat. Genet.* **31**, 347-348.

44. Ravelli, R. B., Gigant, B., Curmi, P. A., Jourdain, I., Lachkar, S., Sobel, A. & Knossow, M. (2004) Insight into tubulin regulation from a complex with colchicine and a stathmin-like domain. *Nature* **428**, 198-202.

45. Slep, K. C. & Vale, R. D. (2007) Structural basis of microtubule plus end tracking by XMAP215, CLIP-170, and EB1. *Mol. Cell* **27**, 976-991.

46. Mishima, M., Maesaki, R., Kasa, M., Watanabe, T., Fukata, M., Kaibuchi, K. & Hakoshima, T. (2007) Structural basis for tubulin recognition by cytoplasmic linker protein 170 and its autoinhibition. *Proc. Natl. Acad. Sci. U S A* **104**, 10346-10351.

47. Guasch, A., Aloria, K., Perez, R., Avila, J., Zabala, J. C. & Coll, M. (2002) Three-dimensional structure of human tubulin chaperone cofactor A. *J. Mol. Biol.* **318**, 1139-1149.

48. Carter, A. P., Garbarino, J. E., Wilson-Kubalek, E. M., Shipley, W. E., Cho, C., Milligan, R. A., Vale, R. D. & Gibbons, I. R. (2008) Structure and functional role of dynein's microtubule-binding domain. *Science* **322**, 1691-1695.

49. Kikkawa, M. & Hirokawa, N. (2006) High-resolution cryo-EM maps show the nucleotide binding pocket of KIF1A in open and closed conformations. *EMBO J.* **25**, 4187-4194.

50. Nogales, E., Wolf, S. G. & Downing, K. H. (1998) Structure of the alpha beta tubulin dimer by electron crystallography. *Nature* **391**, 199-203.

51. Bodey, A. J., Kikkawa, M. & Moores, C. A. (2009) 9-Ångström structure of a microtubule-bound mitotic motor. *J. Mol. Biol.* **388**, 218-224.

52. Stuchell-Brereton, M. D., Skalicky, J. J., Kieffer, C., Karren, M. A., Ghaffarian, S. & Sundquist, W. I. (2007) ESCRT-III recognition by VPS4 ATPases. *Nature* **449**, 740-744.

53. Kieffer, C., Skalicky, J. J., Morita, E., De Domenico, I., Ward, D. M., Kaplan, J. & Sundquist, W. I. (2008) Two distinct modes of ESCRT-III recognition are required for VPS4 functions in lysosomal protein targeting and HIV-1 budding. *Dev. Cell* **15**, 62-73.

54. Toyo-Oka, K., Sasaki, S., Yano, Y., Mori, D., Kobayashi, T., Toyoshima, Y. Y., Tokuoka, S. M., Ishii, S., Shimizu, T., Muramatsu, M., Hiraiwa, N., Yoshiki, A., Wynshaw-Boris, A. & Hirotsune, S. (2005) Recruitment of katanin p60 by phosphorylated NDEL1, an LIS1 interacting protein, is essential for mitotic cell division and neuronal migration. *Hum. Mol. Genet.* **14**, 3113-3128.

55. Hanson, P. I., Roth, R., Lin, Y. & Heuser, J. E. (2008) Plasma membrane deformation by circular arrays of ESCRT-III protein filaments. *J. Cell Biol.* **180**, 389-402.

56. Nickerson, D. P., Russell, M. R. & Odorizzi, G. (2007) A concentric circle model of multivesicular body cargo sorting. *EMBO Rep.* **8**, 644-650.

57. Howard, J. & Hyman, A. A. (2003) Dynamics and mechanics of the microtubule plus end. *Nature* **422**, 753-758.

58. Yang, D., Rismanchi, N., Renvoise, B., Lippincott-Schwartz, J., Blackstone, C. & Hurley J. H. (2008) Structural basis for midbody targeting of spastin by the ESCRT-III protein CHMP1B. *Nat. Struct. Mol. Biol.* **15**, 1278-1286.

59. Sauer, R. T., Bolon, D. N., Burton, B. M., Burton, R. E., Flynn, J. M., Grant, R. A., Hersch, G. L., Joshi, S. A., Kenniston, J. A., Levchenko, I, Neher, S. B., Oakes, E. S., Siddiqui, S. M., Wah, D. A. & Baker, T. A. (2004) Sculpting the proteome with AAA(+) proteases and disassembly machines. *Cell* **119**, 9-18.

60. Lum, R., Tkach, J. M., Vierling, E. & Glover, J. R. (2004) Evidence for an unfolding/threading mechanism for protein disaggregation by Saccharomyces cerevisiae Hsp104. *J. Biol. Chem.* **279**, 29139-29146.

61. Roll-Mecak, A. & Vale, R. D. (2008) Structural basis of microtubule severing by the hereditary spastic paraplegia protein spastin. *Nature* **451**, 363-367.

62. Thompson, J. D., Gibson, T. J., Plewniak, F., Jeanmougin, F. & Higgins, D. G. (1997) The CLUSTAL_X windows interface: flexible strategies for multiple sequence alignment aided by quality analysis tools. *Nucleic. Acids Res.* **25**, 4876-4882.

63. Armon, A., Graur, D. & Ben-Tal, N. (2001) ConSurf: an algorithmic tool for the identification of functional regions in proteins by surface mapping of phylogenetic information. *J. Mol. Biol.* **307**, 447-463.

# CHAPTER 3

# Effect of Ca$^{2+}$ on the Microtubule-severing Enzyme P60-katanin: Insight into the Substrate-dependent Activation Mechanism

## Abstract

Katanin p60 (p60-katanin) is a microtubule (MT)-severing enzyme and its activity is regulated by p80 subunit (adaptor-p80). P60-katanin consists of an N-terminal domain, followed by a single AAA domain. We have previously shown that the N-terminal domain serves as the binding site for MT, the substrate of p60-katanin. In this study, we show that the same domain shares another interface with the C-terminal domain from adaptor-p80. We further show that $Ca^{2+}$ ion inhibits the MT-severing activity of p60-katanin, whereas the MT-binding activity is preserved in the presence of $Ca^{2+}$. In detail, the basal ATPase activity of p60-katanin is stimulated 2-fold by both MTs and the C-terminal domain of adaptor-p80, whereas $Ca^{2+}$ reduces the elevated ATPase activity to the basal level. We identify the $Ca^{2+}$-binding site at the end of helix 2 of the N-terminal domain, which is different from the MT-binding interface. On the basis of these observations, we propose a model in which possible spatial rearrangement of the N-terminal domain relative to the C-terminal AAA domain may be important for productive ATP hydrolysis towards MT-severing. Our model can explain how $Ca^{2+}$ regulates both its severing and ATP hydrolysis activity, since the $Ca^{2+}$-binding site on the N-terminal domain moves close to the AAA domain during MT-severing.

## Introduction

Katanin, spastin, and fidgetin are major three microtubule (MT)-severing enzymes[1-5]. Katanin is a heterodimeric ATPase composed of two subunits, p60 (p60-katanin) and p80 (adaptor-p80). P60-katanin is the catalytic factor responsible for breaking MTs in an ATP-dependent manner, and contains a single AAA domain. Adaptor-p80 is a regulatory factor containing six WD40 repeats, and is not essential for severing activity (Fig. 1)[6,7]. The MT-severing function of katanin is specific in the cell types and cell cycles. For example, katanin promotes mitosis in proliferating cells, where it severs MTs at the mitotic spindle poles and increases the number of minus ends, thereby resulting in accumulation of γ-tubulin at the mitotic centrosomes[8]. On the other hand, katanin exhibits severing activity of the metaphase spindles at the spindle poles[9].

Recently, MT-severing by katanin in neuronal cells has drawn increased attentions, owing to its contribution to neurite outgrowth and implications in neurodegenerative diseases. In nascent neurons, it seems critical that the MTs are chopped by katanin at the cell body prior to being translocated into axons; subsequently, the chopped MT fragments disassemble into tubulin dimers that reassemble into long MTs again[10]. In contrast, excessive MT-severing by exogenous overexpression of p60-katanin results in shortening of the total process length of MTs in hippocampal neuron[11]. In a model of neurodegenerative disease, MT breakdown by katanin triggers the loss of neurite spikes but not apoptosis of neurons, while the MT-associated protein (MAP), tau may function as the protectant of MTs against attack by katanin[12]. Thus, the mechanism of p60-katanin regulation by adaptor-p80 or other factors such as tau in various cells and tissues, and at different developmental stages, is an important and unresolved issue.

We have previously shown that the mechanism of substrate recognition is evolutionarily conserved between p60-katanin and its related AAA ATPase Vps4[13,14]. Vps4 is responsible for the dissociation of membrane skeleton ESCRT-III fibrils. Note that p60-katanin and Vps4 share a

common domain organization typical of type I AAA-ATPases, which consists of an N-terminal substrate-binding region, followed by a single AAA domain at the C-terminus. Despite the low (~20%) amino acid identity, we have shown that the 3D structure of the N-terminal domain of p60-katanin is strikingly similar to that of the MIT (microtubule interacting and trafficking) domain of Vps4 and other MIT domains. Therefore, we named this domain "variant MIT" (vMIT) domain. Helices 2 and 3 of p60-vMIT make up the interface with MTs, which is similar to the interface that Vps4-MIT makes with its substrate ESCRT-III[14]. We further predicted that the binding site for p60-katanin in MTs is located at helix 12 of the α-tubulin subunit. Interestingly, this helix was recently proposed as the binding site for tau[15]. On the basis of our structural model of the p60-MT complex, competition between tau and katanin may occur at this twelfth helix of α-tubulin. This unexpected coincidence is, however, consistent with the hypothesis proposed by Baas *et al.*, in which the physiological role of tau is to protect the MT bundle in axons against the MT-severing activity of p60-katanin[12]. Sudo *et al.* has recently proposed this competition between tau (MT-stabilizing) and katanin (MT-severing) as a new therapeutic target for dementia and other neurodegenerative diseases[16].

In this study, we focused on the role of the vMIT domain in regulating the ATPase activity of p60-katanin in detail. It is known that either MT (substrate) alone or MT + p80 (adaptor) enhances the ATPase activity of p60-katanin[6,17,18], although the underlying molecular mechanism remains unclear. We therefore hypothesized that substrate/adaptor-dependent ATPase activation originates from p60-vMIT by a change in the location of this domain relative to the AAA domain. During the course of biochemical studies, we found that $Ca^{2+}$ ions inhibit the MT-severing activity of p60-katanin. Furthermore, we found that $Ca^{2+}$ directly affects the vMIT domain and then cancels the elevated ATPase activity of p60-katanin that occurs in the presence of either MT or the C-terminal domain of adaptor-p80 (p80-CTD). Given that $Ca^{2+}$ is a key intracellular signal that regulates indirectly MT stability, as well as rearranging the cytoskeleton *in vivo*, we further discuss
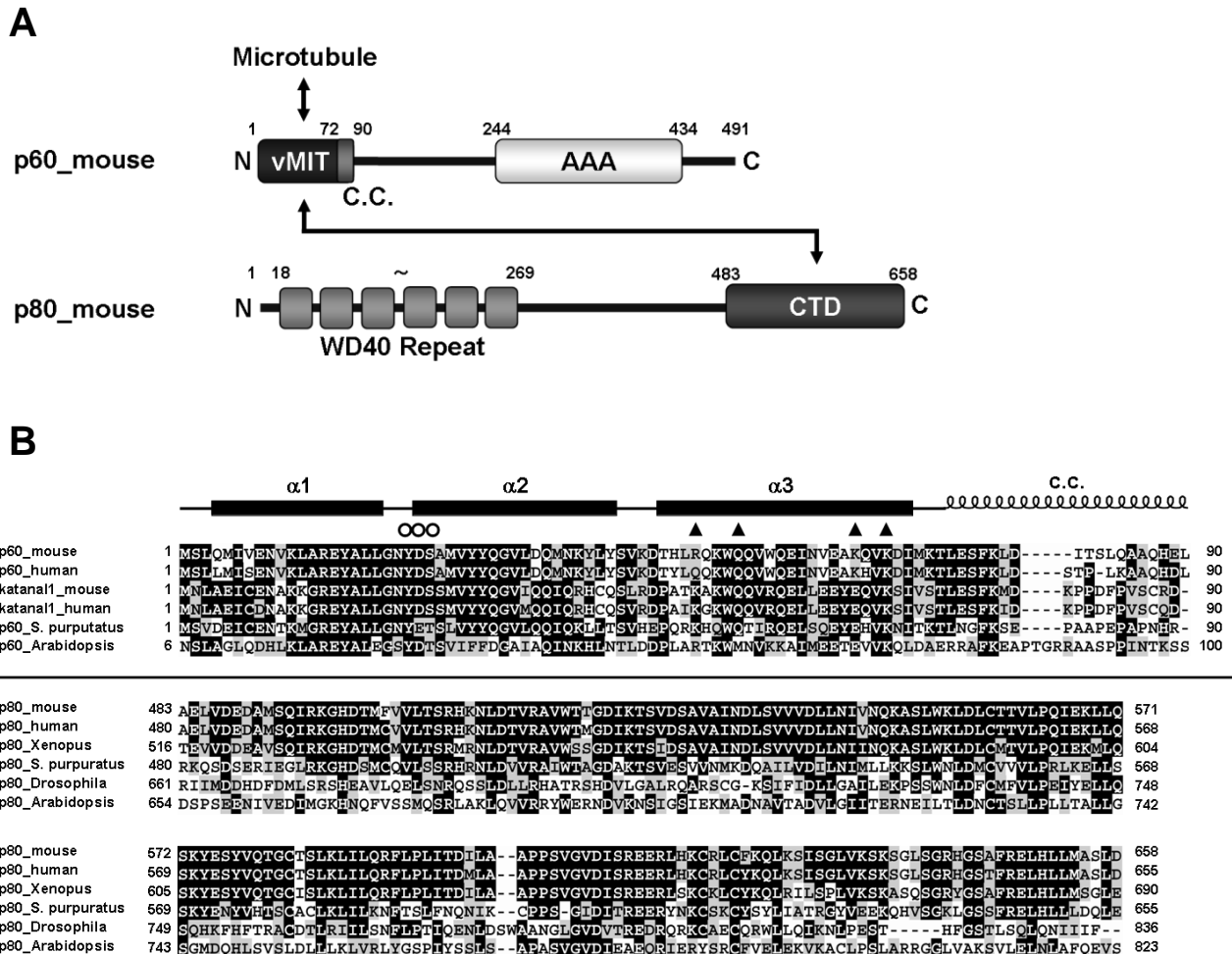
the physiological implications of this finding.



FIGURE 1. **Domain architectures and multiple sequence alignment of p60-katanin and adaptor-p80.** (A) Domain architectures of mouse p60-katanin and adaptor-p80. The regions of interaction between each domain are indicated by an arrow. vMIT, variant MIT domain; c.c., coiled-coil; AAA, AAA domain; CTD, C-terminal domain. (B) Multiple sequence alignment of p60-vMIT and p80-CTD, which interact with each other. The secondary structure elements of p60-vMIT are shown at the top. Filled triangles indicate residues involved in tubulin binding. Open circles indicate residues involved in Ca$^{2+}$ binding (see Fig. 9). The protein names and UniProtKB accession numbers are as follows: p60 mouse (Q9WV86), p60 human (O75449), katanal1 mouse (Q8K0T4), katanal1 human (Q9BW62), p60 *Strogylocentrotus purpuratus* (O61577), p60 *Arabidopsis* (Q9SEX2), p80 mouse (Q8BG40), p80 human (Q9BVA0), p80 *Xenopus* (Q4V7Y7), p80 *Strogylocentrotus purpuratus* (O61585), p80 *Drosophila* (Q9NHF0), and p80 *Arabidopsis* (Q8H0T9). The sequence alignment was generated by ClustalX[45].

## Results

### *P80-CTD interacts with helix 1 of p60-vMIT*

Previous biochemical studies by McNally *et al.*[7,19] showed that the N-terminal half of p60-katanin interacts with the C-terminal half of adaptor-p80, and in our previous study we showed from the 3D structure of p60-vMIT that the MT interface of p60-vMIT is located on the surface of helix 2/3. Here, therefore, we first examined the amino acid sequence of adaptor-p80 to identify the boundary of its C-terminal p60-binding domain. Fig. 1 summarizes the domain organization of p60-katanin and adaptor-p80, and presents multiple sequence alignments of the two domains (p60-vMIT and p80-CTD) that interact with each other. Both subunits are genetically conserved among many higher eukaryotes. We identified the minimum structural domain of p80-CTD as residues 480–655 and succeeded in isolating this domain.

Next, we determined the interface between p60-vMIT and p80-CTD by $^1$H-$^{15}$N HSQC experiments. The binding of p80-CTD induced drastic line broadening of NH signals from $^{15}$N-labeled p60-vMIT (Fig. 2A; Fig. 3). Mapping of the broadened signals upon binding to p80-CTD suggested that a wide area covering the surface of helices 1/2 and helices 1/3 of p60-vMIT might form the binding site for p80-CTD (Fig. 2B; Table 1). We further examined the key residues involved in p80-binding by using Ala-substituted mutants of p60-vMIT in an *in vitro* pull-down assay (Fig. 2C). Wild-type p60-vMIT bound to p80-CTD in nearly a 1 to 1 ratio, as judged from the density of the bands in SDS-PAGE (Fig. 2C, lanes 3 and 14). All Ala mutants also showed similar binding to p80-CTD. Therefore, we assumed that a polar single mutation does not completely inhibit the interaction between p60-vMIT and p80-CTD, probably because the interface is multivalent and covers a wide area including helix 1.
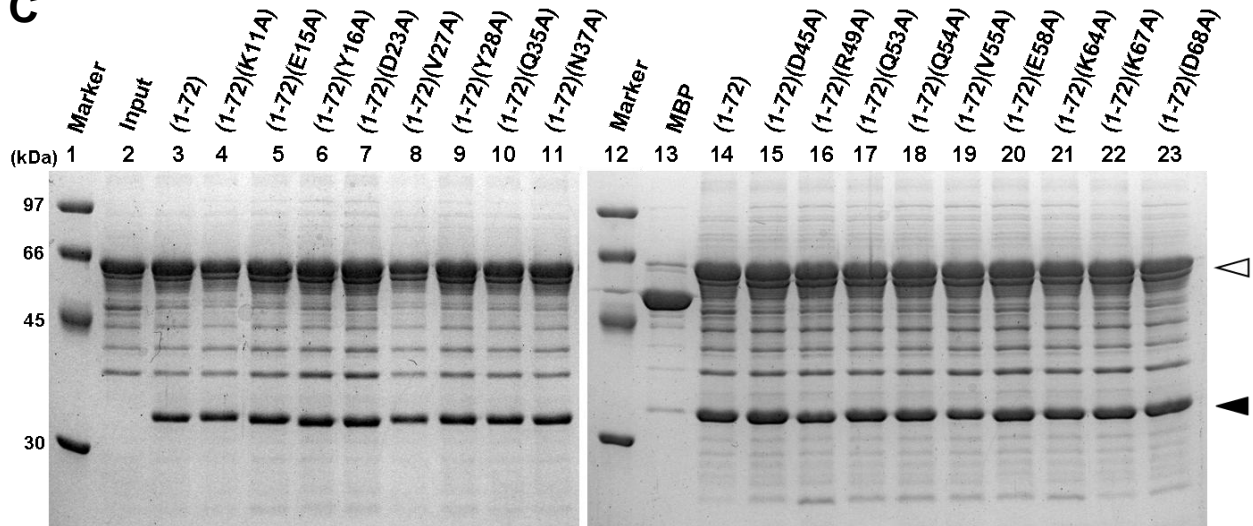
**A**



**B**



**C**
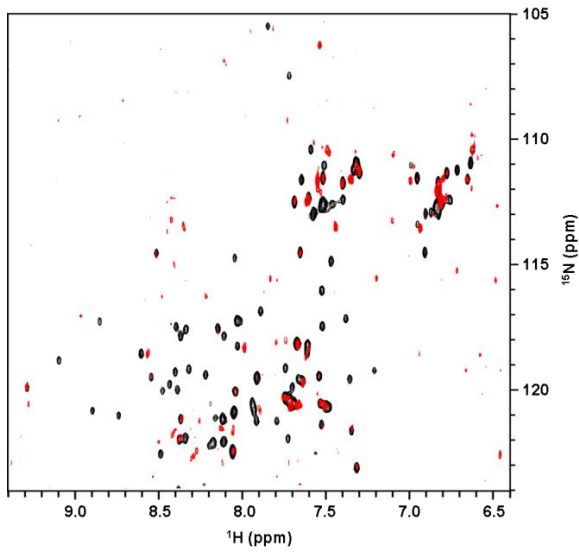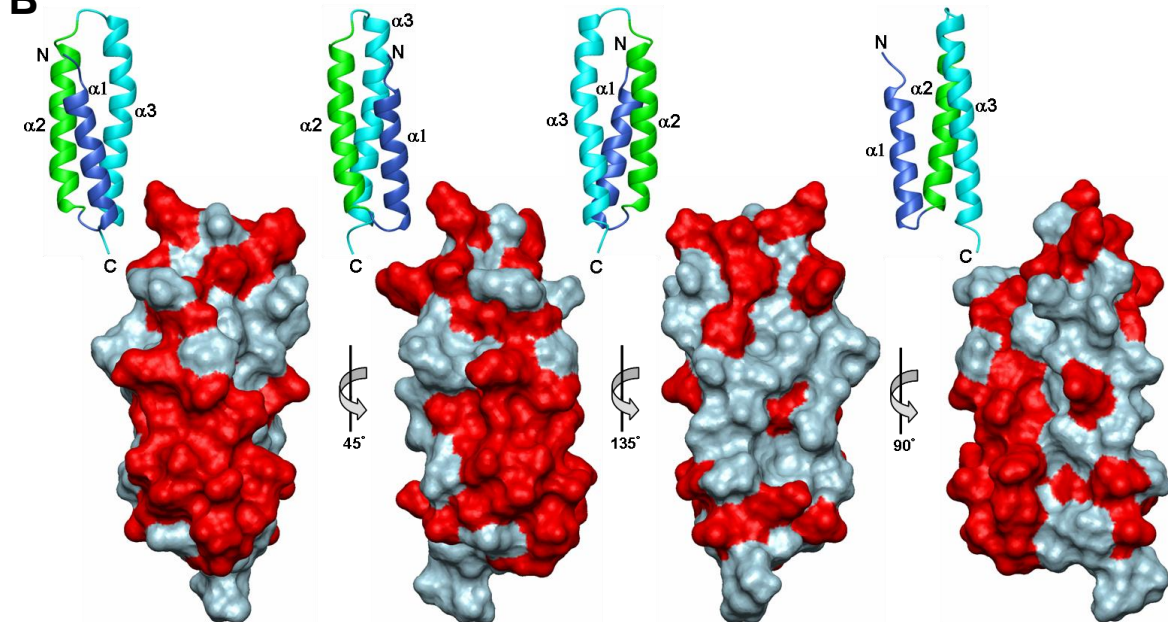
FIGURE 2. **Analyses of the interaction between p60-vMIT and p80-CTD.** (A) $^1$H-$^{15}$N HSQC spectra of p60-vMIT in the absence (black) and presence (red) of p80-CTD. (B) Residues whose NH signals of p60-vMIT were broadening in the presence of p80-CTD are mapped on the surface in red. Orientations of the surface are shown by the ribbon diagram of p60-vMIT (PDB: 2rpa). The residues in helix 1 had mostly eliminated from the $^1$H-$^{15}$N HSQC spectra, because those regions are involved in binding to p80-CTD. (C) Pull-down assays of MBP-tagged p80-CTD with GST-tagged p60-vMIT (wild-type and Ala mutants) *in vitro*. MBP-tagged p80-CTD was used as the input. Molecular sizes are shown in lanes 1 and 12. MBP was used as a negative control (lane 13). Recombinant proteins used for pull-down are indicated at the top of the gel. Filled and open arrowheads show MBP-tagged p80-CTD and GST-tagged p60-vMITs, respectively. The SDS-PAGE gel was stained with Coomassie blue.
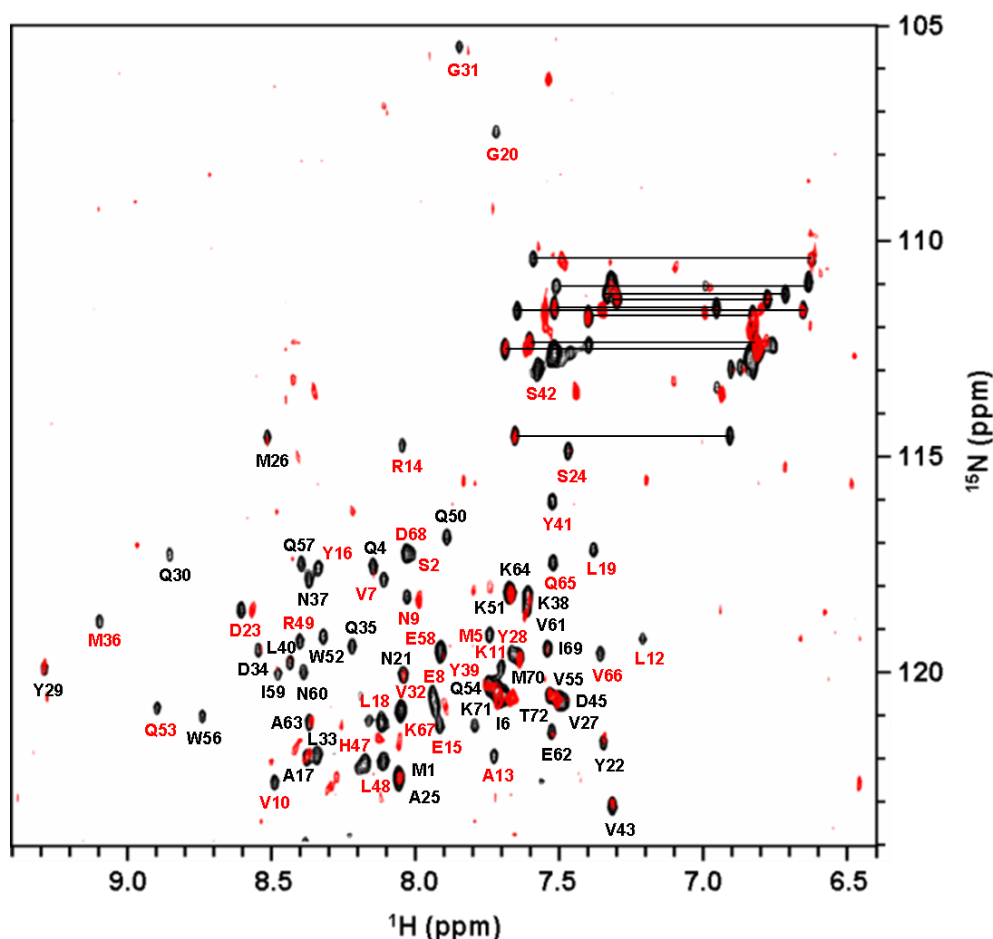


FIGURE 3. **$^1$H-$^{15}$N HSQC spectra of p60-vMIT in the absence (black) and presence (red) of p80-CTD.** Residues whose NH signals of p60-vMIT were broadening in the presence of p80-CTD are shown in red.

TABLE 1. **The broadened signals of ^{15}N-labeled p60-vMIT in the presence of p80-CTD.**

| loop 1 | helix 1 | loop 1-2 | helix 2 | loop 2-3 | helix 3 |
|--------|---------|----------|---------|----------|---------|
| S2     | M5      | G20      | D23     | S42      | T46     |
| L3     | V7      |          | S24     | K44      | H47     |
|        | E8      |          | Y28     |          | L48     |
|        | N9      |          | G31     |          | R49     |
|        | V10     |          | V32     |          | Q53     |
|        | K11     |          | L33     |          | E58     |
|        | L12     |          | M36     |          | Q65     |
|        | A13     |          | Y39     |          | V66     |
|        | R14     |          | Y41     |          | K67     |
|        | E15     |          |         |          | D68     |
|        | Y16     |          |         |          |         |
|        | L18     |          |         |          |         |
|        | L19     |          |         |          |         |

***Binding of either MT or p80-CTD to p60-vMIT stimulates the ATPase activity of p60-katanin***

The ATPase activity of sea urchin and plant p60-katanin is stimulated by MTs alone, or both MTs and adaptor-p80[6,17,18]. In addition, the MT-severing activity of p60-katanin is stimulated by p80/con80 (412-655), according to a DAPI assay[6,7,18,20]. Here, we performed experiments using mammalian full-length p60-katanin and p80-CTD, the domain that we isolated above. We investigated the ability of p60-katanin to hydrolyze ATP in the presence of either MTs or p80-CTD *in vitro* (Fig. 4). Under both conditions, the basal ATPase activity of p60-katanin was stimulated by MTs or p80-CTD in a concentration-dependent manner. In the presence of MTs, stimulation of the ATPase activity of p60-katanin reached almost a maximum at 0.5 μM MTs, corresponding to a p60/MTs molar ratio of 0.8. We also found that the ATPase activity of p60-katanin is stimulated by the addition of p80-CTD alone. Stimulation of the ATPase activity of p60-katanin reached almost a

maximum at 0.4 μM p80-CTD, corresponding to a p60/p80-CTD molar ratio of 1.0. A similar extent of stimulation of p60-katanin was observed in the presence of both MTs and p80-CTD (Fig. 5). These results show that binding of either MTs or p80-CTD to the N-terminal domain of p60-katanin stimulates the basal ATPase activity of p60-katanin. In other words, p60-vMIT serves as a sensory regulator for the ATPase activity of p60-AAA.
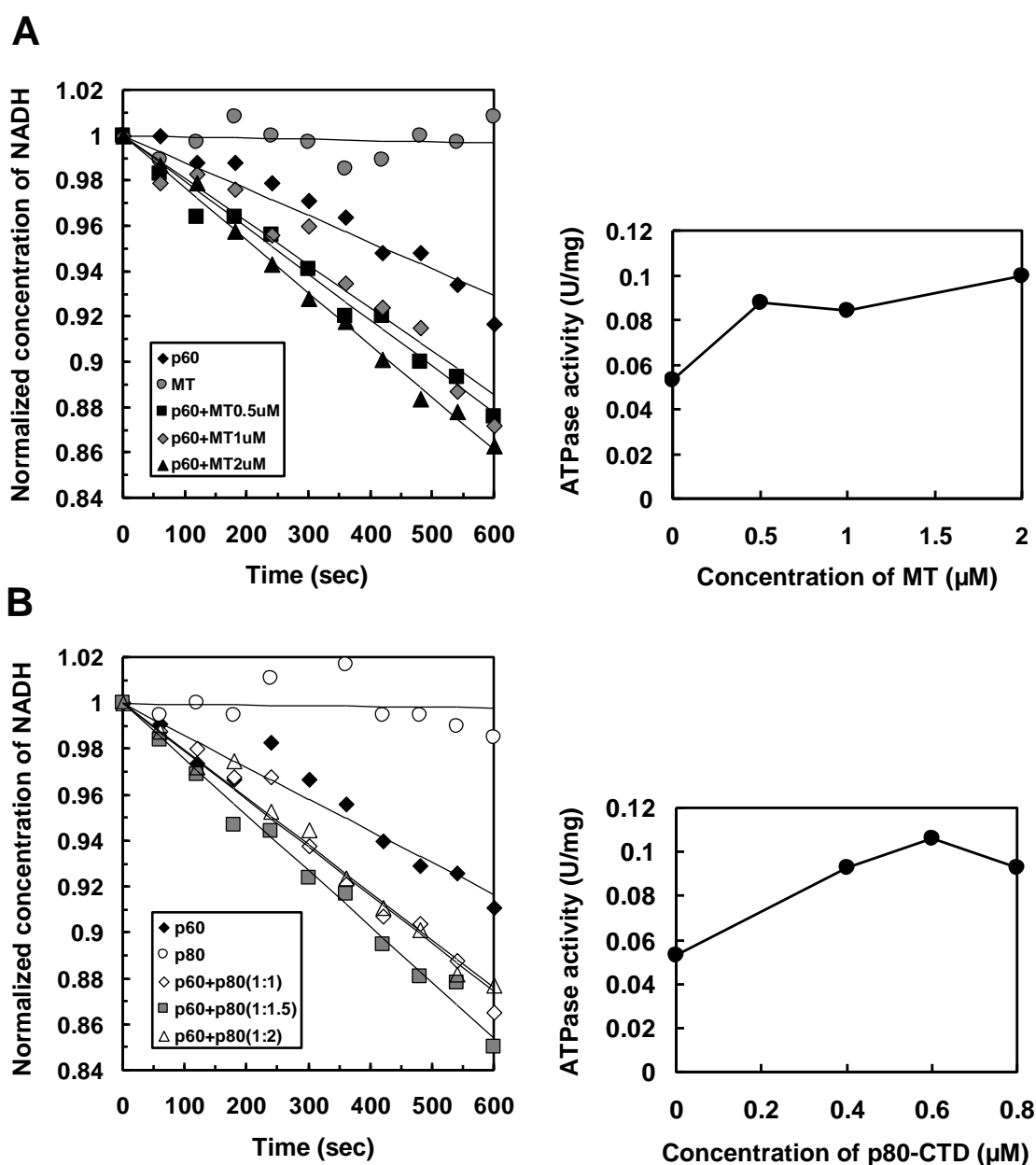
**A**



**B**

FIGURE 4. **ATPase activity of full-length p60-katanin is stimulated in the presence of MT or p80-CTD.** (A) ATPase activity of p60-katanin (0.4 μM) was monitored at 340 nm in the absence (black diamond) or presence of 0.5 μM (black square), 1 μM (gray diamond), and 2 μM (black triangle) of taxol-stabilized MTs (left). Gray circle indicates taxol-stabilized MTs (1 μM) without p60-katanin. ATPase activity was further expressed as μmoles of ATP hydrolyzed per min per mg of p60-katanin (units/mg) in 0, 0.5, 1, and 2 μM of taxol-stabilized MTs (right). (B) ATPase activity of p60-katanin (0.4 μM) was monitored at 340 nm in the absence (black diamond) or presence of 0.4 μM (open diamond), 0.6 μM (gray square), and 0.8 μM (open triangle) of p80-CTD (left). Open circle indicates p80-CTD (0.4 μM) without p60-katanin. ATPase activity was further expressed as μmoles of ATP hydrolyzed per min per mg of p60-katanin (units/mg) in 0, 0.4, 0.6, and 0.8 μM of p80-CTD (right).
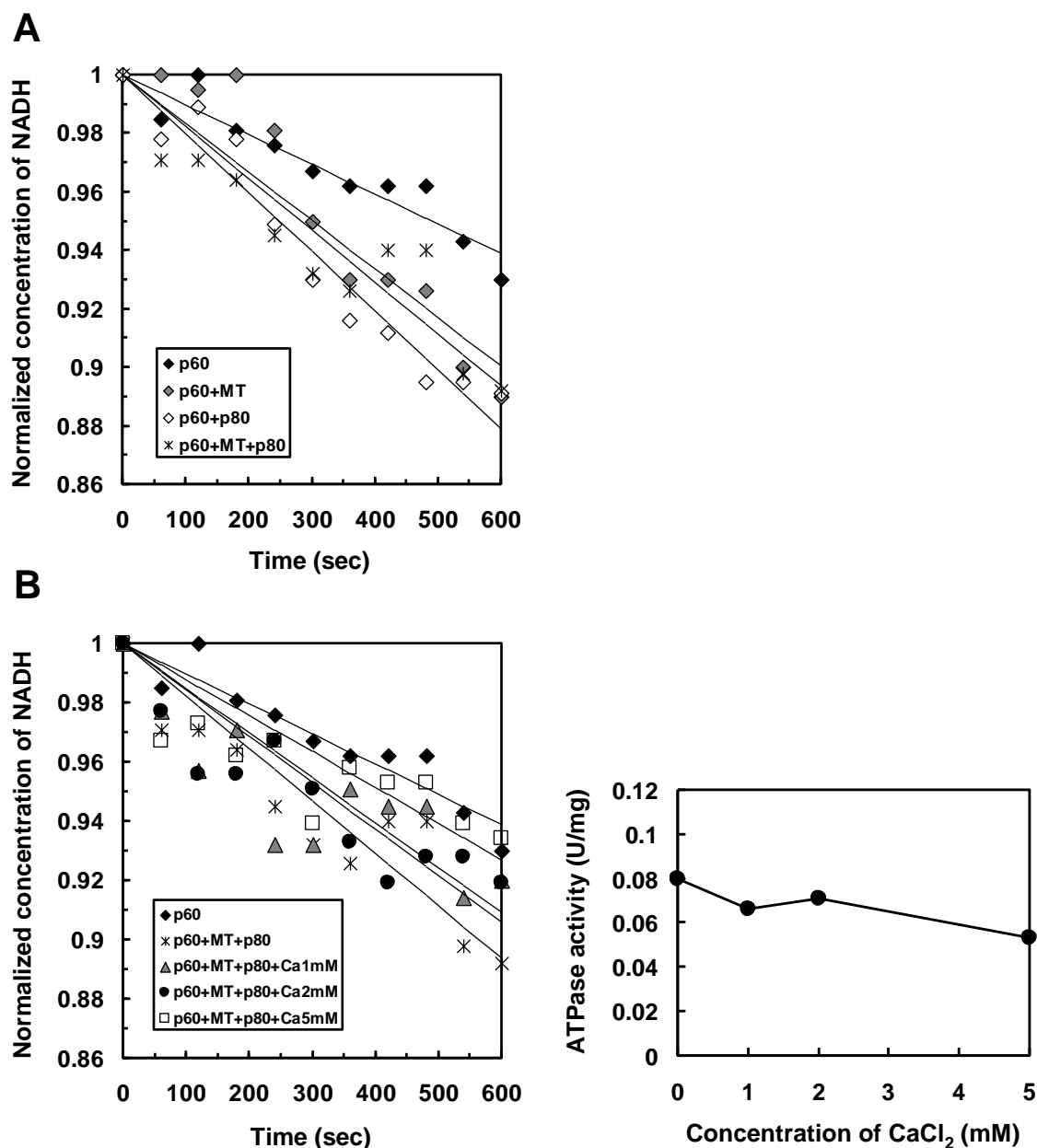
FIGURE 5. **ATPase activity of full-length p60-katanin in the presence of MT, p80-CTD, and increasing concentrations of Ca$^{2+}$.** (A) ATPase activity of p60-katanin (0.4 µM) was monitored at 340 nm in the absence (black diamond) and presence of 1 µM taxol-stabilized MTs (gray diamond), 0.4 µM p80-CTD (open diamond), or both (asterisk). (B) The ATPase activity of p60-katanin (0.4 µM) + taxol-stabilized MTs (1 µM) + p80-CTD (0.4 µM) was monitored at 340 nm in the presence of increasing Ca$^{2+}$ concentrations: 1 mM (gray triangle), 2 mM (black circle), and 5 mM (open square) (left). ATPase activity in presence of MTs and p80-CTD was further expressed as µmoles of ATP hydrolyzed per min per mg of p60-katanin (units/mg) in 0, 1, 2, and 5 mM of Ca$^{2+}$ (right).

## Ca$^{2+}$ negatively regulates the ATPase activity enhanced by MT or p80-CTD

Next, we examined the effect of Ca$^{2+}$ on the ATPase activity of p60-katanin. Interestingly, we found that Ca$^{2+}$ reduced the increase in ATPase activity induced by MTs or p80-CTD to the basal level (Fig. 6). The basal ATPase activity of p60-katanin in the absence of MTs or p80-CTD was not affected by Ca$^{2+}$ (Fig. 6A), even in a higher concentration such as 10 mM (data not shown). In the presence of MTs, however, the ATPase activity of p60-katanin decreased as the Ca$^{2+}$ concentration increased, finally dropping to the basal level at 5 mM Ca$^{2+}$ (Fig. 6B). A similar tendency was observed in the presence of p80-CTD, where the ATPase activity dropped to the basal level at 2 mM Ca$^{2+}$ (Fig. 6C). These results suggest that Ca$^{2+}$ regulates a putative On/Off mechanism for the ATPase activity of p60-katanin, which may be associated with either the vMIT or AAA domain.

FIGURE 6. Substrate-/adapter-stimulated ATPase activity of full-length p60-katanin is suppressed in the presence of Ca$^{2+}$. (A) ATPase activity of p60-katanin (0.4 µM) (black diamond) was monitored at 340 nm with increasing Ca$^{2+}$ concentrations: 1 mM (gray triangle), 2 mM (black circle), and 5 mM (open square) (left). ATPase activity was further expressed as µmoles of ATP hydrolyzed per min per mg of p60-katanin (units/mg) in 0, 1, 2, and 5 mM of Ca$^{2+}$ (right). (B, C) ATPase activity of p60-katanin (0.4 µM) + taxol-stabilized MTs (1 µM) (gray diamond) (B) or p60-katanin (0.4 µM) + p80-CTD (0.4 µM) (open diamond) (C) was monitored at 340 nm with increasing Ca$^{2+}$ concentrations: 1 mM (gray triangle), 2 mM (black circle), and 5 mM (open square) (left). ATPase activity in presence of MTs or p80-CTD was further expressed as µmoles of ATP hydrolyzed per min per mg of p60-katanin (units/mg) in 0, 1, 2, and 5 mM of Ca$^{2+}$ (right).
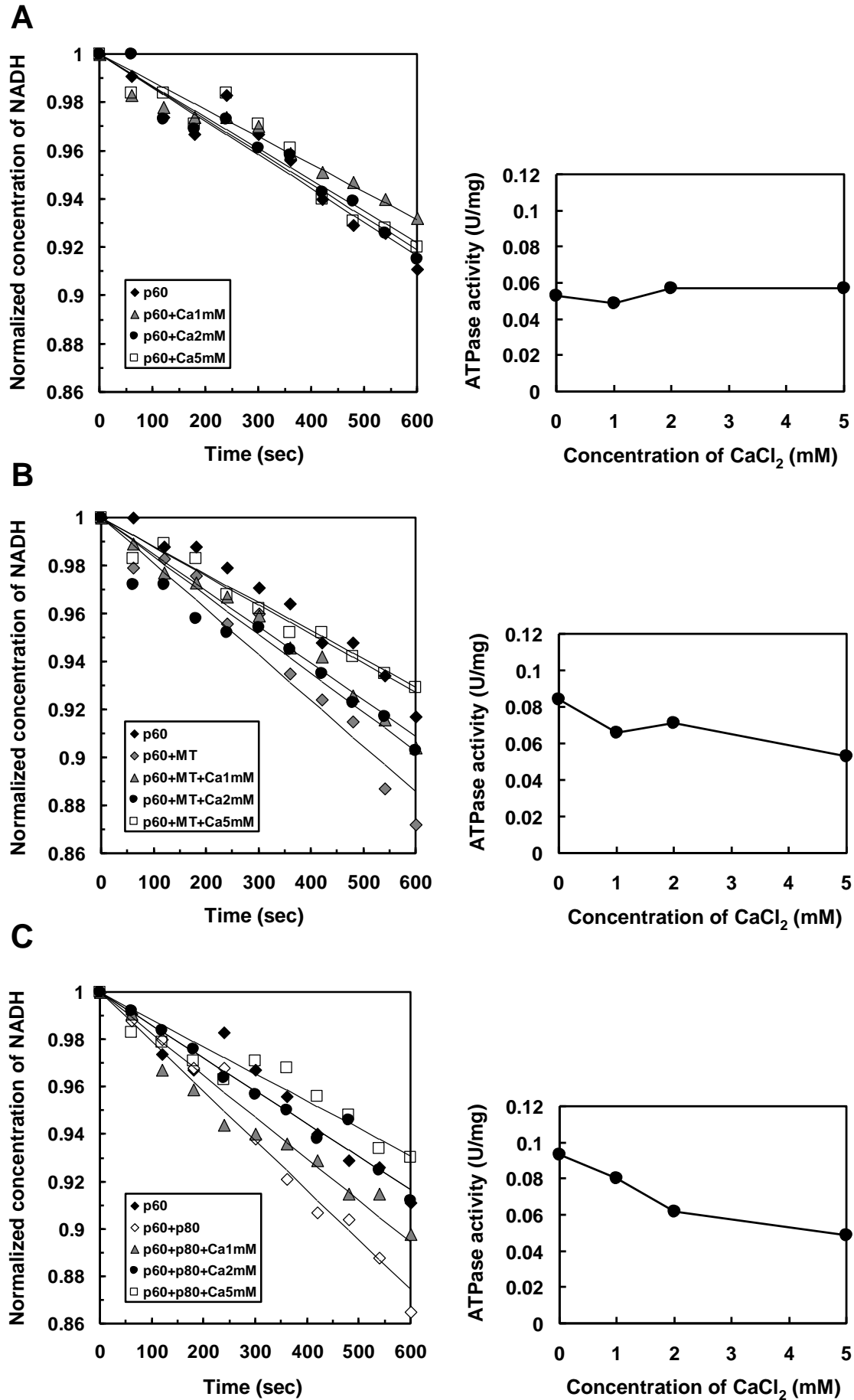
## *Ca²⁺ inhibits the MT-severing activity of p60-katanin, but does not inhibit its binding to MTs*

The dynamics of the polymerization–depolymerization of MTs is called "dynamic instability"[21]. Growing MTs suddenly start depolymerizing rapidly, known as a "catastrophe." However, shortening MTs often are "rescued" and start polymerizing again[22]. *In vitro*, higher concentrations of $Ca^{2+}$ in the mM range induce destabilization of MTs[23,24]; therefore, $Ca^{2+}$ has been used for biochemical experiments to inhibit the polymerization or to induce the depolymerization of MTs. Fig. 7A shows the effects of $Ca^{2+}$ on the interaction between full-length p60-katanin and MTs by a co-sedimentation assay. We then quantified a normalized amount of the degraded tubulin fragments from taxol-stabilized MTs (Fig. 7B, left) and p60-katanin co-sedimented with the remaining MT filaments (Fig.7B, right). In the absence of p60-katanin, marked depolymerization of MT was observed in a $Ca^{2+}$-dependent manner, probably caused by a catastrophe effect[24] (Fig. 7A, lanes 2–7; Fig. 7B, left). In the presence of wild-type p60-katanin, most of the MTs were severed by p60-katanin (Fig. 7A, lanes 8–11; Fig. 7B, left). However, MT-severing by p60-katanin was mostly inhibited by the presence of 10 mM $Ca^{2+}$ (Fig. 7A, lanes 12 and 13; Fig. 7B, left). We observed a partial inhibition in the presence of 5 mM $Ca^{2+}$ in multiple independent experiments (data not shown), thus we concluded that 5 mM of $Ca^{2+}$ is an approximate threshold concentration of inhibition of MT-severing.

We further examined the MT-binding activity of p60-katanin using a K255A mutant, which lacks ATPase activity (data not shown). K255A bound to MTs regardless of $Ca^{2+}$ concentration (Fig. 7A, lanes 14–19; Fig. 7B, right). Furthermore, K255A might stabilize MTs, because the $Ca^{2+}$-dependent catastrophe of MTs was suppressed (Fig. 7A, left, lanes 14–19; Fig. 7B, left). Recently, McNally *et al.*[19] showed that ATPase-deficient katanin promoted the assembly of meiotic spindles. Our observation of K255A is partially consistent with their result. Additionally, we examined the MT-binding activity of p60-katanin with ADP in the absence of $Mg^{2+}$. P60-katanin with ADP bound to MTs regardless of $Ca^{2+}$ concentration without MT-severing (Fig. 7A, right panel). Taken together,

we concluded that Ca$^{2+}$ inhibits the MT-severing activity of p60-katanin without affecting its MT-binding activity.
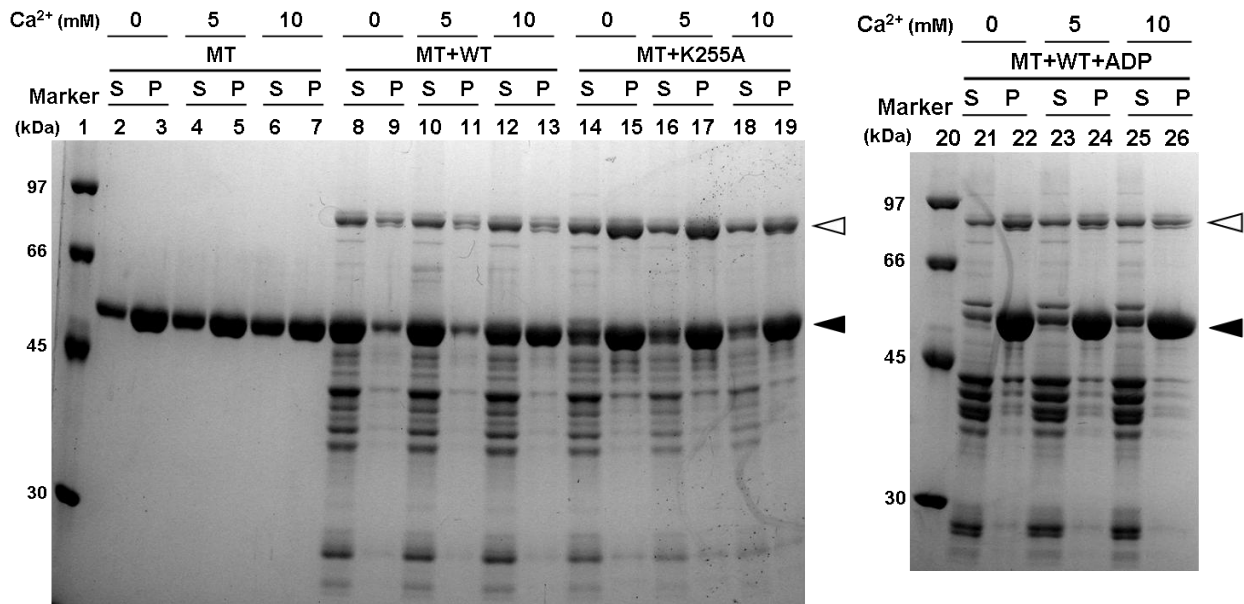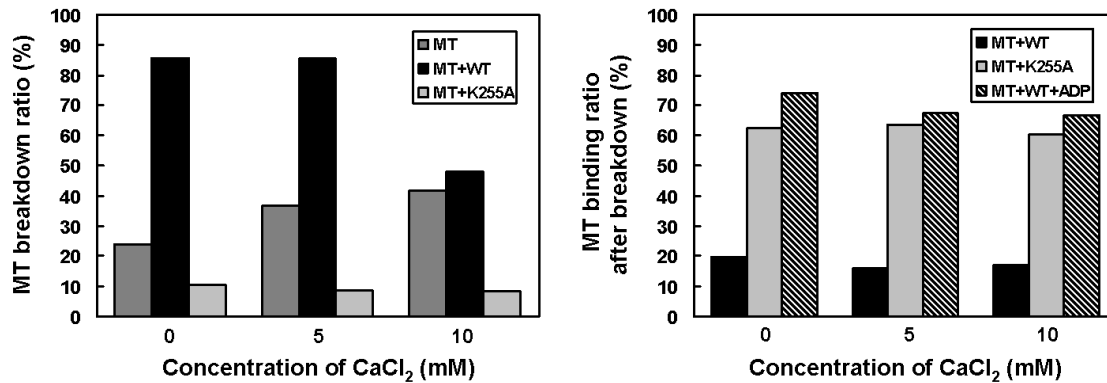


FIGURE 7. **Effects of Ca$^{2+}$ on full-length p60-MT interactions.** (A) *In vitro* MT co-sedimentation assay performed with increasing Ca$^{2+}$ concentrations (0–10 mM) using GST-tagged p60-katanin (wild-type and K255A mutant) in the presense of ATP (left) or using GST-tagged p60-katanin (wild-type) in the presense of ADP without Mg$^{2+}$ (right). Taxol-stabilized MTs and associated p60-katanin were separated from depolymerized tubulin and unbound p60-katanin by sedimentation in a glycerol cushion buffer. P and S represent the pellet fraction and the supernatant fraction, respectively. Molecular sizes are shown in lane 1. Open and filled arrowheads indicate GST-tagged p60-katanin and tubulin, respectively. The SDS-PAGE gel was stained with Coomassie blue. (B) Quantitative analysis of degraded tubulin fragments from taxol-stabilized MTs (left panel) and p60-katanin fragments binding to MT after degradation (right panel). Signals corresponding to the MT/tubulin and p60-katanin fragments in (A) were integrated and normalized by their molecular weights, using ImageJ.

## $Ca^{2+}$ directly binds to p60-vMIT different from the interface with MT

With the aim of obtaining information on the possible involvement of metal ions in the action mechanism of p60-vMIT, we examined its interaction with $Ca^{2+}$ as well as $Ce^{3+}$ as an ideal paramagnetic probe for $Ca^{2+}$ (Fig. 8, Fig. 9A; Fig. 10A)[25,26]. NMR titration analyses of p60-vMIT in various $Ca^{2+}$ concentrations are shown in Fig. 8. In the case of $Ca^{2+}$, the residues showing a major chemical shift perturbation were V66, I69, and K71. Since these residues are adjacent to the C-terminus of p60-katanin vMIT domain (residues 1-72), this binding site is assumed as an artifact of the use of the engineered domain-only construct. When using paramagnetic $Ce^{3+}$ to enhance the chemical shift changes upon metal binding, the residues showing a large change, D23 and S24, were additionally found. Then, we succeeded in determination of this $Ce^{3+}$ binding site by an analysis of pseudocontact shifts due to $Ce^{3+}$ (Fig. 10B). The metal was chelated close to D23 and S24. From these result, we assumed that D23 and S24, which are evolutionarily conserved among many higher eukaryotes, form the binding site of $Ca^{2+}$. This $Ca^{2+}$-binding site differs from the putative interface between p60-vMIT and tubulin/MT, and so is consistent with our observation that $Ca^{2+}$ did not inhibit MT-binding.

From the structural model of the p60–MT complex, we hypothesized that the $Ca^{2+}$-binding site is close to the putative interface between the vMIT domain and hexameric AAA ATPase domains (Fig. 9B and C; Fig. 11), enabling us to propose a model of the regulatory role of the vMIT domain in MT-severing (Fig. 12). P60-katanin may form a putative ring-shaped hexamer, as indicated by Hartman *et al.*[17]. We assumed that hexameric p60-katanin possesses flexible linkers between the vMIT and the AAA domains, and may move over MTs using them freely. In the absence of $Ca^{2+}$, the ATPase activity of p60-katanin is elevated upon binding to an MT through a contact between the vMIT domain and the AAA domain. The enhanced activity of p60-katanin may lead to MT-severing. After the reaction, p60-katanin is released from the MT and goes back to the basal state. In the presence of $Ca^{2+}$, by contrast, p60-katanin does not adopt the activated state regardless of MT-binding.
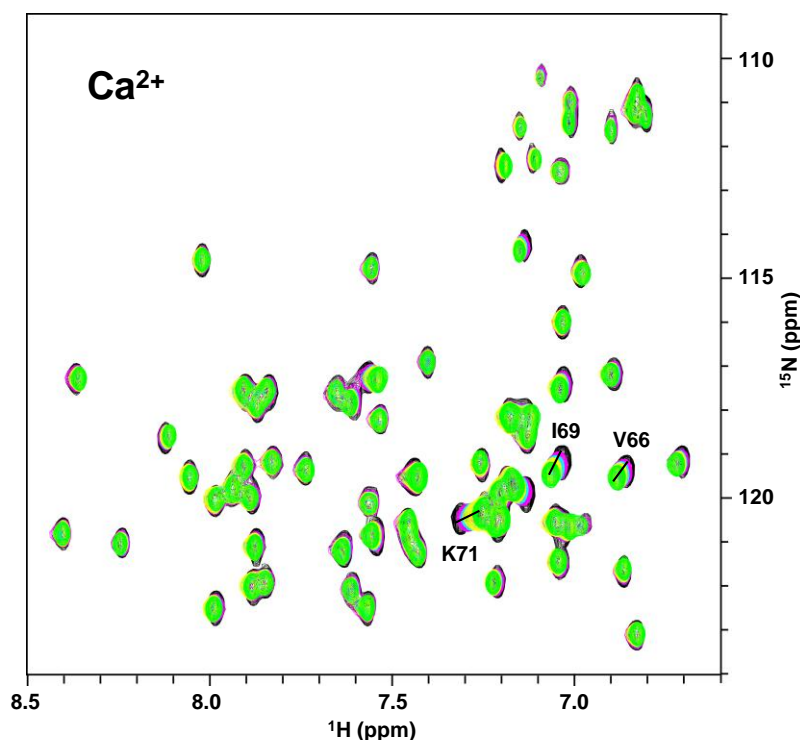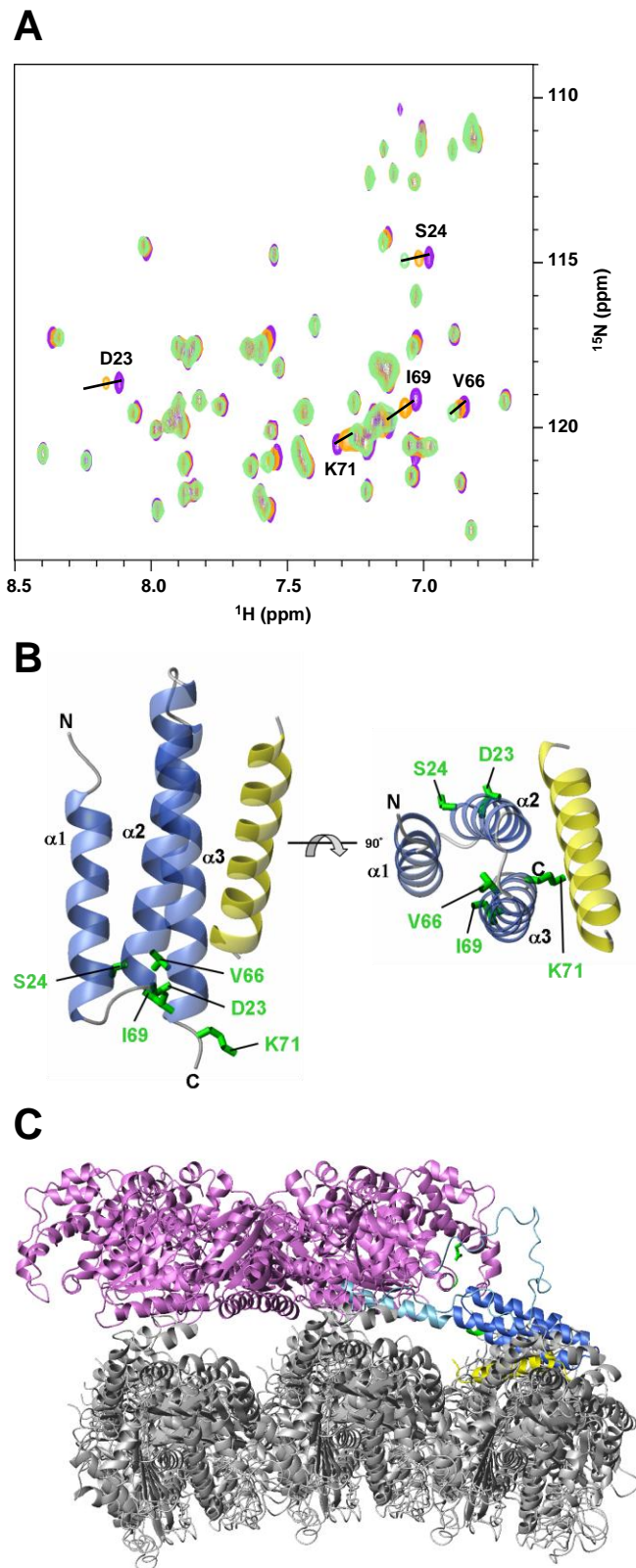
FIGURE 8. **$^{1}$H-$^{15}$N HSQC spectra of p60-vMIT in the absence (black) and presence of 5 mM (magenta), 10 mM (cyan), 15 mM (yellow), 25 mM (green) Ca$^{2+}$.** Residues with the greatest chemical shift perturbations are shown.

FIGURE 9. **Ca$^{2+}$-binding sites of p60-katanin.** (A) $^{1}$H-$^{15}$N HSQC spectra of p60-vMIT in the absence (violet) and presence of 1 mM (orange) and 2 mM (pale green) Ce$^{3+}$ as a paramagnetic probe for Ca$^{2+}$. Residues with the greatest chemical shift perturbations are shown. (B) Side and top views of the ribbon diagram of p60-vMIT (PDB: 2rpa). Side chains of residues binding Ca$^{2+}$ are shown in green. Tubulin helix 12, a putative interface of p60-vMIT, is colored yellow. (C) Proposed model for tubulin binding with full-length p60-katanin. Model complex between tubulin origomer (gray) and hexameric full-length p60-katanin, composed of p60-vMIT (blue), a coiled-coil (light blue), a flexible linker (light blue), and AAA ATPase (violet) domains is shown. One of the six p60-vMITs on the hexameric AAA ATPase is drawn. One helix 12 on tubulin, the putative interface of p60-katanin, is colored yellow. Residues bound to Ca$^{2+}$ on p60-vMIT and residues on hexameric AAA ATPase domains close to the Ca$^{2+}$-binding sites on p60-vMIT are shown in green.

**A**



**B**



**C**
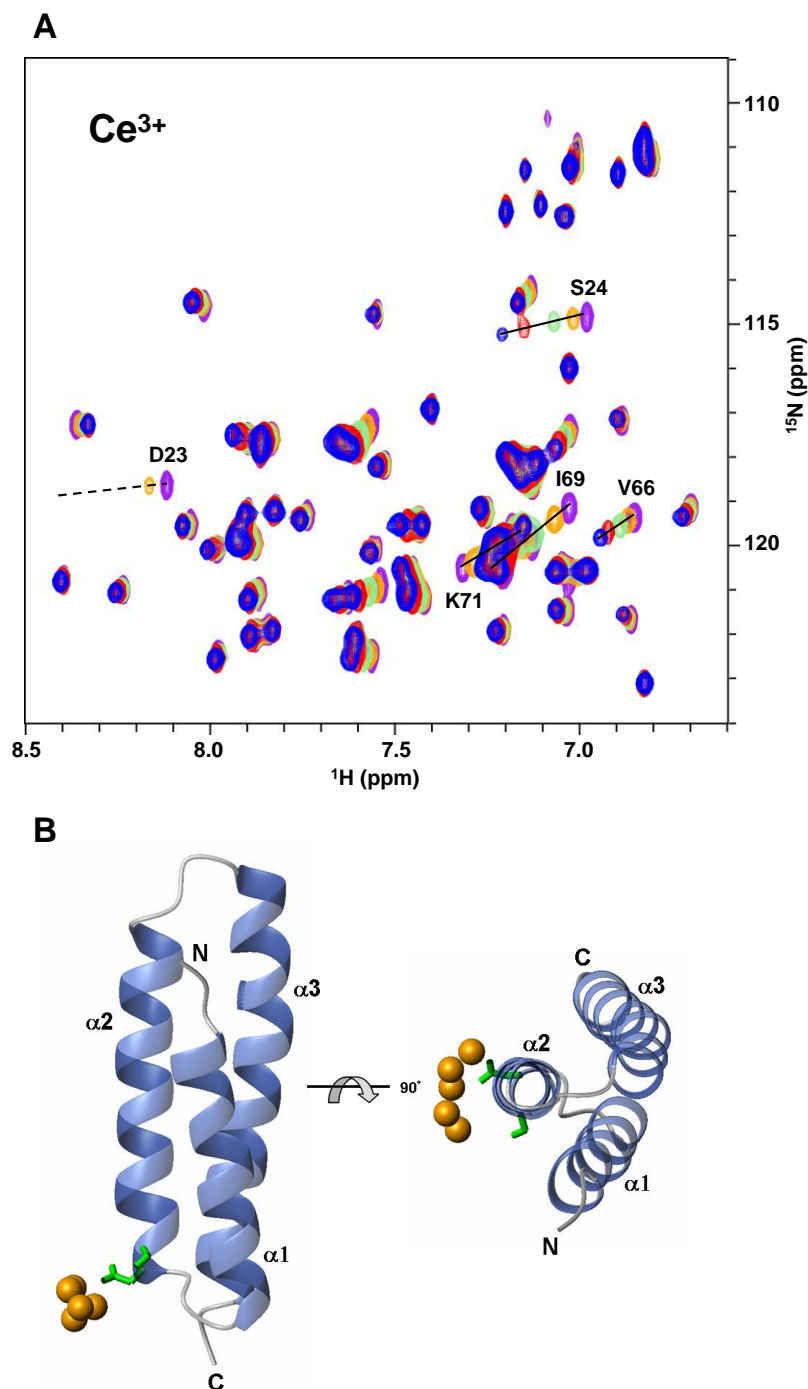
FIGURE 10. **Ce$^{3+}$ titration experiments of p60-vMIT.** (A) $^1$H-$^{15}$N HSQC spectra of p60-vMIT in the absence (violet) and presence of 1 mM (orange), 2 mM (pale green), 5 mM (red), 10 mM (blue) Ce$^{3+}$ as a paramagnetic probe for Ca$^{2+}$. Residues with the greatest chemical shift perturbations are shown. (B) A view of best 5 positions of Ce$^{3+}$ ion (orange) in p60-vMIT (PDB: 2rpa). Side chains of residues binding Ce$^{3+}$ are shown in green. The position of the coordinating Ce$^{3+}$ ion was calculated by using the program FANTASIAN (http://www.cerm.unifi.it./softwares/software- fantasian) coupled with an inhouse grid-search program with 144 pseudocontact shift value of NH signals.
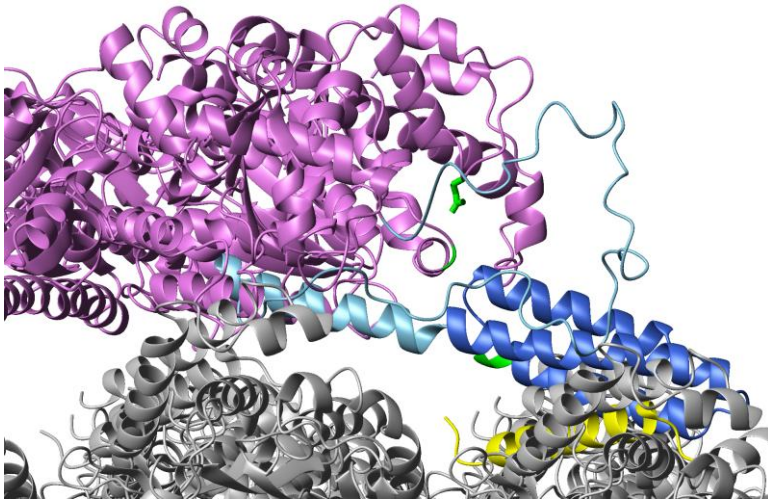
FIGURE 11. **Close-up view of the Ca$^{2+}$ binding region of p60-katanin in Fig. 9C.**
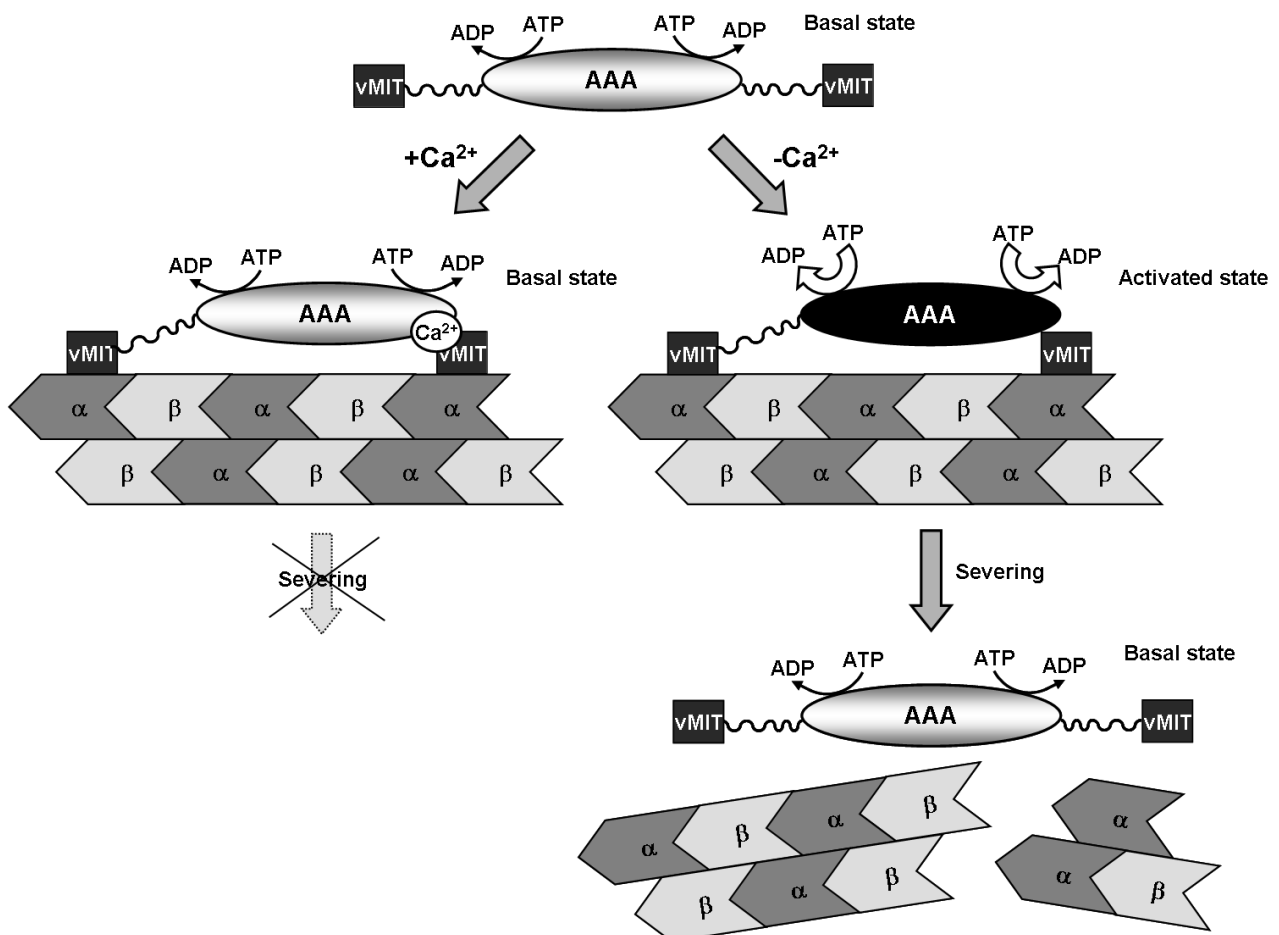


FIGURE 12. **Model of the mechanism of MT-severing by p60-katanin in the absence and presence of Ca$^{2+}$.** Hexameric p60-katanin represents the enzyme in a basal state of ATP-dependent ATPase activity. Four of the six p60-vMIT domains, followed by flexible linkers on the side view of the hexameric AAA ring are not drawn for clarify. In the absence of Ca$^{2+}$, p60-katanin is in an activated state, whereby its ATPase activity is elevated by binding MT through an interaction between the vMIT and AAA domains, resulting in MT-severing. By contrast, when p60-katanin binds Ca$^{2+}$, p60-katanin remains in a basal state regardless of MT-binding and does not sever MT.

## Discussion

### *The function of p80-CTD to capture and release p60-vMIT*

Our NMR experiment and mutation studies suggested that p80-CTD binds to a wide surface of p60-MIT, including helix 1/2 and helix 1/3, which differs from the MT-binding surface, helix 2/3 (Fig. 2B)[14]. If so, p80-CTD and MT could simultaneously bind to p60-vMIT, forming a ternary complex. However, our ATPase assay showed only a limited additive effect of p80-CTD and MT on ATPase activity (Fig. 5A). In addition, p80-CTD was excluded from the p60/MT complex (Fig. 13, lanes 9–12). Thus, in our experiments, we did not observe a ternary complex of p80-CTD, p60-vMIT and MT. Steric hindrance caused by p80-CTD binding to the helix 1/2 and 1/3 surfaces may occur. This unique activity of p80-CTD may explain how adaptor-p80 recruits p60-katanin to MTs. That is, using the N-terminal WD40 domain, adaptor-p80 might localize on γ-TuRC at the minus end of an MT[6], while p80-CTD captures p60-vMIT. P60-katanin would then relocate to the MT, while p80-CTD releases p60-vMIT. Note that, the *in vivo* activity of adaptor-p80 against p60-katanin also remains controversial, because adaptor-p80 localizes p60-katanin to γ-TuRC and stimulates MT severing[8], whereas overexpression of adaptor-p80 suppress the MT-severing activity of p60-katanin in certain types of cell[11].
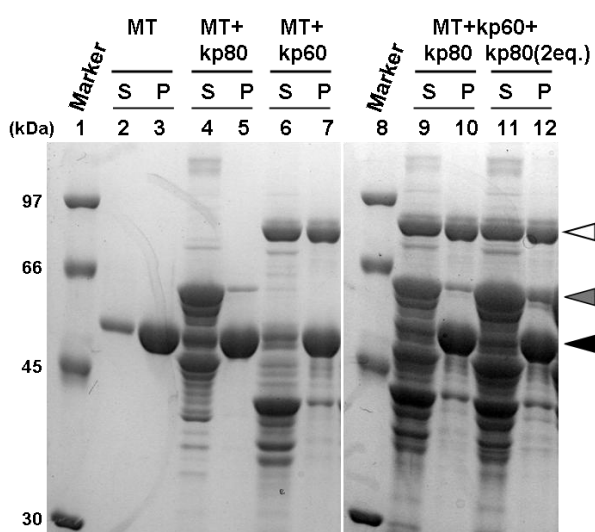


FIGURE 13. **MT co-sedimentation assay in the presence of p60-katanin and p80-CTD *in vitro*.** The assay used a GST-tagged K255A mutant p60 and MBP-tagged p80-CTD. MTs and associated proteins were separated from unbound proteins by sedimentation in a glycerol cushion buffer. The proteins used for co-sedimentation are indicated at the top of the gel. P and S represent the pellet fraction and the supernatant fraction, respectively. Molecular sizes are shown in lanes 1 and 8. Open, gray and filled arrowheads show GST-tagged p60, MBP-tagged p80-CTD and MT, respectively. The SDS-PAGE gel was stained with Coomassie blue.

## *Existence of an MT-/p80-activated state of p60-katanin*

The phenomenon that MT (substrate) as well as p80 (adaptor) binding to p60-katanin increases the ATPase activity of p60-katanin has been reported previously[6,17,18], although the molecular mechanism remains unclear. One explanation might be an equilibrium shift between an inactive dimeric state and an active hexameric state that forms upon binding to substrate and/or adaptor. For example, the katanin-related type I AAA enzyme Vps4 has been shown to act in a dimer–hexamer equilibrium in a nucleotide-dependent manner, although substrate-dependent ATPase activation of Vps4 has not been reported so far[27,28]. Since multivalent binding between active katanin and MT is expected, MT-binding may promote hexamer formation of p60-katanin. We can rule out this possibility, however, because activation of ATP hydrolysis was observed even upon p60-katanin binding to p80-CTD, which was monomeric in solution (data not shown). This suggests the existence of a unique MT-/p80- activated state of p60-katanin. This activated state of p60-katanin is more likely attributed to the intra-molecular spatial rearrangement between the N-terminal vMIT and the central AAA domains, rather than an equilibrium shift.

The regulatory role of p60-vMIT on its own AAA-domain has not been predicted. Nevertheless, it is not surprising if the analogy to other AAA-ATPases, including type II rather than type I enzymes, is considered. In general, the N-terminal domains preceding the AAA domain of type II AAA enzymes may perform three molecular functions: (i) provision of an interface for substrates for ATP hydrolyzing energy; (ii) provision of an interface for adaptor proteins that mainly contribute to subcellular localization; and (iii) modulation of ATPase activity. We previously reported that p60-vMIT serves as an interface for MTs[14]. We also reported that the N-terminal domain of both VCP/p97 and NSF serves as the substrate-binding site, as well as the surface for organelle membrane binding[29]. On the other hand, it has been reported that binding to substrates or membranes regulates the ATPase activity of these proteins[30,31]. In VCP/p97, the residues at the contact site between the N-domain and the first AAA domain (D1-domain) were identified in

conjunction with Paget's disease of the bone and front temporal dementia (IBMPFD) (e.g., R155, A232, T262, and N387)[30,31]. Conformational change of the N-domain relative to the D1-domain in a nucleotide-dependent manner was observed by X-ray crystallography[30,31]. A mutation on A232 (A232E), one of the key residues, is associated with increased severity of the disease[32]. Biochemically, an A232E mutant exhibits elevated ATPase activity[33]. In NSF, a similar mechanism in which the contact site between the N-domain and D1 is associated with enhancement of ATPase activity has also been identified[34]. Note that, although both the sequences and the structures of the N-terminal domains of katanin and VCP/NSF family are rather different, the AAA domains are highly conserved. Finally, we illustrate the MT-activated state of p60-katanin in Fig. 9C, under the assumption that the edge of p60-vMIT becomes close enough to these interfacial residues on the AAA domain with a minimum structural change upon MT-binding. In this model, residues E397 and G237 of p60-katanin are highlighted, which correspond to the interfacial residue N387 and the key residue A232 in VCP, respectively.

### *Ca$^{2+}$ alters the spatial domain rearrangement of p60-katanin in its MT-/p80-activated state*

In this study, we showed that Ca$^{2+}$ inhibits the MT-severing activity of katanin, as well as reducing its MT-elevated ATPase activity to basal levels. Although the mechanism of this modulation seems complicated, studying the effect of Ca$^{2+}$ on p60-katanin may provide clues to the working model of MT-severing, which is driven by ATP hydrolyzing energy and catalyzed by katanin, as shown in Fig. 9C. First, we showed that Ca$^{2+}$ affects p60-katanin activity by directly binding to the vMIT domain (Fig. 9). In contrast, Ca$^{2+}$ does not affect either MT-binding or p80-binding by the domain (Fig. 7, data not shown). Because the Ca$^{2+}$-binding site on p60-vMIT is different from its MT-binding site, these observations are consistent with each other. Next, we found that Ca$^{2+}$ does not affect the basal ATPase activity level of p60-katanin in the absence of MT and/or adaptor-p80 (Fig. 6A). In contrast, Ca$^{2+}$ has an effect only on the MT- and/or p80-elevated ATPase

activity, but not for the basal activity (Fig. 6B and C; Fig. 5B). Because a flexible linker (~114aa) connects the N-terminal vMIT domain and the AAA domain, this $Ca^{2+}$ effect is difficult to explain unless these two domains move spatially close to each other. As discussed above, we assume the existence of the MT-/p80- activated state of p60-katanin in such a domain rearrangement. It is likely that $Ca^{2+}$ affects this MT-/p80-activated state, while the relative orientation of the two domains, which may be a trigger to elevate ATP hydrolysis, is altered by $Ca^{2+}$. This idea is further assessed by visualizing the spatial locations of the vMIT domain, $Ca^{2+}$ ion, and the putative interfacial residues on the AAA domain (Fig. 9C; Fig. 11).

### *Biological implications of the regulatory role of $Ca^{2+}$ in MT-severing by katanin*

In the present study, $Ca^{2+}$ negatively regulated the MT-severing function of katanin. In other words, $Ca^{2+}$ contributed to stabilization of MTs by protecting MTs from attack by katanin. The interaction of $Ca^{2+}$ with MTs has been extensively studied since the inhibitory effect of $Ca^{2+}$ on the *in vitro* assembly of MTs was reported by Weisenberg[23]. $Ca^{2+}$ has been shown to destabilize polymerization of MTs directly or indirectly. Serrano *et al.* determined the $Ca^{2+}$-binding sites on both α- and β-tubulin molecules, which are major components of MTs, and demonstrated that tubulin deprived of these sites could still polymerize in the presence of high concentrations of $Ca^{2+}$ [35]. $Ca^{2+}$ is also known to affect dynamic instability in the assembly of MTs: it enhances the rate of catastrophic degradation of MT[24]. Lefèvre *et al.* recently elucidated that the $Ca^{2+}$-binding sites of tubulin overlapped with the binding sites for MAPs, and thus $Ca^{2+}$ competed with MAPs, resulting in the disassembly of MTs[15].

Indirect $Ca^{2+}$ effect on MT destabilization *via* one of MAPs, tau, has drawn increased attention[36]. In the pathway, calpain, one of calcium-dependent non-lysosomal cysteine proteases, play critical roles. Tau is highly relevant to regulating MT polymerization, or something of that nature. Hyperphosphorylation of tau, however, abolishes its ability to bind tubulin and to promote

MT assembly. When MTs release hyperphosphorylated tau, the protein aggregates into paired helical filaments (PHFs), which are the neuropathological hallmarks of Alzheimer's disease (AD). There are at least three protein kinases responsible for the hyperphosphorylation; cyclin-dependent-kinase 5 (CDK5), glycogen synthase kinase 3β (GSK-3β) and dual-specificity tyrosine-phosphorylation-regulated kinase 1A (DYRK1A)[37-39]. The activity of all the three kinases is regulated by calpain, as follows. In the presence of high concentrations of Ca²⁺, GSK-3β is truncated by calpain, generating two fragments of approximately 40 and 30 kDa. GSK-3β truncation augments its kinase activity[40]. CDK5 is also activated by proteolytic cleavage of its specific activator p35 by calpain[41]. Recently, DYRK1A was elucidated to be proteolyzed and activated by calpain in AD brain[42]. In addition, calpain directly degrades tau, which also causes its loss of MT-stabilizing activity[43,44].

So far, Ca²⁺ has been thought not to stabilize MTs, but to promote the disassembly of MTs, as mentioned above. Our new findings on katanin, however, show that Ca²⁺ can slow down the disassembly of MTs, suggesting that the assembly and disassembly of MT is managed by a more complicated system than expected. Excess of Ca²⁺ is generally harmful to MTs both directly and indirectly. To survive against an accidental increase in Ca²⁺, cells may have developed various fail-safe mechanisms, one of which might be the Ca²⁺-inhibition of katanin. This mechanism would function to avoid the rapid breakdown of MTs for survival of neuronal cells upon a transient Ca²⁺ flux.

In conclusion, we have shown here that p60-katanin, a type-I AAA ATPase, possesses a novel mechanism for regulating its own ATPase activity, probably by a 3D domain rearrangement between the N-terminal vMIT domain and the AAA domain. Ca²⁺ binds p60-vMIT at the edge of this domain, close to the contact site between vMIT and AAA. This putative arrangement can well explain why Ca²⁺ inhibits MT severing without inhibiting either ATPase activity or MT-binding.

## Experimental procedures

### *Production of p80-CTD*

We generated a multiple sequence alignment of the C-terminal sequences of adaptor-p80 excluding the N-terminal WD40 repeats (residues 1–269) by ClustalX[45], from which we decided to clone the sequences 480–614, 480–630, and 480–655 of human and mouse p80. Expression vectors for the recombinant GST-tagged form of the human and mouse p80 fragments were constructed using PRESAT vector methodology[46], as derived from the pGEX-4T3 vector (GE-Healthcare Biosciences). Finally, p80 (480–655), termed p80-CTD, was used for further analysis because this construct produced a protein with greater solubility than the others. Human p80-CTD, prepared by expression in *E. coli* BL21 (*DE3*), followed by affinity purification on glutathione-Sepharose (GE Healthcare Bioscience) and thrombin digestion, was used for ATPase assays. The expression vector for the recombinant MBP-tagged p80-CTD of mouse was also constructed by a standard protocol using PCR, and ligated into the *EcoRI-HindII* sites of pMAL-c2X (NEB). The fusion protein was prepared by expression in *E. coli* BL21 (*DE3*), followed by affinity purification on amylose-sepharose (GE Healthcare Bioscience), and used for NMR experiments and binding experiments with p60-vMIT.

### *Production of p60-katanin*

The expression vector for the recombinant GST-tagged full-length p60-katanin of mouse was constructed by a standard protocol using PCR, and ligated into the *BamH*I-*SalI* sites of pGEX-6P3 (GE Healthcare Bioscience)[14]. An Ala-substituted mutant (K255A) was engineered with the QuikChange site-directed mutagenesis kit (Stratagene). Two complementary oligonucleotides with mutated sequences for each mutant were used as primers (Table 2). The fusion proteins were produced in *E.coli* JM109. Expression was induced with 0.1 mM IPTG, and LB cultures were

grown overnight at 20 °C. For co-sedimentation assays, GST-tagged proteins were purified with glutathione-Sepharose and eluted in the elution buffer (50 mM Tris-HCl, pH 7.4, 100 mM NaCl, 1 mM DTT, 50 mM reduced glutathione, and 5% glycerol). For ATPase assays, proteins were eluted in the elution buffer (20 mM Tris-HCl, pH 7.5, 100 mM NaCl, 1 mM DTT, 1 mM EGTA, 2 mM MgCl$_2$, 0.25 mM ATP, 0.02% Triton X-100, and 5% glycerol) after PreScission Protease digestion on the column.

Production of the recombinant GST-tagged p60-vMIT domains of mouse including wild-type and Ala-substituted mutants was done as previously described (Table 2)[14]. The fusion proteins were expressed in *E. coli* BL21 (*DE3*), affinity-purified on glutathione-Sepharose and dialyzed. These fusion proteins were used for MBP-tagged p80-CTD binding assays. For NMR spectroscopy, a 1 L culture was incubated with [$^{15}$N]-ammonium chloride as the sole nitrogen source by following a standard fermentation protocol at 25°C. Purification of $^{15}$N-labeled p60-vMIT was achieved by glutathione-Sepharose affinity chromatography followed by thrombin digestion, benzamidine-Sepharose chromatography, and gel filtration using a Superdex 75 column (GE Healthcare Bioscience). The complex of $^{15}$N-labeled p60-vMIT with p80-CTD was purified from a mixture of $^{15}$N-labeled GST-tagged p60-vMIT and non-labeled MBP-tagged p80-CTD prepared following FactorXa and thrombin digestion, respectively.

TABLE 1. **Oligonucleotides used as primers for Ala substitution.**

| Primer | Sequence |
| --- | --- |
| K255A_F | CACCTGGCACTGGA**GCG**ACCCTTCTAGCTAAAG |
| K255A_R | CTTTAGCTAGAAGGGT**CGC**TCCAGTGCCAGGTG |

| Primer | Sequence |
|--------|----------|
| K11A_F | CAAATGATTGTTGAGAATGTA**GCC**TTGGCTCGTGAATATGCACTG |
| K11A_R | CAGTGCATATTCACGAGCCAA**GGC**TACATTCTCAACAATCATTTG |
| E15A_F | GAGAATGTAAAATTGGCTCGT**GCC**TATGCACTGCTGGGAAACTATGAC |
| E15A_R | GTCATAGTTTCCCAGCAGTGCATA**GGC**ACGAGCCAATTTTACATTCTC |
| Y16A_F | GAGAATGTAAAATTGGCTCGTGAA**GCC**GCACTGCTGGGAAACTATGAC |
| Y16A_R | GTCATAGTTTCCCAGCAGTGC**GGC**TTCACGAGCCAATTTTACATTCTC |
| D23A_F | GCACTGCTGGGAAACTAT**GCC**TCTGCAATGGTCTACTATCAG |
| D23A_R | CTGATAGTAGACCATTGCAGA**GGC**ATAGTTTCCCAGCAGTGC |
| V27A_F | GGAAACTATGACTCTGCAATG**GCC**TACTATCAGGGAGTTCTTGAC |
| V27A_R | GTCAAGAACTCCCTGATAGTA**GGC**CATTGCAGAGTCATAGTTTCC |
| Y28A_F | GGAAACTATGACTCTGCAATGGTC**GCC**TATCAGGGAGTTCTTGAC |
| Y28A_R | GTCAAGAACTCCCTGATA**GGC**GACCATTGCAGAGTCATAGTTTCC |
| Q35A_F | CAGGGAGTTCTTGAC**GCC**ATGAACAAGTACCTGTACTCAGTC |
| Q35A_R | GACTGAGTACAGGTACTTGTTCAT**GGC**GTCAAGAACTCCCTG |
| N37A_F | CAGGGAGTTCTTGACCAAATG**GCC**AAGTACCTGTACTCAGTC |
| N37A_R | GACTGAGTACAGGTACTT**GGC**CATTTGGTCAAGAACTCCCTG |
| D45A_F | CTGTACTCAGTCAAA**GCC**ACACACCTCCGTCAGAAATGG |
| D45A_R | CCATTTCTGACGGAGGTGTGT**GGC**TTTGACTGAGTACAG |
| R49A_F | GTCAAAGATACACACCTC**GCC**CAGAAATGGCAACAG |
| R49A_R | CTGTTGCCATTTCTG**GGC**GAGGTGTGTATCTTTGAC |
| Q53A_F | CTCCGTCAGAAATGG**GCC**CAGGTTTGGCAGGAAATAAATGTG |
| Q53A_R | CACATTTATTTCCTGCCAAACCTG**GGC**CCATTTCTGACGGAG |

| Primer | Sequence |
| --- | --- |
| Q54A_F | CTCCGTCAGAAATGGCAA**GCC**GTTTGGCAGGAAATAAATGTG |
| Q54A_R | CACATTTATTTCCTGCCAAAC**GGC**TTGCCATTTCTGACGGAG |
| V55A_F | CTCCGTCAGAAATGGCAACAG**GCC**TGGCAGGAAATAAATGTG |
| V55A_R | CACATTTATTTCCTGCCA**GGC**CTGTTGCCATTTCTGACGGAG |
| E58A_F | CAGAAATGGCAACAGGTTTGGCAG**GCC**ATAAATGTGGAAGCTAAG |
| E58A_R | CTTAGCTTCCACATTTAT**GGC**CTGCCAAACCTGTTGCCATTTCTG |
| K64A_F | GTTTGGCAGGAAATAAATGTGGAAGCT**GCC**CAAGTTAAGGATATCATG |
| K64A_R | CATGATATCCTTAACTTG**GGC**AGCTTCCACATTTATTTCCTGCCAAAC |
| K67A_F | GTGGAAGCTAAGCAAGTT**GCC**GATATCATGAAAACATAATAGAGC |
| K67A_R | GCTCTATTATGTTTTCATGATATC**GGC**AACTTGCTTAGCTTCCAC |
| D68A_F | GTGGAAGCTAAGCAAGTTAAG**GCC**ATCATGAAAACATAATAGAGC |
| D68A_R | GCTCTATTATGTTTTCATGAT**GGC**CTTAACTTGCTTAGCTTCCAC |

***Continuous ATPase assays of p60-katanin***

ATPase activity was measured using an ATP regenerating system. The reaction mixture contained 50 mM Tris-HCl, pH 7.5, 50 mM KCl, 2 mM MgCl$_2$, 2 mM phosphoenolpyruvate, 1 mM ATP, 50 μg/ml pyruvate kinase, 50 μg/ml lactate dehydrogenase, and 0.2 mM NADH. The reactions were performed in the presence of 0.4 μM p60-katanin, and ATPase activity was measured by monitoring the decrease in NADH absorption at 340 nm at room temperature using UV-Vis spectrophotometer, UV mini-1240 (Shimadzu, Tokyo, Japan). The shifts in absorption at 340 nm caused by the addition of taxol-stabilizing MTs and p80-CTD were measured. The absorbnce data

were representative of two or three independent experiments and were normalized relative to the level of the time-point zero. ATP hydrolysis activity was then calculated and represented in the unit of μmoles of ATP hydrolyzed per min per mg of p60-katanin (units/mg).

### *In vitro binding experiments*

Maltose binding protein (MBP)-p80 bound to amylose resin was incubated with lysate of GST- tagged p60-vMIT domains in binding buffer (20 mM Tris-HCl, pH 7.4, 200 mM NaCl, and 1 mM EGTA) for 2 hour at 4°C. The beads were washed four times in wash buffer (20 mM Tris-HCl, pH 7.4, 200 mM NaCl, and 1 mM EGTA). The associated proteins were analyzed by SDS-PAGE.

### *Co-sedimentation assays for MT-binding and MT-severing activity of p60-katanin*

Taxol-stabilized MTs (1 μM) and GST-tagged p60-katanin (3.5 μM) were incubated for 30 min at 25°C in binding buffer (80 mM PIPES, pH 7.0, 2 mM $MgCl_2$, 1mM EGTA, 1 mM ATP, and 20 μM taxol). Reaction mixtures (50 μl) were spun through a glycerol cushion buffer (50% [v/v] glycerol in binding buffer; 100 μl) for 30 min at 100,000 g. Supernatants and Pellets ware analyzed by SDS-PAGE. The band intensity of proteins was quantified with Image J (http://rsbweb.nih. gov/ij/).

### *NMR experiments*

$^1$H-$^{15}$N HSQC spectra of $^{15}$N-labeled p60-vMIT in either the presence or the absence of p80-CTD were acquired at 25°C on a Bruker *AVANCE* III 600 MHz spectrometer equipped with a cryogenic probe. These samples were dissolved in 20 mM sodium phosphate, pH 7.5, and 150 mM NaCl, and the protein concentrations were below 50 μM because of the low solubility of p80-CTD. $^1$H-$^{15}$N HSQC spectra for $Ce^{3+}$ titration experiments were recorded using 0.1 mM $^{15}$N-labeled p60-vMIT at 25°C on a Bruker *AVANCE* 500 MHz spectrometer equipped with a cryogenic probe. $^1$H-

$^{15}$N HSQC spectra for Ca$^{2+}$ titration experiments were similarly performed (Fig. 8). The samples were dissolved in 20 mM HEPES, pH 7.5, and 25 mM NaCl. All data were processed using NMRPipe[47] and SPARKY[48] software. The position of the coordinating Ce$^{3+}$ ion was calculated by using the program FANTASIAN[49] coupled with an inhouse grid-search program with 144 pseudocontact shift value of NH signals. For calculation the coordinates of hVps4b-MIT (PDB:1wr0) and p60-vMIT (PDB:2rpa) were used. All of the figures were prepared by MOLMOL[50].

### *Molecular modelling*

A hexameric ring model of the AAA domains of p60-katanin was generated on the basis of the hexameric ring structure of p97 D1 (PDB: 1s3s) using MODELLER (version 9v6) (http://salilab.org/modeller/) as described previously[14]. A molecular model of the complex of p60-vMIT with a tubulin oligomer (PDB: 3du7) was constructed on the basis of the complex between Vps4a-MIT and CHMP1a (PDB: 2jq9)[51] by replacing each component corresponding to p60-vMIT and helix 12 of α-tubulin, respectively[14]. Finally, the complex model of full-length p60-katanin and part of an MT was built by connecting these two models by a flexible linker corresponding to residues 91–204, and by placing the hexameric AAA domain close to the vMIT domain. The model was adjusted and visualized using MOLMOL[50].

# References

1.  McNally, F. J. & Vale, R. D. (1993) Identification of katanin, an ATPase that severs and disassembles stable microtubules. *Cell* **75**, 419-429.

2.  Hazan, J., Fonknechten, N., Mavel, D., Paternotte, C., Samson, D., Artiguenave, F., Davoine, C. S., Cruaud, C., Durr, A., Wincker, P., Brottier, P., Cattolico, L., Barbe, V., Burgunder, J. M., Prud'homme, J. F., Brice, A., Fontaine, B., Heilig, B. & Weissenbach, J. (1999) Spastin, a new AAA protein, is altered in the most frequent form of autosomal dominant spastic paraplegia. *Nat. Genet.* **23**, 296-303.

3.  Errico, A., Ballabio, A. & Rugarli, E. I. (2002) Spastin, the protein mutated in autosomal dominant hereditary spastic paraplegia, is involved in microtubule dynamics. *Hum. Mol. Genet.* **11**, 153-163.

4.  Cox, G. A., Mahaffey, C. L., Nystuen, A., Letts, V. A. & Frankel, W. N. (2000) The mouse fidgetin gene defines a new role for AAA family proteins in mammalian development. *Nat. Genet.* **26**, 198-202.

5.  Frickey, T. & Lupas, A. N. (2004) Phylogenetic analysis of AAA proteins. *J. Struct. Biol.* **146**, 2-10.

6.  Hartman, J. J., Mahr, J., McNally, K., Okawa, K., Iwamatsu, A., Thomas, S., Cheesman, S., Heuser, J., Vale, R. D. & McNally, F. J. (1998) Katanin, a microtubule-severing protein, is a novel AAA ATPase that targets to the centrosome using a WD40-containing subunit. *Cell* **93**, 277-287.

7.  McNally, K. P., Bazirgan, O. A. & McNally, F. J. (2000) Two domains of p80 katanin regulate microtubule severing and spindle pole targeting by p60 katanin. *J. Cell Sci.* **113**, 1623-1633.

8.  Buster, D., McNally, K. & McNally, F. J. (2002) Katanin inhibition prevents the redistribution of gamma-tubulin at mitosis. *J. Cell Sci.* **115**, 1083-1092.

9.  McNally, K., Audhya, A., Oegema, K. & McNally, F. J. (2006) Katanin controls mitotic and meiotic spindle length. *J. Cell Biol.* **175**, 881-891.

10. Baas, P. W. & Qiang, L. (2005) Neuronal microtubules: when the MAP is the roadblock. *Trends Cell Biol.* **15**, 183-187.

11. Yu, W., Solowska, J. M., Qiang, L., Karabay, A., Baird, D. & Baas, P. W. (2005) Regulation of microtubule severing by katanin subunits during neuronal development. *J. Neurosci.* **25**, 5573-5583.

12. Qiang, L., Yu, W., Andreadis, A., Luo, M. & Baas, P. W. (2006) Tau protects microtubules in the axon from severing by katanin. *J. Neurosci.* **26**, 3120-3129.

13. Iwaya, N., Goda, N., Unzai, S., Fujiwara, K., Tanaka, T., Tomii, K., Tochio, H., Shirakawa, M. & Hiroaki, H. (2007) Fine-tuning of protein domain boundary by minimizing potential coiled coil regions. *J. Biomol. NMR* **37**, 53-63.

14. Iwaya, N., Kuwahara, Y., Fujiwara, Y., Goda, N., Tenno, T., Akiyama, K., Mase, S., Tochio, H., Ikegami, T., Shirakawa, M. & Hiroaki, H. (2010) A common substrate recognition mode conserved between katanin p60 and VPS4 governs microtubule severing and membrane skeleton reorganization. *J. Biol. Chem.* **285**, 16822-16829.

15. Lefevre, J., Chernov, K. G., Joshi, V., Delga, S., Toma, F., Pastre, D., Curmi, P. A. & Savarin, P. (2011) The C terminus of tubulin, a versatile partner for cationic molecules: binding of Tau, polyamines, and calcium. *J. Biol. Chem.* **286**, 3065-3078.

16. Sudo, H. & Baas, P. W. (2011) Strategies for diminishing katanin-based loss of microtubules in tauopathic neurodegenerative diseases. *Hum. Mol. Genet.* **20**, 763-778.

17. Hartman, J. J. & Vale, R. D. (1999) Microtubule disassembly by ATP-dependent oligomerization of the AAA enzyme katanin. *Science* **286**, 782-785.

18. Stoppin-Mellet, V., Gaillard, J. & Vantard, M. (2002) Functional evidence for in vitro microtubule severing by the plant katanin homologue. *Biochem. J.* **365**, 337-342.

19. McNally, K. P. & McNally, F. J. (2011) The spindle assembly function of Caenorhabditis elegans katanin does not require microtubule-severing activity. *Mol. Biol. Cell* **22**, 1550-1560.

20. Sudo, H. & Maru, Y. (2008) LAPSER1/LZTS2: a pluripotent tumor suppressor linked to the inhibition of katanin-mediated microtubule severing. *Hum. Mol. Genet.* **17**, 2524-2540

21. Mitchison, T. & Kirschner, M. (1984) Dynamic instability of microtubule growth. *Nature* **312**, 237-242.

22. Walker, R. A., O'Brien, E. T., Pryer, N. K., Soboeiro, M. F., Voter, W. A., Erickson, H. P. & Salmon, E. D. (1988) Dynamic instability of individual microtubules analyzed by video light microscopy: rate constants and transition frequencies. *J. Cell Biol.* **107**, 1437-1448.

23. Weisenberg, R.C. (1972) Microtubule formation in vitro in solutions containing low calcium concentrations. *Science* **177**, 1104-1105.

24. O'Brien, E. T., Salmon, E. D. & Erickson, H. P. (1997) How calcium causes microtubule depolymerization. *Cell Motil. Cytoskeleton* **36**, 125-135.

25. Bertini, I., Lee, Y. M., Luchinat, C., Piccioli, M. & Poggi, L. (2001) Locating the metal ion in calcium-binding proteins by using cerium(III) as a probe. *Chembiochem.* **2**, 550-558.

26. Bertini, I., Janik, M. B., Lee, Y. M., Luchinat, C. & Rosato, A. (2001) Magnetic susceptibility tensor anisotropies for a lanthanide ion series in a fixed protein matrix. *J. Am. Chem. Soc.* **123**, 4181-4188.

27. Gonciarz, M. D., Whitby, F. G., Eckert, D. M., Kieffer, C., Heroux, A., Sundquist, W. I. & Hill, C. P. (2008) Biochemical and structural studies of yeast Vps4 oligomerization. *J. Mol. Biol.* **384**, 878-895.

28. Inoue, M., Kamikubo, H., Kataoka, M., Kato, R., Yoshimori, T., Wakatsuki, S. & Kawasaki, M. (2008) Nucleotide-dependent conformational changes and assembly of the AAA ATPase SKD1/VPS4B. *Traffic* **9**, 2180-2189.

29. Shiozawa, K., Goda, N., Shimizu, T., Mizuguchi, K., Kondo, N., Shimozawa, N., Shirakawa, M. & Hiroaki, H. (2006) The common phospholipid-binding activity of the N-terminal domains of PEX1 and VCP/p97. *FEBS J.* **273**, 4959-4971.

30. DeLaBarre, B. & Brunger, A. T. (2005) Nucleotide dependent motion and mechanism of action of p97/VCP. *J. Mol. Biol.* **347**, 437-452.

31. Tang, W. K., Li, D., Li, C. C., Esser, L., Dai, R., Guo, L. & Xia, D. (2010) A novel ATP-dependent conformation in p97 N-D1 fragment revealed by crystal structures of disease-related mutants. *EMBO J.* **29**, 2217-2229.

32. Watts, G. D., Wymer, J., Kovach, M. J., Mehta, S. G., Mumm, S., Darvish, D., Pestronk, A., Whyte, M. P. & Kimonis, V. E. (2004) Inclusion body myopathy associated with Paget disease of bone and frontotemporal dementia is caused by mutant valosin-containing protein. *Nat. Genet.* **36**, 377-381.

33. Halawani, D., LeBlanc, A. C., Rouiller, I., Michnick, S. W., Servant, M. J. & Latterich, M. (2009) Hereditary inclusion body myopathy-linked p97/VCP mutations in the NH2 domain and the D1 ring modulate p97/VCP ATPase activity and D2 ring conformation. *Mol. Cell Biol.* **29**, 4484-4494.

34. Matveeva, E. A., May, A. P., He, P. & Whiteheart, S. W. (2002) Uncoupling the ATPase activity of the N-ethylmaleimide sensitive factor (NSF) from 20S complex disassembly. *Biochemistry* **41**, 530-536.

35. Serrano, L., Valencia, A., Caballero, R. & Avila, J. (1986) Localization of the high affinity calcium-binding site on tubulin molecule. *J. Biol. Chem.* **261**, 7076-7081.

36. Buee, L., Bussiere, T., Buee-Scherrer, V., Delacourte, A. & Hof, P. R. (2000) Tau protein isoforms, phosphorylation and role in neurodegenerative disorders. *Brain Res. Brain Res. Rev.* **33**, 95-130.

37. Liang, Z., Liu, F., Grundke-Iqbal, I., Iqbal, K. & Gong, C. X. (2007) Down-regulation of cAMP-dependent protein kinase by over-activated calpain in Alzheimer disease brain. *J. Neurochem.* **103**, 2462-2470.

38. Li, T., Hawkes, C., Qureshi, H. Y., Kar, S. & Paudel, H. K. (2006) Cyclin-dependent protein kinase 5 primes microtubule-associated protein tau site-specifically for glycogen synthase kinase 3beta. *Biochemistry* **45**, 3134-3145.

39. Ryoo, S. R., Jeong, H. K., Radnaabazar, C., Yoo, J. J., Cho, H. J., Lee, H. W., Kim, I. S., Cheon, Y. H., Ahn, Y. S., Chung, S. H. & Song, W. J. (2007) DYRK1A-mediated hyperphosphorylation of Tau. A functional link between Down syndrome and Alzheimer disease. *J. Biol. Chem.* **282**, 34850-34857.

40. Goni-Oliver, P., Lucas, J. J., Avila, J. & Hernandez, F. (2007) N-terminal cleavage of GSK-3 by calpain: a new form of GSK-3 regulation. *J. Biol. Chem.* **282**, 22406-22413.

41. Lee, M. S., Kwon, Y. T., Li, M., Peng, J., Friedlander, R. M. & Tsai, L. H. (2000) Neurotoxicity induces cleavage of p35 to p25 by calpain. *Nature* **405**, 360-364.

42. Qian, W., Liang, H., Shi, J., Jin, N., Grundke-Iqbal, I., Iqbal, K., Gong, C. X. & Liu, F. (2011) Regulation of the alternative splicing of tau exon 10 by SC35 and Dyrk1A. *Nucleic. Acids Res.* (in press)

43. Johnson, G. V., Jope, R. S. & Binder, L. I. (1989) Proteolysis of tau by calpain. *Biochem. Biophys. Res. Commun.* **163**, 1505-1511.

44. Yang, L. S. & Ksiezak-Reding, H. (1995) Calpain-induced proteolysis of normal human tau and tau associated with paired helical filaments. *Eur. J. Biochem.* **233**, 9-17.

45. Thompson, J. D., Gibson, T. J., Plewniak, F., Jeanmougin, F. & Higgins, D. G. (1997) The CLUSTAL_X windows interface: flexible strategies for multiple sequence alignment aided by quality analysis tools. *Nucleic. Acids Res.* **25**, 4876-4882.

46. Goda, N., Tenno, T., Takasu, H., Hiroaki, H. & Shirakawa, M. (2004) The PRESAT-vector: asymmetric T-vector for high-throughput screening of soluble protein domains for structural proteomics. *Protein Sci.* **13**, 652-658.

47. Delaglio, F., Grzesiek, S., Vuister, G. W., Zhu, G., Pfeifer, J. & Bax, A. (1995) NMRPipe: a multidimensional spectral processing system based on UNIX pipes. *J. Biomol. NMR* **6**, 277-293.

48. Goddard, T. D. & Kneller, D. G. (2004) Sparky 3. *University of California, San Francisco*.

49. Bertini, I., Cremonini, M. A., Gori-Savellini, G., Luchinat, C., Wuthrich, K., & Guntert, P. (1998) PSEUDYANA for NMR structure calculation of paramagnetic metalloproteins using torsion angle molecular dynamics. *J. Biomol. NMR* **12**, 553-557.

50. Koradi, R., Billeter, M. & Wuthrich, K. (1996) MOLMOL: a program for display and analysis of macromolecular structures. *J. Mol. Graph.* **14**, 29-32.

51. Stuchell-Brereton, M. D., Skalicky, J. J., Kieffer, C., Karren, M. A., Ghaffarian, S. & Sundquist, W. I. (2007) ESCRT-III recognition by VPS4 ATPases. *Nature* **449**, 740-744.

# PART III


# SUMMARY AND GENERAL CONCLUSION

## Similarities of the structure and the molecular mechanism

If the amino acid sequences are highly evolutionarily conserved among proteins, these proteins are expected to have the similar character. While, in proteins with low sequence identities, similarities in both the domain architecture and the 3D structure suggests that the molecular mechanism might be evolutionarily conserved among proteins.

In CHAPTER 1, I identified kp60-NTD as a novel domain suited for structural determination by NMR. In CHAPTER 2, I determined the 3D structure of kp60-NTD for the first time. Kp60-NTD has comprised three anti-parallel $\alpha$-helices, resembling the structure of Vps4-MIT. I further identified the tubulin binding interface of kp60-NTD. The location of the interface of kp60-NTD is similar to that of Vps4-MIT. As expected above, both kp60 and Vps4 resemble in not only the domain architecture and the 3D structure of the $NH_2$-terminal domain but also the molecular mechanism, in which both enzymes contribute to disassemble their macromolecular substrates in an ATP-dependent manner, through binding to substrates using the same surface of their $NH_2$-terminal domains. On the basis of these similarities between kp60 and Vps4, I proposed a model for kp60–MT complex. In this model, the structure of the hexameric AAA domains of kp60 was generated from the known structure of the type II AAA ATPase, whose sequences of the first AAA (D1) domain resemble those of a single AAA domain of kp60 and Vps4.

In type II AAA ATPases VCP/p97 and NSF, the interfacial residues between the N ($NH_2$-terminal) domain and the D1 domain have been thought to be the key to the hydrolysis of ATP. In other word, it has been known that a contact between the N domain and the D1 domain is induced by a domain conformational change from a non-activate (basal) state to an activate state, and may regulate the ATPase activity. In CHAPTER 3, the kp60–MT complex model has suggested that kp60-NTD can move close enough to the AAA domain of kp60, when kp60 binds MTs. At this time, a contact of the putative interface between kp60-NTD and its AAA domain may act as a sensor for regulating the ATPase activities or the MT-severing activities. In fact, locations of the putative

interfacial residues of kp60 are similar to those of the interfacial residues between the N domain and the D1 domain in VCP/p97 and NSF. This putative interface also corresponds to the $Ca^{2+}$-binding site of kp60-NTD. Since I showed that $Ca^{2+}$ inhibits the MT-severing activities of kp60 by biochemical assays, the MT-severing may be regulated in a $Ca^{2+}$-dependent manner. The kp60–MT complex model can explain the biochemical phenomena induced by $Ca^{2+}$. In Vps4, the mechanism such as VCP/p97 and NSF has not been found. It is interesting if there are similarities or differences of the mechanism for regulating the ATPase activities between kp60 and Vps4.

## A model for kp60–MT complex

MT usually has 13 protofilaments and a 3-start helix in which each turn of the helix spans 3 tubulin monomers. Because the start number of this helix is odd, there must always be a 'seam' where α subunits are laterally adjacent to β subunits. The stability of the seam is lower than that of bonds between the other protofilaments, where the same subunits are laterally adjacent. My model for kp60–MT complex demonstrates that a diameter of the hexameric AAA domains of kp60 approximately corresponds to that of about 2.5 tubulin monomers. And, my preliminary biochemical assay has suggested that the central pore of the hexameric AAA domains of kp60 may tug on the COOH-terminal tail of β-tubulin, resulting in the disassembly of MTs (unpublished data). I assume that kp60 has to just attack the seams of MTs so that the pore of the hexameric AAA domain of kp60 tugs on the tail of β-tubulin in an ATP-dependent manner. At this time, while kp60-NTD may contact with the AAA domain, kp60-NTD interacts with α-tubulin in the constant direction, as showed in CHAPTER 3. (Fig. 1) The contact of two domains and the interaction between the kp60-NTD and α-tubulin may increase the ATPase activity of kp60 and accelerate MT-severing by kp60. Additionally, because the seams of MTs could break easily, it seems that it is not surprising that kp60 prefers to attack there.
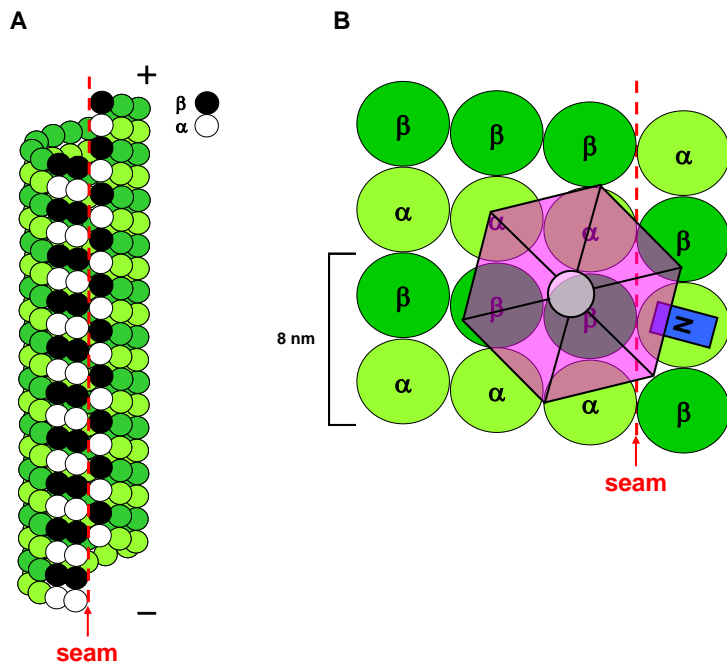
**A**

**B**



FIGURE 1. **A seam of MT and a model of kp60 bound to MT at the seam.** (A) A 13 protofilament MT with seam. Lateral interactions between protofilaments are α to α (yellow-green) and β to β (green), except at the seam. A seam is formed because one turn of a 3-start helix results in a rise of 3 tubulin monomers. (B) Proposed model of kp60 bound to MT at the seam. One of the six kp60-NTDs in a hexamer is drawn. The kp60-NTD binds α-tubulin at the seam, and the pore of the hexameric AAA domain tugs on the COOH-terminal tail of β-tubulin at the seam.

## Structural biology of katanin p60

There are still little 3D structural information on MAPs and complexes between tubulin and MAPs. Therefore, demonstrations of the 3D structure of kp60-NTD and the interface with tubulin on kp60-NTD are crucially important for MT/tubulin studies, and would provide insight into a molecular mechanism for MT disassembly. The further technical developments of the structural analyses such as NMR spectroscopy, X-ray crystallography, and cryo-electron microscopy, and the functional analyses such as single molecule imaging, fluorescent proteins and probes are desirable in structural biology, biochemistry, and molecular cell biology.

Finally, I set up a system to be expressed the full-length kp60 protein in *E.coli*. On the basis of the results in CHAPTER 3, I could elucidate a molecular mechanism of kp60 in detail by monitoring enzymatic activities (the MT-severing activities and the MT-binding activities) of kp60s produced by the molecular engineering, such as mutations in the flexible linker of kp60 and mutations in the putative interface between kp60-NTD and the AAA domain.

## Concluding remarks

In this thesis, I proposed a novel methodology, in which the domain boundary was optimized by combination of bioinformatics and NMR spectroscopy, to obtain a protein sample suitable for the 3D structural analysis. Next, I first determined the 3D structure of the novel NTD of kp60, which is the tubulin binding domain. I further identified the interface with tubulin on kp60-NTD. The structure and the interface with its substrate of kp60-NTD are well similar to those of another type I AAA ATPase, Vps4. There are also the similarities to the molecular mechanisms for their substrates between kp60 and Vps4. These results allowed me to propose a model for kp60–MT complex. Additionally, I showed that kp60-NTD interacts with a minimum region of kp80-CTD, possibly using another interface that differs from the tubulin binding interface. Interestingly, I found that $Ca^{2+}$ ion cancels the enhanced ATPase activity of kp60 in the presence of MT. Furthermore, I found that the MT-severing activity of kp60 is inhibited in $Ca^{2+}$-dependent manner. NMR experiments showed that $Ca^{2+}$ directly binds kp60-NTD at the edge of this domain. It was suggested that this $Ca^{2+}$ binding site is close to the putative interface between the NTD and the AAA domain. Finally, I hypothesized that $Ca^{2+}$ and a spatial rearrangement of kp60-NTD relative to the AAA domain regulate MT-severing by kp60.